Stony Brook University

Structural Changes in the β–Amyloid Precursor Protein Induced by Familial Mutations

A Dissertation Presented

by

Tzu-chun Tang

to

The Graduate School

In Partial Fulfillment of the Requirements

for the Degree of

Doctor of Philosophy

in

Biochemistry and Structural Biology

Stony Brook University

August 2013

Stony Brook University

The Graduate School

Tzu-chun Tang

We, the dissertation committee for the above candidate for the

Doctor of Philosophy degree, hereby recommend

acceptance of this dissertation.

Steven O. Smith, Ph.D. - Dissertation Advisor
Professor, Department of Biochemistry and Cell Biology

Erwin London, Ph.D. - Chairperson of Defense
Professor, Department of Biochemistry and Cell Biology

Huilin Li, Ph.D.
Professor, Department of Biochemistry and Cell Biology

William E. Van Nostrand, Ph.D.
Professor, Research of Medicine

This dissertation is accepted by the Graduate School

Charles Taber

Interim Dean of the Graduate School

Abstract of the Dissertation

Structural Changes in the β–Amyloid Precursor Protein Induced by Familial Mutations

by

Tzu-chun Tang

Doctor of Philosophy

In

Biochemistry and Structural Biology

Stony Brook University

2013

The proteolysis of the β-amyloid precursor protein (APP) yields Aβ peptides with lengths of 38-42 amino acids by a two-step sequential cleavage involving β- and γ-secretase. Aβ40 is the most abundant product, while Aβ42 is the most toxic species to neurons. An increase in the ratio of Aβ42/Aβ40 and an overall increase in secreted Aβ peptides have both been correlated with early-onset familial Alzheimer's disease (FAD). I have focused on two sites where FAD mutations are clustered. The first cluster is in the extracellular domain close to the transmembrane boundary. Within the clusters, the A21G (Flemish), E22Q (Dutch), E22G (Arctic), E22K (Italian), and D23N (Iowa) mutations have very different effects on APP processing. Mutations at Glu22 and Asp23 decrease the level of secretion of the Aβ peptides, while A21G increases total Aβ secretion by more than 3-fold. The second cluster is within the TM domain, below the γ-cut site that releases Aβ42. A stretch of four β-branched amino acids when mutated individually increases the

Aβ42/Aβ40 ratio. I have focused on the T43I mutation, which increases the Aβ42/Aβ40 ratio by 8-fold. Structural studies have been undertaken in membrane bilayers using NMR and FTIR spectroscopy. These studies have provided several insights into the structure of APP and how structural changes induced by mutation influence APP processing. First, the extracellular sequence from Leu17 to Ala21 has β-secondary structure, while the transmembrane region is helical starting at Gly29. Second, the A21G mutation reduces the β-secondary structure near the site of the mutation and increases α-helical structure in the region between Gly25 and Gly29. Third, both the wild-type protein and the A21G mutant form transmembrane homodimers mediated by the $G^{33}xxxG^{37}$ interface. Fourth, the T43I mutation shifts the transmembrane dimer toward the monomeric state. Measurements of Aβ secretion resulting from the A21G and T43I mutations show that both affect the intramembranous γ-cleavage, but in very different ways. A21G destabilizes the β–structure of $L^{17}VFF^{20}$ sequence, which has previously been suggested as inhibitory to the γ–secretase. In contrast, T43I destabilizes transmembrane dimerization. As a result, the A21G mutation leads to an increase in total Aβ secretion, while the T43I mutation results in an increase in the Aβ42/Aβ40 ratio.

Table of content

List of Figures:

List of Abbreviations

AD, Alzheimer's disease

ATR, attenuated total reflection

AUC, analytical ultracentrifugation

Aβ, **β** amyloid peptide

CFP, Cyan fluorescence protein

α-CTF, α C-terminal fragment

β-CTF, β C-terminal fragment

DDT, dithiothrietol

DMPC, 1,2-dimyristoyl-sn-glycero-3-phosphocholine

DMPG, 1,2-dimyristoyl-sn-glycero-3-phosphoglycerol

DPC, dodecylphosphocholine

EC, extracellular

ECLIA, electrochemiluminescence assay

EDTA, ethylenediamine tetraacetic acid

ER, endoplasmic reticulum

FTIR, Fourier transform infrared

FRET, Fluorescence resonance energy transfer

HFIP, hexafluoroisopropanol

HPLC, high performance liquid chromatography

IC, intracellular

IPTG, isopropyl -D-1-thiogalactopyranoside

JM, juxtamembrane

MAS, magic angle spinning

MW, molecular weight

NMR, nuclear magnetic resonance

β-OG, n-octyl- β -D-glucopyranoside

POPC, 1-palmitoyl-2-oleoyl-*sn*-glycero-3-phosphocholine

POPS, 1-palmitoyl-2-oleoyl-*sn*-glycero-3-phospho-L-serine

PAGE, polyacrylamide gel electrophoresis

TGN, trans Golgi network

TM, Transmembrane domain

UV-Vis, ultraviolet-visible

WT, wild-type

YFP, Yellow fluorescence protein

Acknowledgements

This thesis is dedicated to my lovely family, Jennifer and Lucas. Without their support, and accompany, I cannot accomplish my PhD thesis by myself. I am also especially grateful to my father, mother, sister, and brother. Even though they are far away in Taiwan, their timely encouragement always help me out from the bottom, when I confront difficulties.

I particularly like to thank my research advisor Dr. Steven. O. Smith for his guidance in many aspects. Dr. Smith sets himself as an excellent model of a scientist. I was impressed by and also benefited from his extensive knowledge in various aspects of science, his diligence, enthusiasm for projects, and the way of critical and scientific thinking. His suggestions and problem solving thinking made me solve many research problems in a more logical/global way. All these characteristics will significantly benefit, and extend my future career for my research.

I would also like to give my sincere thanks to all the current and former members of Dr. Smith's lab. Dr. Martine Ziliox helped me to improve my solid- and solution-state NMR background, and practical experimental skills with electronics. I am also grateful to have been working with my former, and present colleagues: Ass. Prof. Markus Eilers, Dr. Shivani Ahuja, Dr. Mahiuddin Ahmed, Dr. Ian Brett, Dr. Joseph Goncalves, Dr. Miki Itaya, Darryl Aucoin, and Yi Hu. Their generous help, knowledge, and fulness helped me to integrate into my projects in the very early year of my PhD life in Dr. Smith's lab.

Besides those in Dr. Smith's lab, Dr. James I. Elliott, his wife, Margie (Yale University) and Dr. Takeshi Sato (Osaka University) helped me prepare the synthetic peptides.

I also want to thank the professors on my thesis committee: Dr. Erwin London (Chairperson), Dr. William Van Nostrand, and Dr. Huilin Li. Their generous time, and insightful comments navigated me through my research projects smoothly, and help me to enrich my scientific background.

It would have been impossible for me to fulfill my study during the last seven years. I also want to express my sincere thanks to all my friends at Stony Brook, all professors and fellow students in the Department of Biochemistry of Cell Biology.

Chapter 1. Introduction

1.1 Amyloid Precursor Protein (APP)

1.1.1 Biology of APP

Alzheimer's disease (AD) is the most common form of dementia and neuron degeneration in the elderly nowadays. An estimated 5.4 million of all Americans have AD in 2012. The disease is characterized by two pathogenic hallmarks, deposition of extracellular amyloid β peptides (Aβ), and the intracellular accumulation of twisted highly phosphorylated tau proteins. The proteins result in damage to neuronal cells and inflammation of microglials. The center of amyloid cascade hypothesis is the overload of toxic Aβ peptides originating from the imbalance of its clearance and production. Aβ

peptides are generated by the two-step sequential cleavage at juxtamembrane and transmembrane (TM) domain of APP by β-secretase and then γ-secretase within TM helices. APP is a type I transmembrane protein, containing a bulky extracellular domain (ECD) and a short intracellular (IC) tail. Three isoforms of APP are biosynthesized by alternatively splicing. Overexpression of APP770 and APP751 are ubiquitous in a spectrum of different cell types. APP695, the shorter isoform with the alternative splicing at Kunitz protease inhibitor (KPI) domain, is the most abundant in neuronal cells.

Despite being overexpressed ubiquitously in different cell types, APP-gene knockout experiments suggest that the existence of APP is not essential to cell survival. One explanation is the existence of other homologous proteins, e.g. APLP-1 (APP-like protein 1) that share APP function. However, APP is the one protein containing the full Aβ sequence. Although much more attention has been put on its role of generating the toxic Aβ peptides, several cellular functions have been proposed for APP. The N-terminus of APP (e.g. sαAPP) has been proposed to function as a membrane receptor involved in neutrite growth, neuronal adhesion, Ca^{+2} homeostasis, apoptosis pathway (e.g. P31 peptide) [(1)] and synaptic plasticity, while C-terminal fragments (AICD, amyloid intracellular domain) are believed to regulate the downstream transcription of specific genes in the nucleus complexed with Fe65 [(2)] (see Figure 1-1).

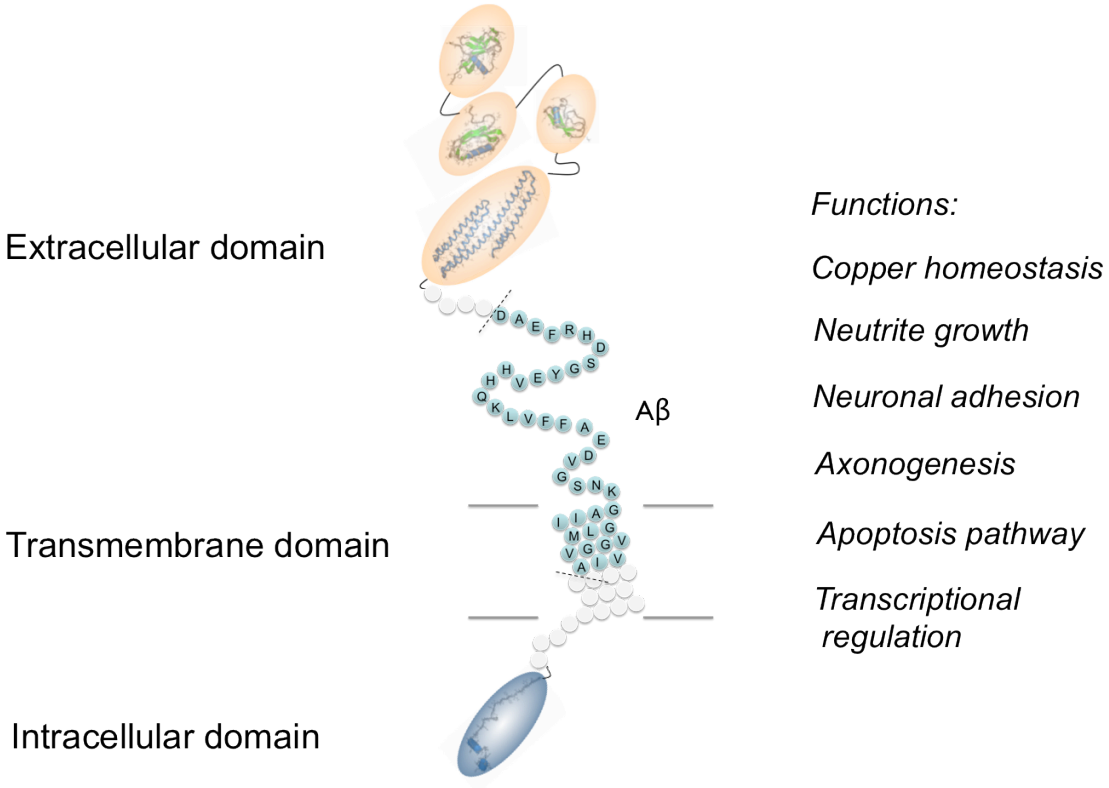

Figure 1-1. Structure domains and functions of APP. The structure domains are made derived from coordinates deposited in the PDB and the black letters in circle is the Aβ sequence.

1.1.2 Trafficking of APP

The biosynthesis and trafficking of APP is of particular of interest, since these cellular events can influence the secretion of Aβ peptides from APP[3]. The overexpression of APP is ubiquitous across different cell types. In non-polarized cells, several post-translational modifications occur during the transit of freshly biosynthesized APP from the nucleus to the plasma membrane. About 90 % of APP is post-transnationally modified by N-, O-glycosylation, phosphorylation or tyrosine sulphation on the EC or IC domain and localized in the Golgi apparatus and trans Golgi network (TGN) at steady state. Only ~ 10% of nascent APP can be trafficked to the plasma membranes but rapidly internalized through the endocytosis pathway because of the internalization sequence of YENPTY (APP 682-687 in the APP695 isoform numbering). In neuronal cells, the trafficking and distribution of synthesized APP from endoplasmic reticulum (ER) are highly polarized in soma (cell body), axons and dendrites where distinct sets of lipid or protein molecules can regulate the trafficking and processing. In neuronal cells, the trafficking of APP from ER to Golgi apparatus and trans Golgi network (TGN) is similar to the case in non-polarized cells and the neuronal soma. The route to axons and dendrites is transmitted through post-Golgi transport vesicles. (i.e. APP delivery to axons uses the axonal fast transport system where kinesin-1 serves as a micro tubular motor protein with a unidirectional movement. Retrograde transportation is also observed with slightly slower kinetics by Kaether et *al.,* 2000.

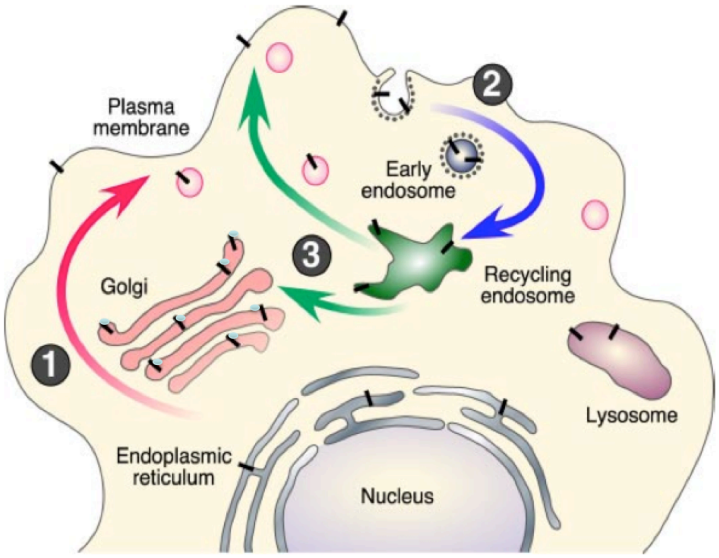

Figure 1-2. **Secretion and intracellular trafficking of APP in non-polarized cells.** In step 1, newly biosynthesized APP (shown in a black bar) is secretory to the plasma membrane through ER and Golgi. Most of the APP are post-translationally modified and kept in the Golgi apparatus (**1**)(shown in a black bar with light blue circles). About 10 % of nascent APP is transited to the plasma membrane and rapidly internalized through the endocytosis pathway where the β–cleavage occurs (**2**), or through the recycling organelles to the cell surfaces (**3**). The illustration is adapted and modified from the review article [(3)].

1.1.3 APP degradation and Aβ secretion in the non- amyloidogenic and amyloidogenic pathway

Other than the generation of Aβ from the metabolism with β- and γ-secretase, several degradation pathways have been found, i.e. FBL-2 (F-box and leucine rich repeat protein 2) binding in the C-terminus of APP can promote the ubiquitination-dependent degradation and the inhibition of endocytosis where Aβ are generated [(4)] and HtrA2, a stress-responsive chaperone-protease which acts as a binding protein to the N-terminal cysteine rich domain of APP, regulates ER-associated degradation via the proteasome degradation pathway. The processing of APP via the endocytosis pathway has been classified as non-amyloidogenic or amyloidogenic pathway depending on the generation of amyloid Aβ peptides. In the non-amyloidogenic pathway, APP is first cleaved at K16/L17 by α–secretase in plasma membranes, which releases a soluble fragment, called soluble α APP (sαAPP) and C-terminal fragment (α-CTF, or called C83). Shorter, non-amyloidogenic Aβ, 17-42 or 17-40 species (P3 fragments), are generated from the cleavage of α-CTF by γ–secretase with the fact that the α-CTF serves as a γ–secretase inhibitor by blocking the secretion of Aβ40 or Aβ42 [(5)]. In the amyloidogenic pathway, APP is cleaved at the β-cut site (Met596-Asp597, Asp597 corresponding to the Asp1 in the Aβ numbering) by β-secretase (BACE-1 or -2). The cleavage also releases an extracellular soluble fragment, call soluble β APP (sβAPP) and β-CTF (or also called C99) in bilayers. Aβ peptides (38, 40 and 42) are released from β-CTF peptides after intramembranous cleavage by γ–secretase complex (see Figure 1-3). BACE1 is the first enzyme catalyzing the β-site cleavage. The overexpression of BACE-1 can enhance Aβ production, while the knockout BACE-1 and -2 can completely block Aβ generation [(6)].

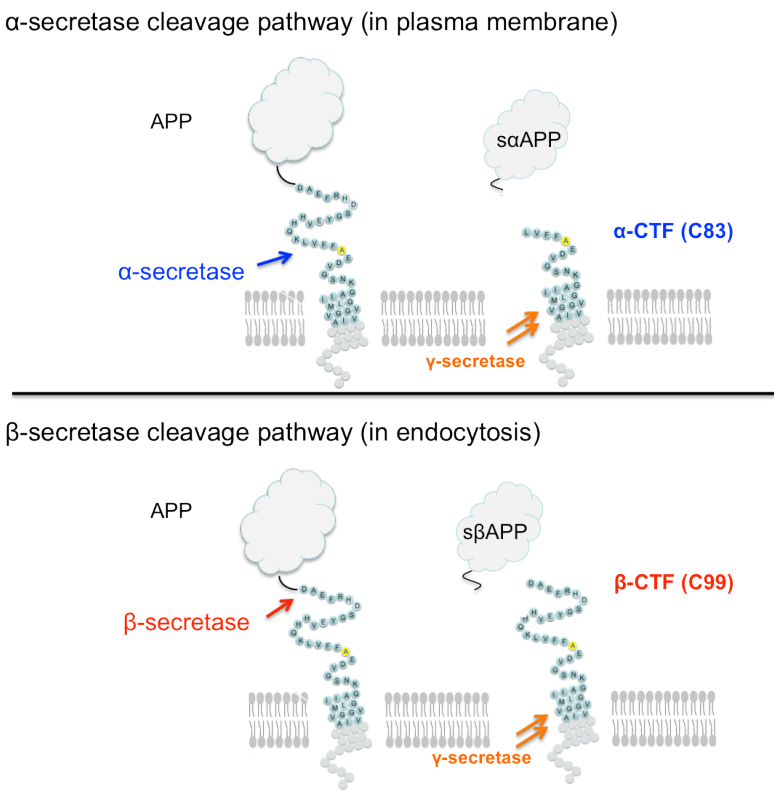

Figure 1-3. Processing of APP and Aβ secretion. Processing of APP is a two-step sequential cleavage. Depending on the Aβ secretion, the processing can be classified as non-amyloidogenic (α–secretase pathway) and non-amyloidogenic (β–secretase pathway).

The γ-secretase complex is composed of several proteins (Presenilin 1/2 (PS1/2), Nicastrin (Nct), Pen2, and Aph1) that are considered to be necessary and sufficient for the enzymatic activity. The catalytic subunit of the γ-secretase complex is Presenilin 1 (or its isoform, Presenilin 2), a nine-TM helix intramembraneous aspartyl protease. The catalytic core contains two aspartic acids residues, Asp257 and Asp385 in TM helix 6 and 7, respectively that catalyze that cleavage of multiple peptide bonds stretching from the middle of TM helix of β-CTF to the intracellular side of the TM helix [(7)]. Aβ peptides with different lengths are resulted from this loose enzymatic specificity. Two major proteolytic fragments are Aβ40 and Aβ42 peptides. Aβ40 peptides are preferentially released and less toxic, while the minor products, Aβ42 peptides are capable of initiating the nucleation of Aβ peptides in vitro and show highly toxic to neurons in vivo [(8)] (see Figure 1-4 below).

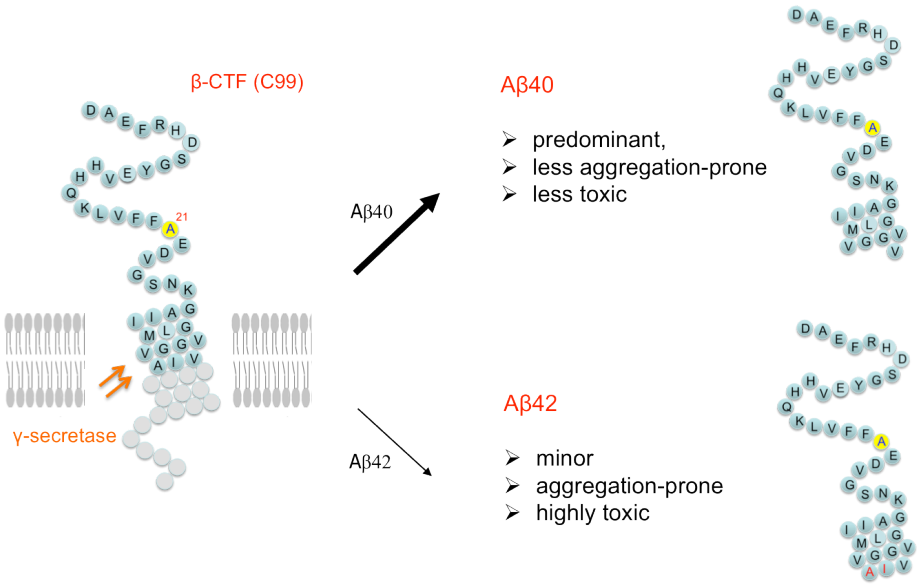

Figure 1-4. The second cut on TM domain is a multiple-site cleavage by the γ-secretase complex. Aβ 1-38, 1-40 and 1-42 peptides are three major cleavage products. Aβ1-40 and 1-42 productions are shown here.

During the sequential processing, several fragments are sequentially produced. C99 (or referred as β-CTF), C-terminal 99 residues, containing the full length of Aβ peptides, is residing on the membrane bilayers after the liberation of soluble EC domain by β-secretase (Figure 1-4). C99 is an accessible substrate of the γ-secretase complex and the enzymatic cleavage of C99 will release Aβ peptides into EC space or lumen and liberate amyloid precursor protein intracellular domain (AICD) into the cytosol, which has been suggested to mediate the transcriptional signaling in the nucleus by complexing with Fe65 and the histone acetyltransferase, Tip60, or to activate the organization of actin dynamics by regulating some specific gene transcription [(2)].

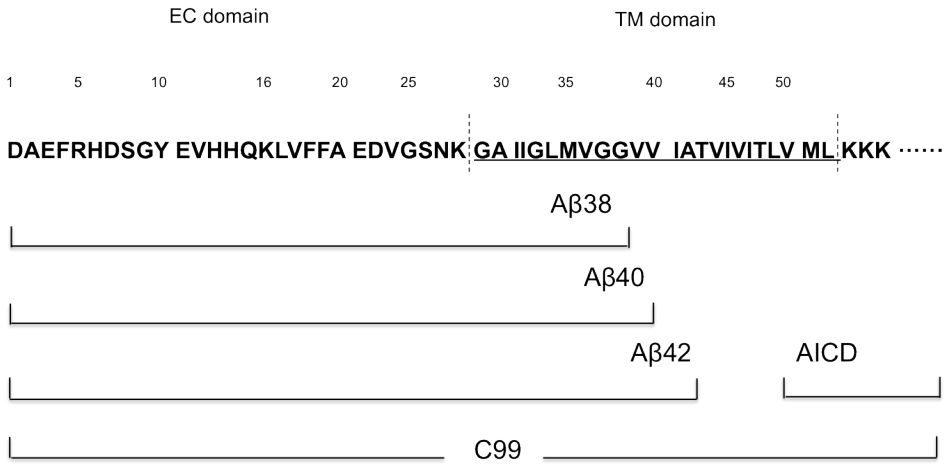

Figure 1-5. APP processing fragments. Different-length cleavage products during secretase proteolysis are shown.

The detection of Aβ peptides and AICD was used to identify the APP intramembraneous proteolytic processing by the γ-secretase complex. Since the secretion of Aβ peptides has been identified from the regular metabolism processing of APP in cells, it was first proposed that two distinct proteases or a single enzyme could process the γ-cleavage with loose specificity. In one model, the lack of correlation between AICD and Aβ peptides production was used to propose that multiple-site cleavages might be associated with two distinct enzymes [9, 10]. In disagreement with the first model, a lack of detection of a longer form of AICD has raised the possibility of progressive cleavage [11, 12]. More recently, the detection of equal molar of Aβ peptides and AICD production by the immunoblotting has further supported to build up the progressive model by a single enzyme [12, 13], the γ-secretase complex, where the ε-site cleavage is first to be processed near the boundary of TM and JM domain, while the following cleavages are carried out every three residues till the release of Aβ40 or 42 into EC space or lumen. Additional evidence supporting this model is the identification of the intermediates, Aβ46 peptides, during the processing by analytical MASS spectroscopy and western blotting with length-dependent antibodies [14] Importantly, the suppression of Aβ40 can lead to the accumulation of this longer peptide regardless of Aβ42 secretion where two distinct cleavage pathway for Aβ40 (i.e. Aβ49 - Aβ46 - Aβ43 - Aβ40) and Aβ42 (i.e. Aβ48 - Aβ45- Aβ42- Aβ38) have been proposed [15-17] . Longer Aβ peptides are successively processed till TM region is not long enough to reside in the catalytic cavity and eventually partitions out of the membrane. An alternative explanation is the loose specificity caused by the adjustment of TM position in the membrane bilayer, in which the thickness of bilayers varies in different subcellular locations [18].

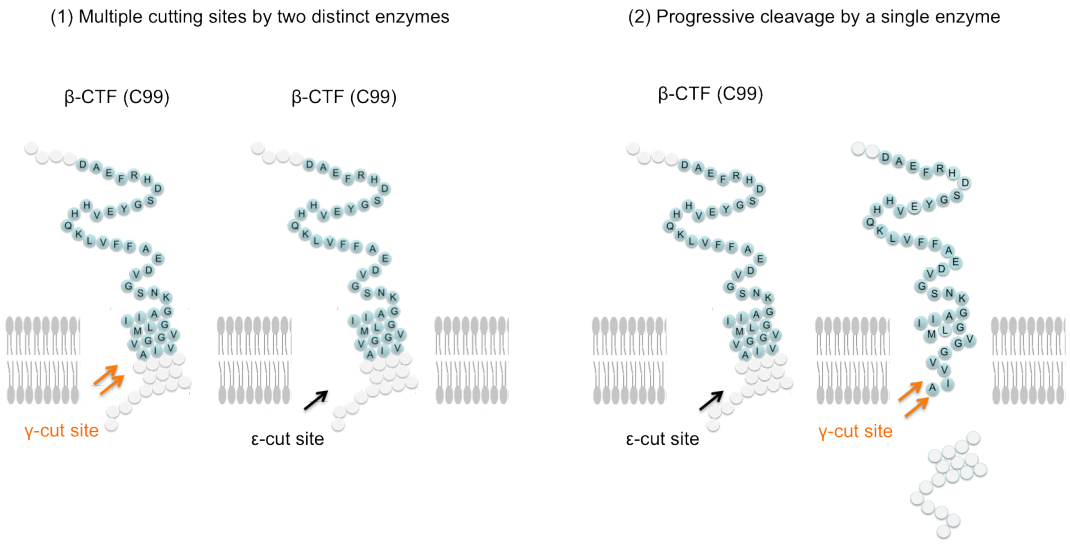

Figure 1-6. Two proposed cleavage models. In multiple-site cleavage by two distinct enzyme model (1), different length Aβ peptides are released by two different enzyme cleavage. In progressive cleavage by single enzyme model (2), different length Aβ peptides are released from sequential cleavage by single enzyme.

1.2 TM domains mediate the homodimer formation of β-CTF

The TM segment of β-CTF is unusual in containing three consecutive GxxxG motifs in the N-terminal sequence and a GxxxA motif about halfway of TM domain, which both are well known for mediating TM dimerization in bilayers. Several *in vivo*, or *in vitro* studies have targeted this motif, and found that mutations alter the Aβ secretion [19-24]. The fluorescence resonance energy transfer (FRET) experiments by Munter *et al*. showed that wild-type APP labeled with YFP and CFP can co-localize in the membrane of living cells of SH-SY5Y cells and the mutations on G29A and G33A can impair the TM dimerization leading to reduced Aβ42 production [23]. The studies of chemical-induced dimerization by Eggert *et al.* also show that induced dimerization of APP or β-CTF can reduce the total Aβ production without changing the Aβ42/Aβ40 ratio [22]. Additionally, biophysical studies by Gorman *et al* showed that the TM domain of APP can form homodimer in micelles or lipid bilayers and suggested that the dimer-to-monomer transition of APP TM peptide upon familial mutation below the GxxxG motifs causes higher Aβ42/Aβ40 ratio [25]. Our structure studies further identified three consecutive GxxxG motifs can mediate the dimerization of TM domain in bilayers, but not the GxxxA motif that is comparable to the TM interface in Glycophorin right-handed homodimer structures can not (see Figure 1-7 below). Taken together, structure studies and mutation studies all point to a model in which the dimerization can affect the APP processing, although how the TM dimerization influences the cleavage by γ–secretase is not conclusive. The other distinct feature of the APP TM sequence is the cluster of β–branched amino acids (Thr, Val and Ile) in the C-terminus right below the γ-cut site releasing the Aβ42 peptides. The bulky and steric side chains of β–branched amino acids

are known to destabilize the typical α–helix. Several familial mutations found at this four-residue cluster (Thr43-Val44-Ile45-Val46) can influence Aβ secretion.

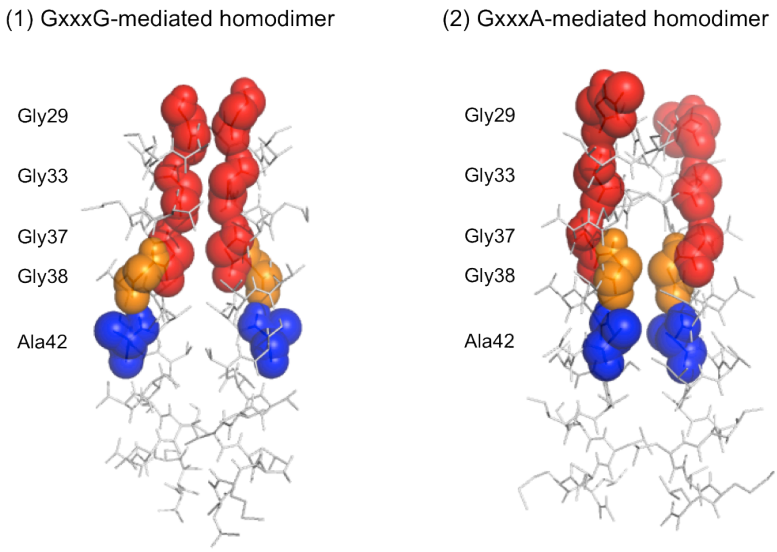

Figure 1-7. Two potential homodimer structures. Two low energy structures are generated from CHI simulation with GxxxG and GxxxA dimeric interface (see the detail in the Chapter 2 and Chapter3).

1.3 Extracellular domains of β-CTF regulates the Aβ production

Unlike the mutations within TM sequence that can directly influence the catalytic core of the enzyme, several allosteric sites on the γ–secretase complex have been identified as the drug target binding sites to modulate the cleavage of Aβ peptides from β-CTF. Recently, several familial mutations on the EC sequence have been verified to influence the APP processing allosterically, Aβ aggregation or neuronal toxicity. The studies by Tian *et al.* showed that the extracellular sequence from Leu17 to Asp23 including the hydrophobic core of Leu17-Val18-Phe19-Phe20 sequence that mediates the formation of Aβ oligomers and fibrils, and a tri-residue mutational cluster at Ala21-Glu-22-Asp23, influence production of Aβ peptides cleaved from β-CTF. Deletion of this seven-residue sequence promotes the secretion of total Aβ peptides by increasing the activity of γ-secretase, suggesting that in the wild-type protein it functions as an inhibitory domain [(26)]. Furthermore, the mutation at Ala21 to Gly but not at Glu22 and Asp23 can disrupt this inhibitory domain without changing the upstream hydrophobic sequence of Leu17-Val18-Phe19-Phe20.

1.4 Familial and artificial mutations in APP sequence

Aβ38, 40, and 42, are most abundant secreted peptides from β-CTF generated by the γ-cleavage [(27) (8)]. There are at least three clusters of FAD mutations in APP that are located close to the α, β and γ-cleavage sites, which may influence the proteolytic processing to favor increased total, or Aβ42/Aβ40 production. The first cluster is located near the position of the β-secretase cleavage site at Met596-Asp597. (The substrate numbering is based on the APP695 isoform of APP. Asp597 corresponds to the first

residue (i.e. Asp1) of the β-CTF. In the following, we use the β-CTF numbering, which coincides with the numbering of the Aβ peptides.) Several of the mutations within the first cluster can increase cleavage by β-secretase [28, 29], and engineered mutations within this cluster are widely used to enhance the secretion of Aβ from APP [30]. The second cluster is between the γ-cleavage site (Ala42) that releases the Aβ42 peptide and the cytoplasmic end of the TM domain. Familial mutations within the third cluster increase the ratio of Aβ42/ Aβ40 [31], which has been found to be correlated with the onset age of AD [32] (in Figure 1-8).

The third cluster is located near the α-secretase cleavage site at Lys16-Leu17. The Lys16Asn mutation is right on top of the cleavage site, and increases the production of Aβ peptides preferentially with higher concentration of β-CTF. The single mutations at three consecutive amino acids, Ala21, Glu22 and Asp23, right after the hydrophobic sequence of Leu17 to Phe20, have very different influence on the APP processing [33]. The site of the A21G Flemish mutation [34] is adjacent to the E22Q (Dutch), E22G (Arctic), E22K (Italian), and D23N (Iowa) mutations [35-37]. The A21G mutation increases Aβ production [26] but not via a change in α-secretase cleavage, whereas the mutations at Glu22 generally decrease total secreted Aβ peptides [26, 33, 38]. The E22Q [35, 39] and D23N [37, 40] are associated with cerebral amyloid angiopathy (CAA), but are not associated with an increase in Aβ secretion [40]. We are interested in how the simple alanine to glycine mutation at position 21, which is midway between the β and γ cleavage sites, can have such a dramatic influence on APP processing.

Several residues surrounding the A21G mutation that have not been implicated in early-onset AD are found to influence APP processing. Tian *et al.* [26] suggested that the L17-V18-F19-F20-A21 sequence is part of an inhibitory motif that modulates γ-secretase processing. Upon deletion of this motif, the catalytic efficiency of γ-secretase increases 42-fold compared to the full-length β-CTF. The A21G mutation can severely impair the inhibitory effect of this region, generating more Aβ species (Aβ38, Aβ40 and Aβ42), implying that the interaction between APP and γ-secretase is altered upon mutation. In contrast, mutations in the G25-S26-N27-K28 region, which is a few residues C terminal to position 21, have the opposite effect. Ren *et al.* [41] found that mutations at Ser26 and Lys28 reduce secreted Aβ without a corresponding loss of the AICD cleavage product.

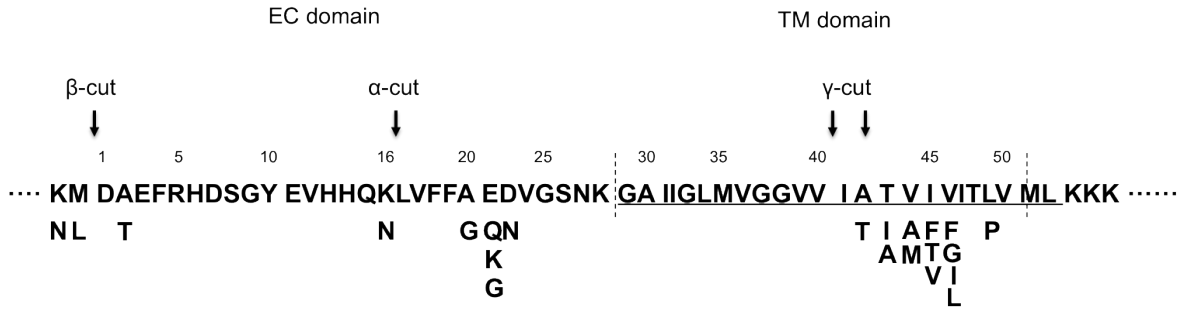

Figure 1-8. The diagram of familial mutations on APP. Three clusters of mutations on APP are shown corresponding to the α-, β- and γ-secretase cleavage site.

1.5 Structure of Presenilin / SPP homologue (PSH) and proposed molecular mechanism for the processing of APP

The γ-secretase complex has a diverse set of type I membrane protein substrates (a single-pass TM helix with N-terminus in the extracellular space versus C-terminus in the cytoplasm). Notch, Cd44, ErbB4, and E-cadherin are cleaved by the γ-secretase in vivo. These substrates are all cleaved near the intracellular TM-JM boundary. However, like APP, Notch, and Cd44 are also cleaved in the middle of the TM domain, although their sequences are not conserved.

The γ-secretase complex composed of Presenilin 1/2 (PS1/2), Nicastrin (Nct), Pen2, and Aph1 has been thought to be necessary and sufficient for its full enzymatic activity. Nicastrin, and Aph1 help the stabilization of enzyme. Pen2, a two-helix transmembrane protein is required for the maturation of enzymatic activity. The catalytic subunit of the γ-secretase complex is Presenilin 1/2, a nine-helix intramembraneous aspartyl protease. The catalytic aspartyl core containing two aspartic acids, Asp257 in TM helix 6 and Asp385 in helix 7 performed the multiple scissions of peptide bonds spanning from C-terminus to the middle of TM helix of APP [(7)]. Several familial mutations near the TM6 and TM7 have been found to influence the processing of its substrate. For instance, G384A can promote the production of Aβ42 [(16)].

Only fragments of Presenilin structures have been reported. No atomic resolution full structure of γ–secretase complex has been resolved. However, several studies have targeted to elucidate the intramembranous mechanism of Presenilin 1/2 by looking at its homologous protein. Similar to the other aspartyl protease, like pepsins, the proteolytic

reaction need water molecules accessible to the enzymatic core and two catalytical aspartic acids lie within hydrogen-bonding distance. The structure study of homologous Presenilin family by Xiaochun Li *et al.* in 2012 that shares a 53% sequence similarity with Presenilin shows two distinct structure features, i) a hydrophobic hole surrounding by TM2/TM3/TM5/TM7 allowing a potential tunnel for ion passage, lipid binding or other regulatory protein binding and ii) a large solvent accessible cavity in facing the cytoplasm where two catalytic aspartic acids reside (the homology modeling of PS1 based on PSH structures in Figure 1-9). The structure feature is consistent with precious cryoEM structure with potential water accessible space. The studies also showed that the two catalytic aspartic acids in Helix 6 and Helix 7 are in distance of 6.7 Å, more than two times distance of hydrogen bonds that implies the induce-to-fit mechanism upon the binding of substrate to the enzyme. The organization of TM helices presents a plausible explanation of how the hydrophobic substrates enter into the hydrophilic catalytic environment that is maintained or packed by hydrophobic helices and segregated from membrane bilayers. Two potential routes via the space between TM6 and TM9 or TM6 and TM2 are proposed to involve in the substrate entry. Several lines of experiments support the first possibility, e.g. TM9 is directly involved in the substrate binding by photo-affinity labeling results. In contrast, the entry between TM6 and TM2 is hindered by the bulky residues of Trp161 in TM6 and Met216/Met223 in TM7 in the lateral passage. The structure studies provides a molecular mechanism where the β–CTF substrate can be accommodated and processed. However, how the abnormal secretion of Aβ peptides (i.e. increased total secretion or Aβ42/ Aβ 40 ratio) upon mutation occurs is still elusive and can attribute to the structure change of substrates or the alteration of substrate-to-enzyme

interaction.

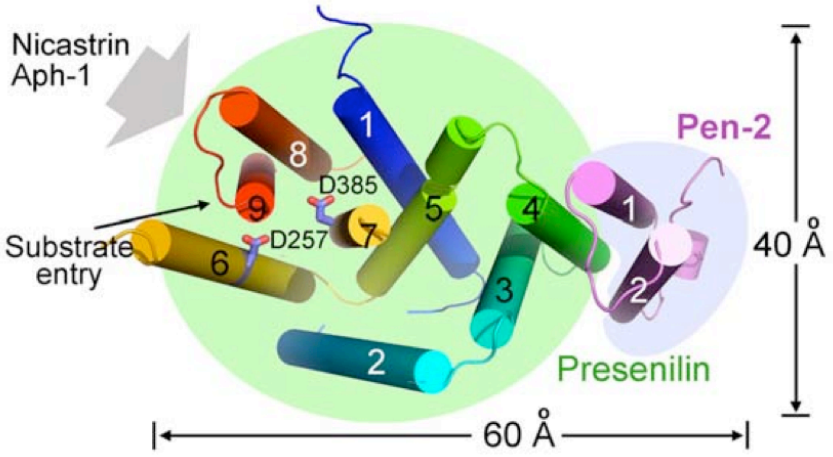

Figure 1-9. The proposed orientation for the γ–secretase complex. The two TM helices in Pen-2 interact with TM4 of PS1, whereas both NCT and Aph-1 were reported to bind the CTF of PS1. (The picture is adapted from Xiaochun Li *et al*.)

1.6 Cholesterol and the processing of APP

Both familial mutations and environmental factors are known to influence Aβ processing by γ-secretase. For example, a higher concentration of serum cholesterol has been statically observed in AD patients as risk factor for Alzheimer's disease [42]. The hypercholesterolemia leads to increase more Aβ deposition, and intraneuronal accumulation of toxic Aβ oligomers on transgenic mice [43, 44]. Many cellular factors appear to influence the overall level of secreted Aβ peptides and the Aβ42/ Aβ40 ratio. The presence of cholesterol and cholesterol-rich domains is linked to β-secretase, γ-secretase activity and the level of secreted Aβ [45]. Depletion of cholesterol inhibits γ-secretase and Aβ secretion, while addition of cholesterol enhances γ-secretase activity [46, 47]. Using γ-secretase functionally reconstituted into proteoliposomes, Selkoe and coworkers [48] found that the optimal cholesterol concentration for Aβ42 production was the same as that for Aβ40. This observation implies that cholesterol does not influence the Aβ42/ Aβ40 ratio, but rather the overall level of secreted Aβ peptide.

1.7 Summary and objectives

The intramembranous cleavage by γ–secretase is unusual on the multiple-site cuts releasing Aβ peptides with 38-42 residue in length. Early-onset AD familial mutations can influence the production of Aβ peptides. In this thesis, I have focused on two sites on the APP protein where FAD mutations are clustered.

The first cluster is in the extracellular domain of the protein close to the TM boundary. The A21G (Flemish), E22Q (Dutch), E22G (Arctic), E22K (Italian), and D23N

(Iowa) mutations are at the positions that link the extracellular (EC) hydrophobic residues of L17-V18-F19-F20 and TM domain and have very different effects on APP processing. I have focused on the A21G mutation, which increases the Aβ secretion by more than 3-fold from APP.

The second cluster is within the TM domain, below the position of Ala42, the γ-secretase cut site that releases the Aβ42 peptides. A stretch of four β -branched amino acids when mutated individually increases the Aβ42/Aβ40 ratio. I have focused on the T43I mutation, which increases the Aβ42/Aβ40 ratio by 8-fold.

Chapter 2. Materials and Methods

We mainly use the biophysical methods to study the structures of N-terminal EC and TM domain of the amyloid precursor proteins in bilayer systems. We intend to correlate the structural variation of wild-type and mutant β-CTF to the processing event, e.g. the production of Aβ42 and Aβ40 peptide, and the Aβ42/40 ratio upon familial AD or non-genetic mutations on EC and TM sequence.

2.1 Lipids, detergents, and amino acids

Dimyristoylphosphocholine (DMPC), dimyristoylphospho-glycerol (DMPG), 1,2-dihexanoyl-*sn*-glycero-3-phosphocholine (DHPC), 1-myristoyl-2-hydroxy-*sn*-glycero-3-phosphate (sodium salt) (LMPG), octyl-β-glucoside (β-OG), 1-palmitoyl,2-oleoyl-

phosphocholine (POPC), 1-palmitoyl-2-oleoyl-*sn*-glycero-3-phospho-L-serine (POPS) and Cholesterol were obtained from Avanti Polar Lipids (Alabaster, AL). ^{13}C and ^{15}N-labeled amino acids were purchased from Cambridge Isotope Laboratories (Andover, MA).

2.2 Synthetic APP TM and JM (juxtamembrane) peptides

2.2.1 Peptide synthesis

Synthetic peptides corresponding to the juxtamembrane and transmembrane domain of the amyloid precursor protein were synthesized by the solid-phase methods at the Keck Biotechnology Resource Laboratory in Yale University (for C55 peptides corresponding to the TM and JM regions of APP, residues 1-55 in the Aβ sequence numbering) or at the Institute for Protein Research, Osaka University (C43 peptides, residues 22-65 in the Aβ sequence numbering). The purity was confirmed with MALDI mass spectrometry and analytical reverse phase HPLC. The synthesized peptides incorporated with ^{13}C labeled amino acids on the sequence for APP TM peptides and C55 are listed below.

A) Selectively labeled APP-TM wild-type peptides for the Glycine-rich region and β-branched amino acid regions:
1) APP TM peptide: EDVGSNKGAIIG(2-13C)LMVGGVVIATVIVITLV(1-13C)ML KKKQYTSIHHGV
2) APP TM peptide: EDVGSNKGAIIG(1-13C)LMVGGVVIATV(U-13C)IVITLVMLK KKQYTSIH HGV
3) APP TM peptide: EDVGSNKGAIIGLMVG(1-13C)GVV(U-13C)IATVIV ITL(2H) VMLKKKQYTSIHHGV
4) APP TM peptide: EDVGSNKGAIIGLMVG(2-13C)GVVIATVI(U-13C)VITLVML(2H)KK KQYTSIHHGV
5) APP TM peptide: EDVGSNKGAIIGL(2H)MVGG(1-13C)VVI(U-13C)ATVIVITL VMLKK KQYTSIHHGV

6) APP TM peptide: EDVGSNKGAIIGLM(2H)VGG(2-13C)VVIA(3-13C)TVIVITLV MLKK KQYTSIHHGV
7) APP TM peptide: EDVGSNKGAIIGLMVGG(2-13C)VVIA(1-13C)TVIVITLVMLK KKQY TSIHHGV

(B) Selectively labeled wild-type APP-TM peptides for the TM-JM boundary:
8) APP TM peptide: EDVGSNKGAIIGLMVGGVVIATVIVITL(1-13C)VMLKKKQYT SIHHGV
9) APP TM peptide: EDVGSNKGAIIG(2-13C)LMVGGVVIATVIVITLV(1-13C)MLK KKQY TSIHHGV
10) APP TM peptide: EDVGSNKG(2-13C)AIIGLMVGGVVIATVIVITLVM(1-13C)LK KKQ YTSIHHGV
11) APP TM peptide: EDVGSNKGAIIGLMVGGVVIATVIVITLVML(1-13C)KKKQY TSI HHGV

(C) Selectively labeled APP-TM T43I mutant peptides:
12) APP TM peptide: RREPPEDVGSNKGAIIGLM(2H)VG(1-13C)GVVIATV(U-13C)IVITLVMLKKKQYTSIHHGV
13) APP TM peptide: RRWPPEDVGSNKGAIIGLM(2H)VG(2-13C)GVVIA(U-13C)TVI(U-13C)VITL VMLKKKQYTSIHHGV
14) APP TM peptide: EDVGSNKGAIIGLMVGGVVIAIVIV(U-13C)ITLVM(U-13C)LKKKQYTSIHHGV
15) APP TM peptide: EDVGSNKGAIIGLMVGGVVIAIVIVI(U-13C)TLVML(U-13C)KKKQYTSIHHGV
16) APP TM peptide: EDVGSNKGAIIGLMVGGVVIAIVIVITL(U-13C)V(U-13C) MLKKKQYTSIHHGV

(D) Selectively labeled C55 peptides for the intrahelical contact (G25xxxG29):
17) APP TM peptide (wild-type): DAEFRHDSGYEVHHQKL(1,2-Leu)VFFAEDVG(1-13C Gly)S N KG(2-13C Gly)A(U-13C Ala) IIGLMVGGV VIATVIVITLVMLKKK
18) APP TM peptide (Flemish): DAEFRHDSGYEVHHQKL(1,2-Leu)VFFGEDVG(1-13C Gly) SNKG(2-13C Gly)A(U-13C Ala) IIGLMVGGV VIATVIVITLVMLKKK

(E) Selectively labeled C55 peptides for the dimeric interface (G33xxxG or GxxxA42) and TM regions:
19) APP TM peptide (wild-type): DAEFRHDSGYEVHHQKLVFFAEDVGSNKGA I(1-13C) IG(1-13C)LMVGGV VIA(3-13C)TVIVITLVMLKKK
20) APP TM peptide (wild-type): DAEFRHDSGYEVHHQKLVFFAEDVGSNKGAI IG(2-13C)LMVGGV VIA(1-13C)TVIVITLVMLKKK

21) APP TM peptide (Flemish): DAEFRHDSGYEVHHQKLVFFGEDVGSNKGA I(1-13C) IG(1-13C)LMVGGV VIA(3-13C)TVIVITLVMLKKK
22) APP TM peptide (Flemish): DAEFRHDSGYEVHHQKLVFFGEDVGSNKGAI IG(2-13C)LMVGGV VIA(1-13C)TVIVITLVMLKKK

(F) Selectively labeled C55 peptides for the extracellular and TM regions:
22) APP TM peptide (wild-type): DAEFRHDSGYEVHHQKLVF(U-13C,15N)FAEDV(U-13C,15N)G(U-13C,15N)SNKGAIIGLMVGGV VIATVIVITLVMLKKK
23) APP TM peptide (Flemish): DAEFRHDSGYEVHHQKLVF(U-13C,15N)FGEDV(U-13C,15N)G(U-13C,15N)SNKGAII GLMVGGV VIATVIVITLVMLKKK
24) APP TM peptide (wild-type): DAEFRHDSGYEVHHQKLVFF(U-13C,15N) AENVGSNKG(U-13C,15N)AIIGLMVGGV VIATVIVITLVMLKKK
25) APP TM peptide (Flemish): DAEFRHDSGYEVHHQKLVFF(U-13C,15N) GEDVGSNKG(U-13C,15N)AIIGLMVGGV VIATVIVITLVMLKKK
26) APP TM peptide (wild-type): DAEFRHDSGYEVHHQKLV(U-13C,15N)FFA(U-13C,15N)EDVGSNKGAIIGLMVGGV VIATVIVITLVMLKKK
27) APP TM peptide (Flemish): DAEFRHDSGYEVHHQKLV(U-13C,15N)FFG(U-13C,15N)EDVGSNKGAIIGLMVGGV VIATVIVITLVMLKKK

(G) Selectively labeled C55 peptides for Dutch (E22Q) and Iowa (D23N) mutant:
28) Dutch C55 mutant: DAEFRHDSGYEVHHQKLVF(U-13C,15N)FAQDV(U-13C,15N) G(U-13C,15N)SNKG AIIGLMVGGV VIATVIVITLVMLKKK
29) Iowa C55 mutant: DAEFRHDSGYEVHHQKLVF(U-13C,15N)FAENV(U-13C,15N) G(U-13C,15N) SNKG AIIG LMVGGV VIATVIVITLVMLKKK

2.3 Recombinant C55 (N-terminal 55 residue of β-CTF)

2.3.1 Peptide expression in bacteria

The 55 residues containing the full-length Aβ, transmembrane domain and a few residues in the juxtamembrane sequence (KKK) of amyloid precursor protein are subcloned into a pET21a vector with the added N-terminal methionine (start codon), and an attached linker/6 His-tag (KLAAALEHHHHHH) at the end of sequence. The plasmid

harboring target DNA sequences then is transformed into BL21 *E. coli* strain, and plated on Lauria-Bertani broth (LB)/Ampicillin plates. A single colony on the plate is inoculated in 5 ml of LB/Ampicillin medium overnight at 37 °C at 180 rpm ($O.D._{600}$ ~1.8). The cultured medium is spun down at 4 °C, and cells are re-suspended and cultured in 25 ml of sterilized LB medium or M9 minimal medium (40 mM Na_2HPO_4, 20 mM KH_2PO_4, 10 mM NaCl, 0.1% NH_4Cl, 0.2% glucose, and pH 7.0 supplemented with 0.1 mM $CaCl_2$, 1 mM $MgSO_4$, trace elements, and vitamin B) containing Ampicillin (0.1 mg/ml), until the $O.D._{600}$ reaches 0.6. The cultured medium is inoculated to the sterilized 1 L of LB broth medium or (M9 minimal medium) at 37 °C at 180 rpm, until the O.D. reaches ~ 0.8. The cells are induced with 1 mM of isopropyl-thiogalactoside (IPTG) for 16 h at 23 °C at 180 rpm. The induced cells (~1.5 gram) are then spun down at 6,000 g, re-suspended in the 35 ml of ice-cold lysis buffer (75 mM Tris, 300 mM NaCl, 0.2 mM EDTA, and pH 7.8), and passed through a French pressure cell press (SLM AMINCO) twice at 1000 psi. The harvested cells are spun down at 25,000 g, and the pellets containing C55 proteins are subjected to the subsequent purification.

2.3.2 Recombinant peptide purification

The pellets are washed with the 35 ml of lysis buffer, and spun down at 25,000 g for 20 min till the washed solution becomes clear (usually with 3 iterations). The spun-down pellets are dissolved in 35 ml of urea/SDS buffer (20 mM Tris, 150 mM NaCl, 8 M urea, 0.2% SDS, pH 7.8). The pellet is first homogenized with an 18G 11/2 needle to increase the solvent exposed surface, and mixed well overnight (~ 16 hours) at room

temperature until the pellet is dissolved. The dissolved pellets are centrifuged at 25,000 g for another 20 min. The supernatants are pooled with the pre-equilibrium Nickel beads for 2 hours (2.5 ml of resin for 1 gram of cells pellet). The beads are then washed with 8 bed volumes of urea/SDS buffer, 8 bed volumes of SDS rinse buffer (20 mM Tris, 150 mM NaCl, 0.2% SDS, pH 7.8), and 8 bed volumes of detergent-contained Tris-buffered saline buffer (20 mM Tris HCl, 200 mM NaCl, pH 7.8) in a pulsed manner. The proteins are refolded, and eluted with 250 mM imidazole in Tris-buffered saline solution (pH 7.8) containing detergent. The eluted fractions are collected, and checked by SDS-PAGE. The protein concentration is estimated with 280 nm absorbance using an extinction coefficient of 1490 M^{-1} cm^{-1}, after removal of imidazole with an Amicon ultra spin concentrator (3 kDa MWCO). The residual imidazole is checked with the SEC column or solution NMR 1D ^{1}H spectrum. The protein purity was further confirmed with mass spectroscopy (MALDI-TOF).

2.4 Reconstitution of TM and C55 peptides

2.4.1 Reconstitution of C55 peptides in detergent micelles

The C55 peptides were solubilized in detergent, e.g. dodecyl phosphocholine (DPC) or octyl-β-glucoside (β-OG) in hexafluoroisopropanol (HFIP) depending on purposes. The molar ratio of peptide: detergent was 1: 200. The mixture containing C55 peptide was incubated for 3 hours at 27 °C, and then the solvent is removed under a stream of argon gas and then under vacuum overnight. MES buffer (5 mM MES, 50 mM

NaCl, pH 6.2) was added to the solids from the previous step and gently mixed at room temperature for 3 hours.

2.4.2 Reconstitution of peptides in lipid bilayers

The C55 peptides were co-solubilized in DMPC, DMPG, and octyl-β-glucoside in HFIP. The peptide: lipid molar ratio was 1:50. The molar ratio for DMPC: DMPG was 10: 3. (POPC: POPS in 10:3, and POPC: POPS: Cholesterol in 10: 3: 5.2). POPC is abundant in plasma membranes and exhibits a continuous transition from a liquid disordered state to liquid ordered state with the addition of cholesterol [(49)]. The mixture containing C43 peptide was incubated for 3 hours at 37 °C (C55 peptide at 30 °C), and then the solvent is removed under a stream of argon gas and then under vacuum overnight. MES buffer (5 mM MES, 50 mM NaCl, pH 6.2) was added to the solid from the previous step and gently mixed at 30 °C for C55 peptides for 6 h. The octyl-β-glucoside was removed by dialysis [(50)]. The reconstituted membranes (100 μl) were subject to FTIR analysis, and then the samples are pelleted and loaded into NMR rotors.

2.4.3 Reconstitution of C55 into bicelles.

The C55 peptides were eluted from the Ni column and refolded with 16 mM DHPC (Avanti lipids) in the elution buffer as described above. The fractions containing purified protein were collected on the basis of the absorbance at 280 nm. The peptide-to-lipid ratio was 1: 50 in bicelles with different q values (0.25, 0.35, 1.0, and 2.0) by adding proper amounts of lipids in the protein stock solutions. The samples of peptides

reconstituted into bicelles were prepared as described in [51] by several cool-and-thaw cycles until the samples appear clear or homogeneous.

2.5 Polarized attenuated total reflection (ATR) Fourier transformed infrared (FTIR) analysis

ATR FTIR spectra were obtained on a Bruker IFS 66V/S spectrometer with a vacuum system (down to 5 mtorr). ATR-FTIR spectroscopy was used to characterize the global secondary structures, and the orientation of transmembrane domain of C55 in bilayers. The reconstituted peptides in bilayers were layered down on a germanium plate with the incident IR beam at 45°. The laser beam (wavelength at 633 nm) is used to calibrate the distance in the interferometer corresponding to the IR beam. The amide I vibrational frequency (1600 – 1700 cm^{-1}) is sensitive and used to characterize the secondary structures. The amide I frequency between 1650 - 1660 cm^{-1} is characteristic of α-helix, while the amide I frequency between 1640 - 1620 cm^{-1} is characteristic of β-sheet conformation for the non-isotope labeled proteins. The absorbance difference between 90° and 0° of polarized light provides information on the orientation of transmembrane helices relative to the normal of bilayers. The dichroic ratio (I_{90}/I_0) on transmembrane helices is used to calculate the tilt angle, with the value of $\alpha = 41.8°$ based on parallel measurements on bacteriorhodopsin [50]. The dichroic ratio is also used to estimate the reconstitution quality (homogeneity) of TM helix in membrane bilayers.

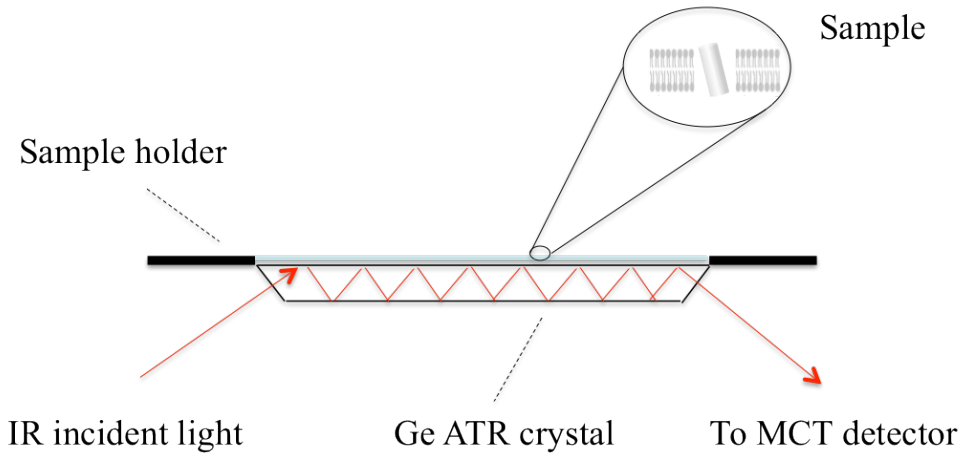

Figure 2-1. The diagram for the ATR plate. Samples are gently layered on the Germanium window, which is an optical element with a high refractive index for total reflection.

2.6 Magic angle spinning (MAS) nuclear magnetic resonance (NMR) spectroscopy

MAS NMR experiments were performed at a ^{1}H frequency of 500 MHz and 600 MHz (or at ^{13}C frequency of 125 MHz and 150 MHz) on a Bruker AVANCE spectrometer. The MAS spinning rate was set to 9-11 KHz ± 10 Hz. The ramped amplitude cross polarization contact time was 2 ms. Two-pulse phase-modulated decoupling was used during the evolution and acquisition periods with the field strength of 80 kHz. Internuclear $^{13}C\ldots^{13}C$ distance constraints were obtained from 2D DARR (dipolar assisted rotational resonance) NMR experiments [52] using a mixing time of 600 ms. The sample temperature was maintained at 198 K ± 2 K.

DARR (Dipolar assisted recoupling resonance)

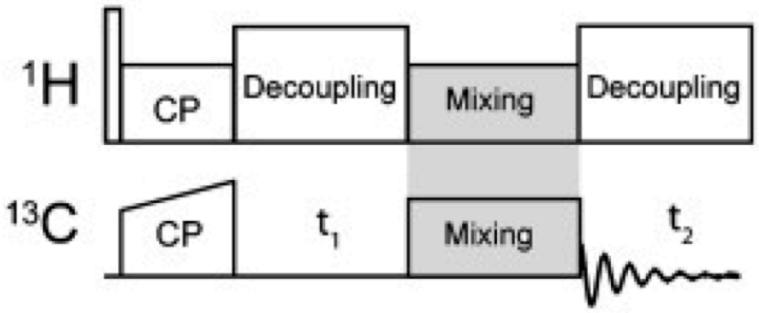

Figure 2-2. The 2D DARR (Dipolar assisted recoupling resonance) pulse sequence used in characterization of dimeric interfaces in APP TM or C55 peptides in bilayers. CP stands for cross polarization. t1 and t2 are time increments for the second and first dimension. Dipolar re-coupling is during mixing time.

2.7 Solution nuclear magnetic resonance (NMR) spectroscopy

2.7.1 TROSY HSQC spectrum of wild-type C55 in different detergent systems (Heteronuclear Single Quantum Coherence)

The recombinant proteins are produced, purified and reconstituted into different detergent systems as described above. The concentration of reconstituted protein is about 0.8 mM based on UV_{280nm} with a distinction coefficient of 1490 M^{-1}. cm^{-1}. The spectrum are collected at 45 degree to increase the molecular tumbling and better resolution. The detergent systems of SDS, DHPC, β-OG and LMPG are screened to optimize the best condition for multi-dimensional experiments. To get backbone chemical shift information (e.g. C=O, Cα and Cβ) of C55 protein in micelles, multi-dimensional NMR experiments are performed. TROSY (transverse-relaxation optimized spectroscopy) type of HNCO, CBCA(CO)NH and CBCANH spectrum are collected and analyzed for the sequential assignment.

2.8 Computational simulations

The CNS Helix Interactions (CHI) simulation protocol is a computational global searching program for determining low-energy conformations of helix-helix interaction with improved packing interactions between helices [(53)]. Computational searches were carried out on the wild-type APP TM (from Gly29 to Leu52) sequences. Input parameters, such as the peptide sequence, the separation between helices, and sampling step size, were initiated, and two canonical helices were generated based on the sequence for calculation. Each helix was rotated relative to one another from 0° to 360° with a sampling step size of

45° at helix separations of 8.5 Å to 10.5 Å to find low energy conformations of helix dimers. Both right-handed and left-handed conformations were searched. The crossing angles and rotations were variable. Energy minimized conformations were first placed on an initial grid. When there were more than five structures with a root mean square deviation of 1 Å or less, these conformations is categorized as a "cluster" and the individual minimized structures in each low energy cluster were averaged and re-minimized. The computational search was done under vacuum conditions (dielectric constant $\varepsilon = 1$) to mimic the low dielectric environment within the hydrophobic core of bilayer membranes.

2.9 Measurement of Aβ secretion from APP, β-CTF (or C99) and C55 in vivo

Secretion of Aβ peptides is measured by MESOSCALE kit (Meso Scale Discovery, Gaithersburg, MD, USA) in Professor Pascal Kienlen-Campard's lab in Institute of Neuroscience in University Catholique de Louvain in Belgium. Aβ production was monitored in the culture media 48 h after transfection in CHO (Chinese Hamster Ovary) cell lines. Briefly, samples were cleared by centrifugation (12,000 *g*, 3 min, 4 °C). The level of APP, the β-CTF, or C55 overexpression is normalized by the method of Western blotting. Aβ38, Aβ40 and Aβ42 secretions were quantified in 25 μl of cellular medium by multiplex ECLIA (Electrochemical Luminescence) to its corresponding anti-Aβ catch antibody. The measurement is carried out according to the manufacturer's instructions for detail, and the schematic illustration is shown in Figure 2-2 (the illustration is adapted from the website of Meso Scale Discovery, Gaithersburg, MD,

USA). Three steps of signal amplification are involved, including electrochemistry ignition step, chemical energy conversion and luminescence light as measured signal. The detection sensitivity and accuracy can be calibrated based on the corresponding purified Aβ peptides, e.g. Aβ38, Aβ40 and Aβ42 and optimized to the range of sub pg /ml for Aβ peptides and the dynamic range is increased to 3-4 logs compared to a normal ELISA (enzyme-linked immunosorbent assay) measurement.

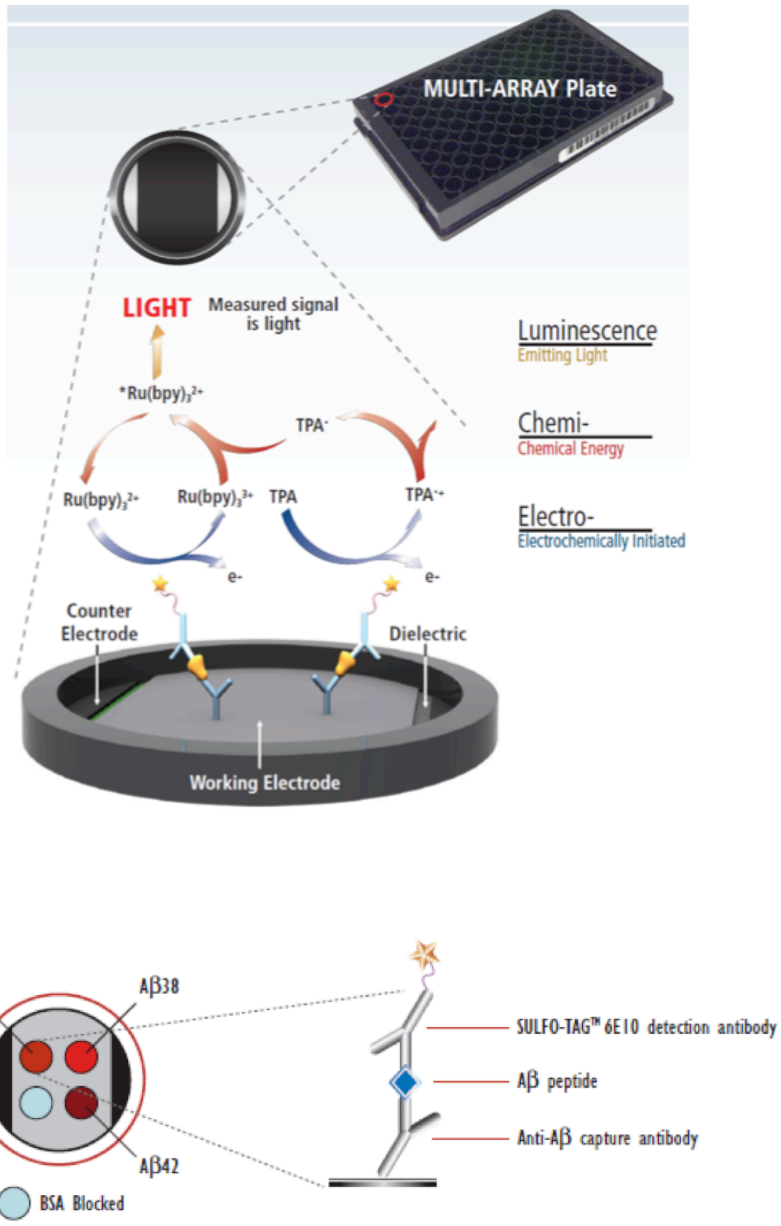

Figure 2-3. Illustration of ECLIA method. The upper panel show the three-step amplification and the lower panel presents that the Aβ peptides recognized by the pre-immobilized anti-Aβ capture antibody on the carbon surface well are conjugated with the SULFO-TAG^{TM} labels, which sequentially initiates the electrochemiluminescence reaction. The measurement by ECLIA provides several advantages, including i) background signals are minimal because the stimulation mechanism (electricity) is decoupled from the signal (light). ii) SULFO-labels are stable, non-radioactive and offer a choice of convenient coupling chemistry. They emit light at ~620 nm, eliminating problems with color quenching. iii) 3x cycles of each label amplify the signal to enhance light levels and improve the sensitivity. (the illustration is adapted from the website of Meso Scale Discovery, Gaithersburg, MD, USA)

Chapter 3 GxxxG motifs mediate the TM dimerization of APP in bilayers

3.1 Introduction

The most unusual feature of APP proteolysis is the intramembraneous cleavage by the aspartyl protease, the γ-secretase complex. Several cleavage sites have been identified that generate different length Aβ peptides from 38-42 residues. The γ-cleavage site cuts the APP sequence in the middle of the TM domain to predominantly produce the Aβ40 peptide, and to a lesser extent the Aβ42 and Aβ38 peptide. Aβ42 has a higher propensity to form aggregates than the shorter isoforms and is the most toxic species generated by γ-site cleavage. There is another cleavage site, referred to as the ε-cleavage site, a few residues downstream between Leu49 and Val50 that has been identified by N-terminal

sequencing of the AICD peptide.

To address the mechanism of intramembranous proteolysis, we focus on the structure of the TM domain of APP in membrane bilayers. Proteolysis requires local unraveling of the helical secondary structure of the TM domain to expose backbone carbonyl carbons for nucleophile attack by polarized water and carboxyl group of two Aspartic acids in the enzyme active cavity. This requirement raises the question of whether there are sequence motifs in the TM domain of APP that destabilize the helical structure in cell membranes in a fashion similar to that proposed for the conserved Asn-Pro sequence in the sterol regulatory element binding protein (SREBP), the substrate of the site-2 protease [(54)].

3.1.1 Two unusual features of the TM sequence of APP

There are 2 unusual features of the TM sequence of APP that have the potential to distort or destabilize local helical secondary structure (see Figure 3-1). The first is the high density of β-branched amino acids surrounding the Aβ40- and Aβ42-cleavage sites. The β-branched amino acids (Val, Thr, and Ile) are known for a high propensity for forming extended β-structure. Sequential β-branched residues can have a destabilizing effect on the secondary structure of TM helices.

Figure 3-1. **Two unusual features on APP TM sequence.** i) High occurrence of glycine residues (in red) in the N-terminus of TM region. ii) High density of β-branched amino acids (Val, Ile and Thr in orange) in the C-terminus of TM sequence.

The second unusual feature in the TM domain of APP is the high occurrence of glycines upstream of the Aβ40- and Aβ42-cleavage sites. Li *et al.* [55] have shown that in the aqueous environment of SDS micelles, glycines in TM domains can promote extended secondary structure. In the APP TM helix, glycines may play a role in helix destabilization, particularly within the context of the γ-secretase complex.

Several of the glycines in the APP TM domain occur in GxxxG motifs. However, rather than destabilizing helical secondary structure, GxxxG motifs within TM sequences are well known to mediate helix dimerization in membrane bilayers. Mutational studies of APP indicate that these GxxxG glycines are important in both dimerization and APP processing. Whereas the mutation of the GxxxG motifs has been shown to significantly decrease the generation of Aβ40, the influence on dimerization is less clear. For example, mutation of Gly29 and Gly33 to isoleucine diminishes the ability of APP to dimerize, whereas mutation of these same residues to leucine leads to SDS-resistant dimers that apparently adopt an interface nonproductive for γ-processing [21]. In contrast, recent studies by Gorman *et al.* [25] have shown using fluorescence energy transfer that peptides corresponding to the TM domain of APP dimerize and proposed that a GxxxA motif, rather than the GxxxG sequences, mediate dimerization. They found that dimerization influences the ratio of Aβ40 to Aβ42 produced by the γ-secretase complex. Consequently, to address the role of the TM sequence in APP processing, not only is it important to establish the secondary structure of APP, but also to determine the helix interface that mediates dimerization.

3.2 Results

3.2.1 TM region of APP is globally helical in membrane bilayers

Glycines and β-branched amino acids both contribute to helix destabilization in soluble proteins [(56)]. As a result, the abundance of these residues within the TM region of APP raises the question of whether the secondary structure is locally unraveled at either the γ- or ε-cut sites. Polarized IR spectroscopy can be used to establish the global secondary structure of peptides reconstituted into membrane bilayers. In Figure 3-2, polarized IR spectra of APP TM JM peptides exhibit an amide I vibration at 1,657 cm^{-1}, a frequency characteristic of α-helical structure (1650 cm^{-1}–1660 cm^{-1}). Deconvolution of the amide I band of APP TM domain reveals only a small shoulder at lower frequency (1,630 cm^{-1}). The dichroic ratio of the amide I band is sensitive to the orientation of the TM helix relative to the plane of membrane. The observed dichroic ratio of 3.46 ± 0.2 corresponds to a helix orientation of 15.5° relative to the membrane normal (see the section 2.6 of Chapter 2 for calculation). The high dichroic ratio, which also provides a way to assess our ability to reconstitute TM peptides in a homogeneous fashion, indicates that the APP TM peptide can be reconstituted into DMPC: DMPG (10:3) bilayers in a stable (non-aggregated) and homogenous helical TM orientation.

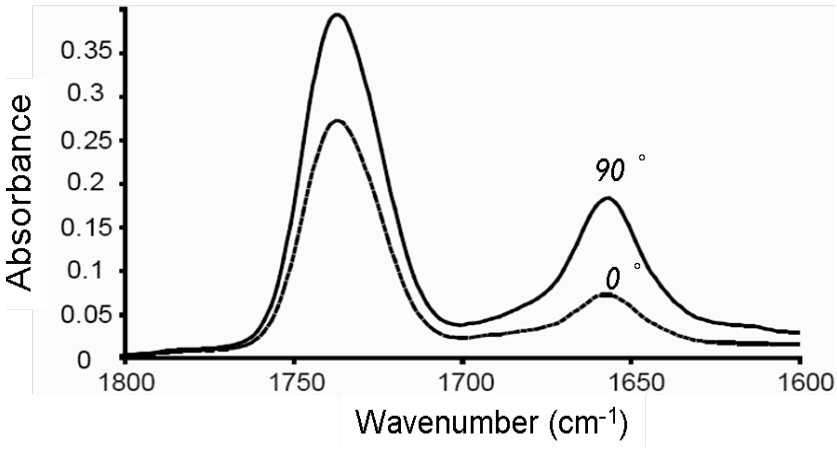

Figure 3-2. **FTIR spectrum of APP TM peptide in DMPC: DMPG bilayers.** The IR absorbance at 1736 cm^{-1} is the stretching frequency of lipid carbonyls. The vibration frequency at 1654 cm-1 is the stretching of helical carbonyls in APP TM peptides. The ratio of integration at 1654 cm^{-1} to 1736 cm^{-1} is approximately equal to 1: 2, and indicates the molar ratio of TM peptides (43 residues) to lipids is 1: 50. The averaged dichroic ratio (the integration ratio of I_{90} to I_0) of 3.46 indicates the TM helical tilt angle of 15.5° relative to the bilayer normal.

3.2.2 Two possible TM homodimer structures in computational searches

The ability of APP to dimerize has been suggested by cross-linking and gel filtration, and more recently by FRET and TOXCAT measurements [57]. On the basis of the helical secondary structure observed for the TM domain of APP, we undertook computational searches of low-energy dimer structures involving the TM domain of APP. The strategy behind these searches is described in the section 2.9 of Chapter 2 in more detailed.

Two clusters of low energy symmetric dimer structures are typically found in the computational searches of APP dimers. The results at a crossing angle of 9.5 Å are presented in Figure 3-3. Similar cluster distribution is observed at a crossing angle of 8.5 Å, 9 Å, 10 Å, and 10.5 Å. The conformations in these two clusters have helices with right-handed crossing angles (shown in black and red circles in the right panel). In the first cluster (cluster 17 in black circle), the GxxxG motifs mediate dimerization. In the second cluster (cluster 22 in red circle), the G37xxxA42 sequence mediates dimerization.

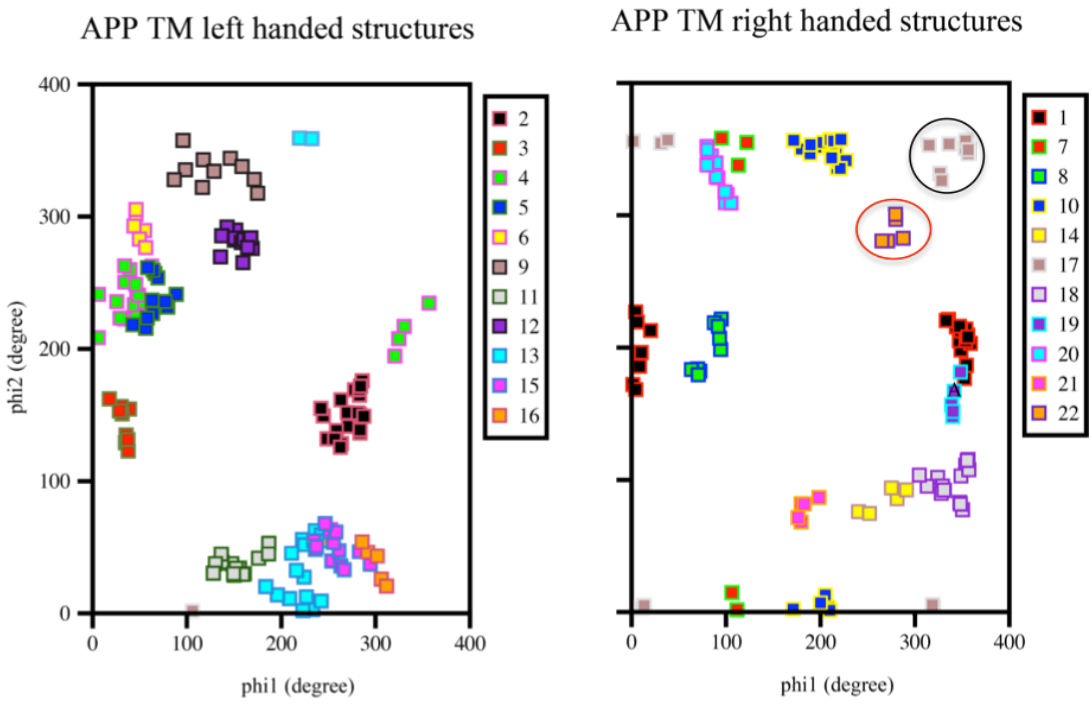

Figure 3-3: CHI searching of APP TM peptide with right handed coiled coil and left handed coiled coil structure. Low energy structures with similar conformations are clustered and shown as possible ensembles.

The energy diagram in figure 3-4 shows that the dimer structures mediated by the GxxxG and GxxxA motifs adopt different interhelical contact in the C-terminus with varied free energy through hydrophobic residues. In the dimer structures mediated by the GxxxG, Ile41, Ile45, Thr48 and Leu52 are potentially located at the inter-helical interface where Thr45 is potentially forming H-bonding. In contrast, Ile41, Ala42, Ile45, Val46 and Leu49 are putative residues in the inter-helical interface in the GxxxA-mediated structures.

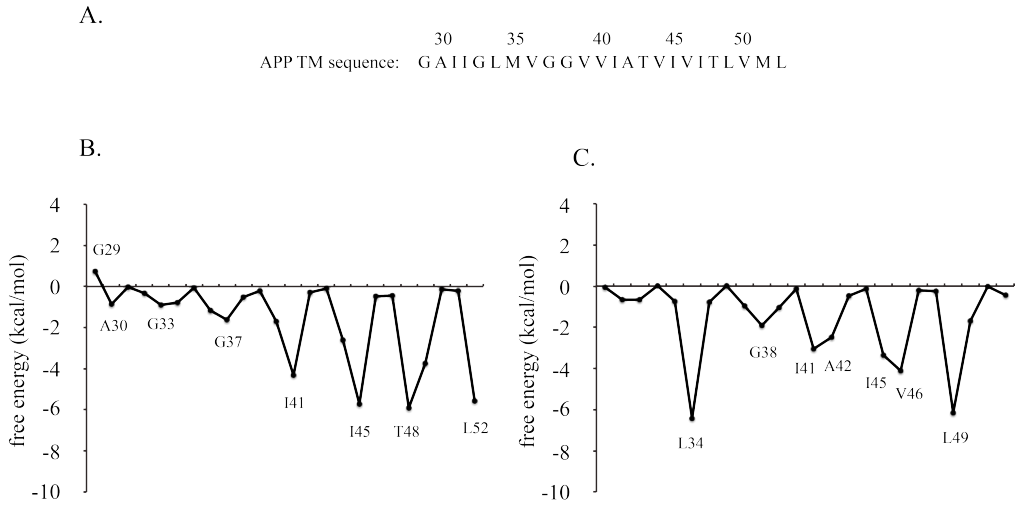

Figure 3-4. **Averaged energy diagram for two low energy clusters of symmetric right-handed structures found in CHI searching.** APP TM sequence used in simulation is shown in panel A. B panel represents the TM homodimer structures mediated by GxxxG motifs. The homo TM dimer structure mediated by GxxxA motif is shown in panel C. Residues involved in the dimeric interface are labeled with the corresponding free energy.

3.2.3 APP TM helix forms homodimers through sequential GxxxG motifs.

To test whether any of the low energy dimer structures seen in the computational studies actually occur in membrane bilayers, namely whether the GxxxG or the GxxxA motifs contact one or another in the APP TM dimer, solid-state NMR experiments were undertaken of the membrane-reconstituted APP TM domain. Figure 3-5 presents the results of NMR measurements between APP TM peptides labeled at Gly33, Gly37 and Gly38 on the putative dimeric interface. Two peptides were synthesized for these experiments; one with ^{13}C=O of Gly and the second with ^{13}Cα of Gly at each of the 3 glycine positions. These resonances have distinct chemical shifts from other amino acids. Two peptides were reconstituted in a 1:1 molar ratio. The observation of a ^{13}Cα…^{13}C=O cross peak (see boxed cross-peak in Figure 3-5) in the 2D dipolar-assisted rotational resonance (DARR) NMR experiment indicates that these carbons are in contact. The observation of a contact is highly significant because it indicates that stable and well-defined APP homodimers are present in our reconstituted samples. The dimers must be in a head-to-head orientation and tight association (i.e., little or no monomer). On the basis of the intensity of the interhelical 13Cα…13C=O contacts observed, we can estimate that >50% of the dimers are associated in a stable uniform structure (at least in the region of glycine contacts).

To verify the translational position of the glycine residues in the dimer and to address the possibility that the GxxxA sequence mediates dimerization, we undertook DARR NMR experiments on APP TM peptides labeled at individual glycines: Gly33,

Gly37, and Gly38. Figure 3-5 A presents the 2D NMR spectrum obtained using APP TM peptides reconstituted as before and separately labeled at position 33 with ^{13}Cα-Gly (peptide 1) and ^{13}C=O Gly (peptide 2). The results show an interhelical cross peak between the Gly33 residues consistent with the packing shown in our GxxxG-mediated dimer structures. In a similar fashion, we observe a cross peak in the 2D DARR NMR spectrum of an equimolar mixture of APP peptides containing either ^{13}Cα and ^{13}C=O Gly at position 37 (Figure 3-4 B). In contrast, DARR NMR spectra (Figure 3-5 C) obtained in a parallel experiment using APP peptides separately labeled at position 38 with ^{13}Cα Gly and ^{13}C=O Gly did not exhibit a Gly - Gly peak.

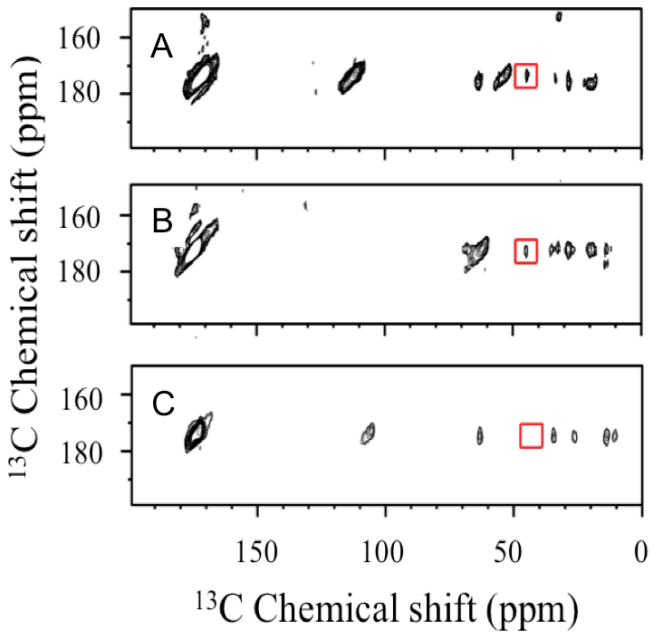

Figure 3-5. 2D DARR ^{13}C spectrum of mixed APP TM peptides labeled with ^{13}Cα-^{13}C glycine and ^{13}C=O-glycine on two peptides. Panel A is the mixed APP TM peptides with ^{13}Cα-Gly33 and ^{13}C=O Gly33. Panel B is the mixed APP TM peptides with ^{13}Cα-Gly37 and ^{13}C=O Gly37. Panel C is the mixed APP TM peptides with ^{13}Cα-Gly38 and ^{13}C=O Gly38 in bilayers (DMPC: DMPG). The comparison shows that only are Gly33 -- Gly33 and Gly37 -- Gly37 cross peaks are observed but not Gly38 -- Gly38 that indicated the dimeric interface of GxxxG motifs is picked up in APP TM peptides.

3.2.4 TM helix of APP breaks at the cytoplasmic membrane surface

The sensitivity of the ^{13}C chemical shifts to secondary structure allows us to determine whether there is a change in the local structure around the ε-cut site (Leu49-Val50). In Figure 3-6, we compare the ^{13}C MAS NMR spectra of APP TM peptides specifically ^{13}C-labeled at Leu49, Val50, Met51, and Leu52. The bold lines correspond to the lipid-reconstituted peptide; dotted lines correspond to lipid alone. The ^{13}C MAS NMR spectrum of Leu49 exhibits 2 resonances at 175.0 and 172.1 ppm, assigned to the backbone ^{13}C = O of Leu49 and the lipid C = O, respectively. The ^{13}C chemical shift indicates that Leu49 is in α-helical secondary structures. Comparison of the Leu49 spectrum with the spectra of Val50, Met51 and Leu52 shows that the peptide carbonyl resonances shift to lower frequency, characteristic of random coil structures.

The above data indicate that there is a break in helical secondary structure near the ε-cut site at the TM-JM boundary. Nicholson and coworkers [(58)] have previously shown that the N-terminal residues of the isolated JM domain of APP are unstructured in solution and suggested that the transient local structure and prolyl cis/trans isomerization induced by phosphorylation at Thr72 may function as a regulatory switch.

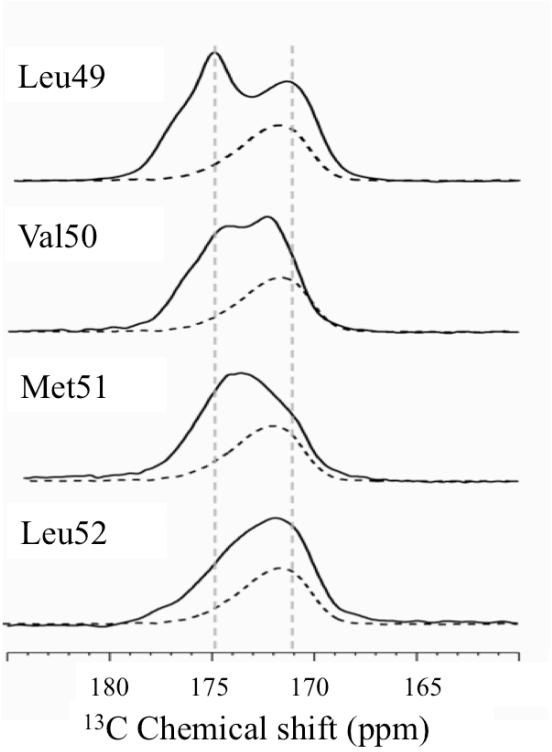

Figure 3-6. **1D CP ^{13}C spectrum of wild-type APP TM peptide labeled with 1-^{13}C Leu49, Val50, Met51 and Leu52.** The spectrum for each labeling is shown in solid line. The dashed line is the lipid (DMPC: DMPG) only spectrum served as control.

3.2.5 Extension of the APP TM helix leads to an accumulation of CTFs

To test the proposal that the secondary structure at the TM-JM boundary in the C-terminus is critical for APP processing, we present the data on APP with 2 distinct insertions at the intracellular TM-JM boundary (see Figure 3-7). The insertion of 3 leucines before the intracellular KKK sequence (APP 3L) is designed to extend the length of the TM helix. The insertion of 3 glycines (APP 3G) should maintain the helix break point as in the wild-type protein. To verify that the 3L insertion extended the α-helical structure at the TM-JM boundary, whereas the 3G extension retained the helix-to-coil transition, ^{13}C MAS NMR spectra were obtained of APP TM peptides containing the 3L and 3G inserts, and labeled at position 52 with ^{13}C=O leucine. The carbonyl chemical shifts of the 3L and 3G peptides observed in Figure 3-8 clearly indicate that the TM helix has been extended only with the 3L insertion (Figure 3-8).

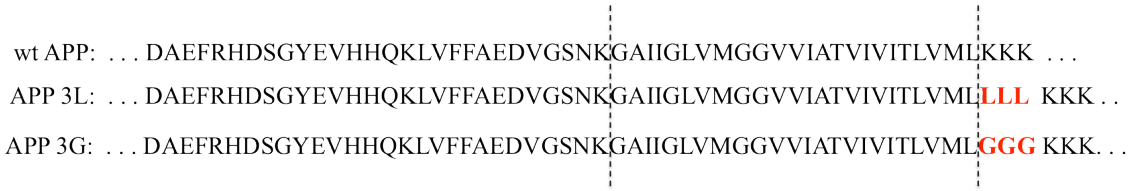

Figure 3-7. Sequences of the JM-TM domains of human APP, APP 3L and APP 3G. Insertion of 3 leucines and 3 glycines are in red.

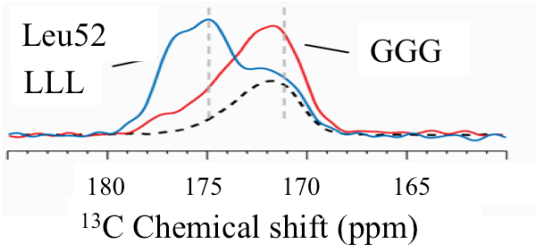

Figure 3-8. 1D CP ^{13}C spectrum of APP TM mutant peptides with KKK to GGG (in red) and KKK to LLL (in blue) labeled with ^{13}C′-^{13}C Leu52 in bilayers. The downfield (higher frequency) chemical shift of 1-^{13}C Leu52 in KKK to LLL mutant peptides indicates the helix-to-coil transition is missing with longer helix structures. The dashed line is the lipid (DMPC: DMPG) only spectrum served as control.

The wild-type APP and mutants were expressed in Chinese Hamster Ovary (CHO) cells. The insertion of 3G or 3L did not alter APP expression (Figure 3-9 A below). The production of sαAPP, an indicator of non-amyloidogenic processing, was not impaired in cells expressing APP 3L or APP 3G. Significant accumulation of APP C-terminal fragments, mainly α-CTF, occurred in cells expressing APP 3L and to a lesser extent in cells expressing APP 3G (shown in Figure 3-9 B). In the context of unmodified α-cleavage, the accumulation of α-CTF is likely a result of an impairment of the γ-cleavage of C-terminal fragments. This result was confirmed by the quantification of extracellular Aβ40. The release of Aβ40 (normalized to sαAPP) decreased by 70% in cells expressing APP 3L (Figure 3-9 C). Importantly, there was no AICD detected in cells expressing APP 3L as compared with wild-type APP. To further test whether the APP 3L mutation influences the cleavage by γ–secretase, DAPT (N-[N-(3,5-difluorophenacetyl)-L-alanyl]-S-phenylglycine t-butyl ester), a γ-secretase inhibitors of dipeptidic type, targets the C-terminal fragment of Presenilin, the TM domain of helix 7 is added. The data analysis in Figure 3-9 C and D shows that DAPT inhibitor can affect more the cleavage by the secretase on wild-type than the mutant.

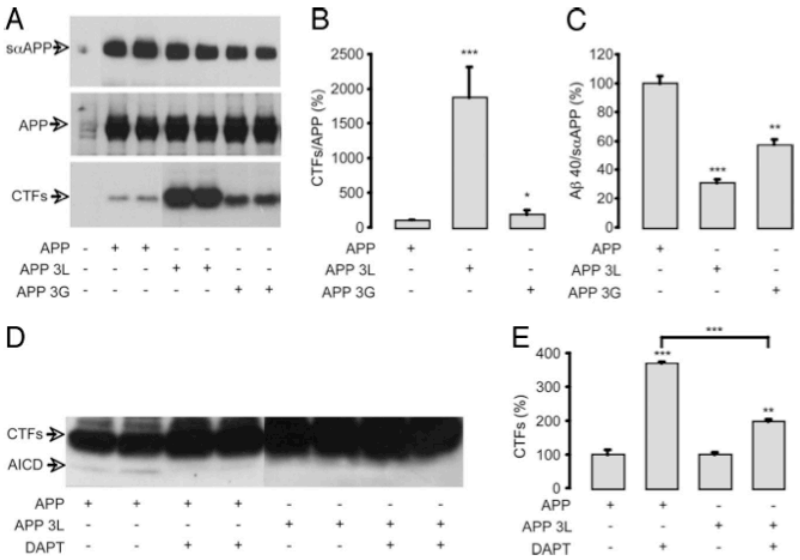

Figure 3-9. Influence of the 3L and 3G insertions in the intracellular TM-JM boundary of APP. (A) Expression of cellular APP and soluble αAPP (sαAPP) were analyzed by Western blotting analysis using the WO-2 antibody (epitope at Aβ residue 5-8) on cell lysates and cell supernatants, respectively. The CTFs (α- and β-CTF) were detected in cell lysates by the C17 antibody (i.e. the polyclonal antibody recognizing the last 17 amino acids of APP). (B) The ratio of CTF to full-length APP was calculated and represented as a percentage of the CTF/APP level in non-mutated APP controls. (C) The ratio of Aβ40/sαAPP was calculated and represented as a percentage of Aβ40/sαAPP production in non-mutated controls. In Figure 9 D, AICD was detected by Western blot analysis using the C17 antibody. The effects of DAPT on CTF accumulation were quantified in the same experiments and given as a percentage of CTF levels in APP or APP 3L for non-treated controls (E). Values are means ± SEM, $n = 4$; * = 0.05, ** = 0.01, *** = 0.001, compared with control or as indicated in B and *C*.

3.3 Discussion

The detailed molecular mechanism of intramembraneous proteolysis is poorly understood. However, proteolysis by aspartyl proteases, e.g. renin, HIV-1 protease and β-secretase, shares the commonality. The proteolysis by aspartyl proteases needs one water molecule, two aspartyl acids and the exposed carbonyl of substrate in proximity. This key step of catalysis is involved in the formation of a tetrahedral intermediate that requires the local unraveling of helical TM secondary structure to expose a backbone carbonyl (see Figure 3-10). In hydrophobic environment (i.e. membrane bilayers), hydrophobic TM peptides tends to form helical structure to compensate the polar group of C=O or NH; in hydrophilic environment (catalytic core of enzyme), hydrophobic TM peptides tends to unravel or expose the polar group to gain solvation free energy. Here, we have investigated the structure of the TM-JM regions of the APP protein in membrane bilayers to gain insight into how γ-secretase catalyzes proteolysis.

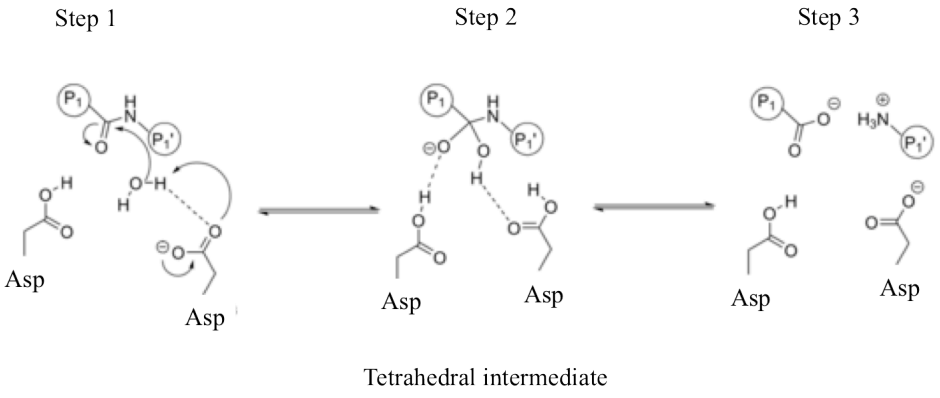

Figure 3-10. Common features of mechanism of aspartyl protease. The catalysis requires one water molecule, two aspartyl acids and the free carbonyl. The proteolysis is involved in the tetrahedral intermediate.

Figure3-11 presents the structure of the APP TM dimer. The ε-cut site lies at the boundary between the hydrophobic core and the polar head group region of the bilayer, whereas the γ-cut site is at the bilayer center. The TM dimer structure is consistent with the ε-cleavage site being the sole active site in the γ-secretase complex and with proposals for progressive cleavage from the ε- to the γ-cut site [20].

The progressive cleavage model is consistent with i) the detection of Aβ peptides with lengths intermediate between Aβ49 (ε-cleavage) and Aβ42 (γ-cleavage), ii) measurements of equimolar production of Aβ and AICD and iii) the fact that it has not been possible to detect longer AICD peptides that would be expected if γ-cleavage occurs before ε-cleavage.

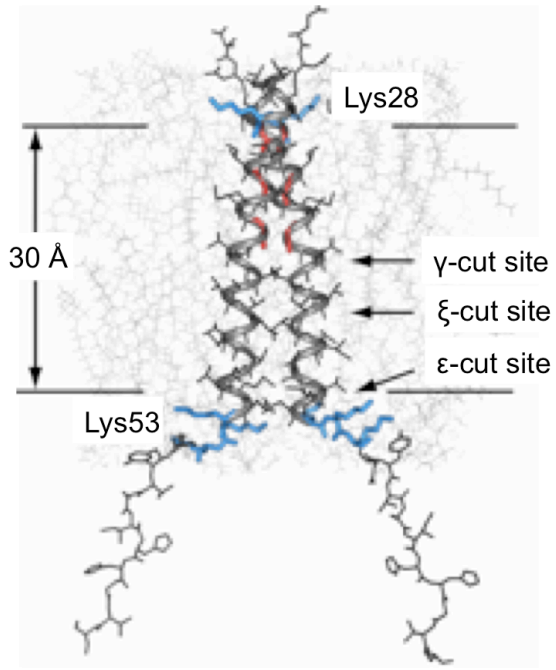

Figure 3-11. Structural model of the APP TM domain. Proposed structure of the APP TM dimer in relation to a DOPC membrane bilayer (downloaded from http://persweb.wabash.edu/facstaff/fellers/). The structural studies of the APP TM domain indicate that the γ-cut site is approximately 30 Å from Lys28. Cleavage at a single site would lead to local unraveling of the helix and a shift of amino acids into the binding site. To place the Aβ42- cleavage site at the same position would result in unraveling of the TM helix to the Gly37-Gly38 sequence.

3.3.1 Wild-type β-CTF forms a homodimer in vivo

In addition to the break in helical secondary structure at the TM-JM boundary, dimerization of the TM domain may be a common feature of γ-secretase substrates. The role of dimerization of APP and other γ-secretase substrates in proteolysis, however, remains controversial. Based on mutational studies, Munter *et al.* [23] concluded that dimerization facilitates Aβ42 production. In contrast, several studies have indicated the opposite. Gorman *et al.* using FAD mutants and our studies using TM glycine mutants found that increased dimerization can reduce the Aβ42/Aβ40 ratio [25]. Surprisingly, Eggert *et al.* using the FKBP (FK506-binding protein)/AP20187–induced 70 % dimerization leads to the decreased Aβ production by 50% without changing the Aβ42/Aβ40 ratio [22]. One possibility is that helix orientation within the TM dimer, and the strength of dimerization, controls APP processing. We have determined the orientation of the TM helices in the wild-type APP TM dimer, where GxxxG motifs (rather than the GxxxA sequence) mediate dimerization. However, it will be necessary to correlate the detailed structures of the TM and JM regions of APP mutants with the generation of different length Aβ peptides to fully address the influence of structure on processing.

The structural model in Figure 3-11 shows the APP TM dimer with a break in helical secondary structure at the TM-JM boundary. To show that the helix-to-coil transition is required for APP processing of full length APP by the γ-secretase complex, we inserted 3 additional leucines at the TM-JM boundary to extend the TM helix without

changing the TM region mediating dimerization. The 3L insertion was found to block APP processing by γ-secretase, whereas the processing of APP with the GGG insertion was similar to the WT protein. The lack of γ- and ε-cleavage of the 3L mutant of APP is consistent with the requirement that the TM domain must be locally unstructured for proteolysis and that there is only a single cleavage site at the TM-JM boundary.

3.4 Conclusions

Processing of APP by the γ-secretase complex is the last step in the formation of the Aβ peptides associated Alzheimer's disease. Here, solid-state NMR spectroscopy is used to establish the local structural features of the TM and JM domains of APP that facilitate proteolysis. Using peptides corresponding to the APP TM and JM regions, we show that the TM domain forms an α-helical homodimer mediated by consecutive GxxxG motifs but not GxxxA. We find that the APP TM helix is disrupted at the intracellular membrane boundary near the ε-cleavage site. This helix-to-coil transition is required for γ-secretase processing; mutations that extend the TM α-helix inhibit ε-cleavage, leading to a low production of Aβ peptides and an accumulation of the α- and β-CTF. Our data support a progressive cleavage mechanism for APP proteolysis that depends on the helix-to-coil transition at the TM-JM boundary and unraveling of the TM α-helix.

Chapter 4. Structure determination of wild-type C55 in bilayers

4.1 Introduction

Processing of APP occurs by the sequential action of several proteases. The α- or β-secretase (either one in two different pathways) first cleave between the extracellular and the TM domain of APP to generate a N-terminal soluble fragment (either soluble αAPP or soluble βAPP) and a membrane-anchored C-terminal fragment (α- or β-CTF). The γ-secretase complex cleaves the CTFs, e.g. β-CTF (also referred to as C99, C-terminal 99 residues) at multiple-cut sites within their TM domain and releases the Aβ in different length. C55, a shorter version of the C-terminal truncated form of β-CTF, is a 55-

residue protein corresponding to the juxtamembrane (JM) and transmembrane (TM) sequence of β-CTF including full length Aβ peptide. Several studies show that shorter version of β-CTF can be processed in a similar fashion to the full-length substrate, in which the Aβ42/Aβ40 ratio stays the same but the total Aβ production is less because of the deletion of intracellular domain including the sorting sequence in the mammalian cell lines [(59)].

Three major cleavage products include Aβ38, Aβ40 and Aβ42. Aβ40 is the major γ-cleavage product accounting for ~ 85% of total secreted peptides that is comparable to previous studies of soluble Aβ peptides in cerebrospinal fluid (CSF) of AD patients [(60)]. Aβ38 (accounting for ~ 10%), a 2-residue shorter species, has a similar toxicity to neuronal cells and propensity to form aggregates as Aβ40 isoforms and is concomitantly implicates as a γ-cleavage product of its precursor, the longer Aβ42 peptides. Aβ42, a 2-residue longer species, has a much higher propensity to form aggregates than the shorter isoforms and is the most toxic peptide generated by γ-cleavage, although only accounting for ~ 5 % of total secreted peptides [(8)]. Aβ42 is the principal component of extracellular amyloid plaques in AD patients [(27)]. Several FAD mutational clusters have been found on APP proteins. Not unexpectedly, these mutations are located on top of or near the α-, β- and γ-cleavage sites. The first cluster is located at the position of the β-secretase cleavage site at Met596-Asp597. The substrate numbering is based on the APP695 isoform of APP (the most abundant isoform in neuronal cells). Asp597 corresponds to the first residue (i.e. Asp1) of the β-CTF. These mutations within the first cluster can increase the cleavage by β-secretase [(28)] [(29)], and engineered mutations within this cluster are widely used to

enhance the production of Aβ from APP [30]. The second cluster is right below the γ–cut site at Ala42 that generates the toxic Aβ42 peptides. Single mutations at four consecutive β–branched residues of Thr43, Val44, Ile45 and Val46 can lead to the increased Aβ42/Aβ40 ratio that has been correlated to the early-onset AD.

The third cluster is located just near the α–cut site, including the Lys16 right before the hydrophobic $L^{17}VFF^{20}$ sequence and Ala21, Glu22 and Asp23 before the TM sequence, which is near the position of the α-secretase cleavage site at Lys16-Leu17. The finding of this mutational cluster near the α–cleavage site in the extracellular sequence of APP is particularly of interest because of its transition position between two sequential secretase-cleavages. One can image that the position about half way of the β-CTF protein can potentially influence the extracellular cleavage event by α- or/and β-secretase or the intramembranous cleavage by the γ–secretase complex.

Previous studies by Tian *et al.* [26] suggested that the L17-V18-F19-F20-A21 sequence is part of an inhibitory motif that modulates γ-secretase processing. Upon deletion of this motif, the catalytic efficiency of γ-secretase increases 42-fold compared to full-length β-CTF. The A21G mutation can severely impair the inhibitory effect of this region, generating more Aβ species (Aβ38, Aβ40 and Aβ42), implying that the interaction between APP and γ-secretase is altered upon mutation. Mutations in the G25-S26-N27-K28 region, which is a few residues C-terminal to position 21, also influence Aβ processing. Moreover, Ren *et al.* [41] found that mutation of Ser26 and Lys28 reduces secreted Aβ without a corresponding loss of the AICD cleavage product. Kukar *et al.* [61] found that the K28A or K28Q mutations shift the major cleavage site upstream to Gly33

from Val40 without changing the production of AICD. Therefore, these results suggest that the transition region between the EC and TM domains can have a regulatory effect on the position of γ-cleavage.

An open question is whether any structure elements in the extracellular sequence of the β-CTF regulate the enzymatic processing of APP. The structure of the 99-residue β-CTF was determined in LMPG detergent micelles by Sanders and coworkers using solution NMR methods [45]. They observed α-helical structure in the K16-L17-V18-F19-F20 sequence, the hydrophobic TM domain and in the last ~10 residues of the cytoplasmic sequence. The structure in this region is of particular interest because of its role as an inhibitory motif [26], but also as an key element in amyloid oligomer or amyloid fibril formation by the Aβ peptides [62]. In the structure determined by solution NMR, the LVFF sequence seems to insert into the detergent micelles [63]. Here, I proposed to extend our structural studies from TM domains to the extracellular sequence. I mainly focus on the structure of this extracellular hydrophobic stretch and the transition region between TM domain and the LVFF sequence where a mutational cluster occurs.

4.2 Results

4.2.1 C55 peptides served as a physiologically relevant substrate by the γ-secretase complex

As mentioned previously, Aβ40 is the predominant γ-cleavage product taking ~ 85% of total secreted peptides. Less Aβ38 and Aβ42 peptides are produced. Aβ42

peptides are the most toxic peptide generated by γ-cleavage and also the major component of amyloid plaques (senile plaques) in AD patients' brain and the ratio of Aβ42/Aβ40 are frequently linked to estimate the neuronal toxicity of Aβ42 in AD pathology. Aβ secretion (Aβ38, Aβ40 and Aβ42) from β-CTF and C55 is quantified by ECLIA method. Our structure studies are mainly on C55, the truncated form of β-CTF. To identify whether C55 is a physiologically relevant substrate by the γ-secretase complex in our system, we compare the Aβ secretion from β-CTF and C55. Figure 4-1 B-D shows that the C55 peptides release a decreased total Aβ peptide secretion by 35 %. The ratio of Aβ42/ Aβ40 (~ 6%) or Aβ42/ Aβ38 (~ 75 %) are approximately the same. The similar ratio of Aβ42 versus Aβ40 or Aβ38 indicates the shorter version of β-CTF serves as a mechanistic relevant substrate to the γ-secretase complex and can mimic the intramembranous γ–cleavage of full-length substrate.

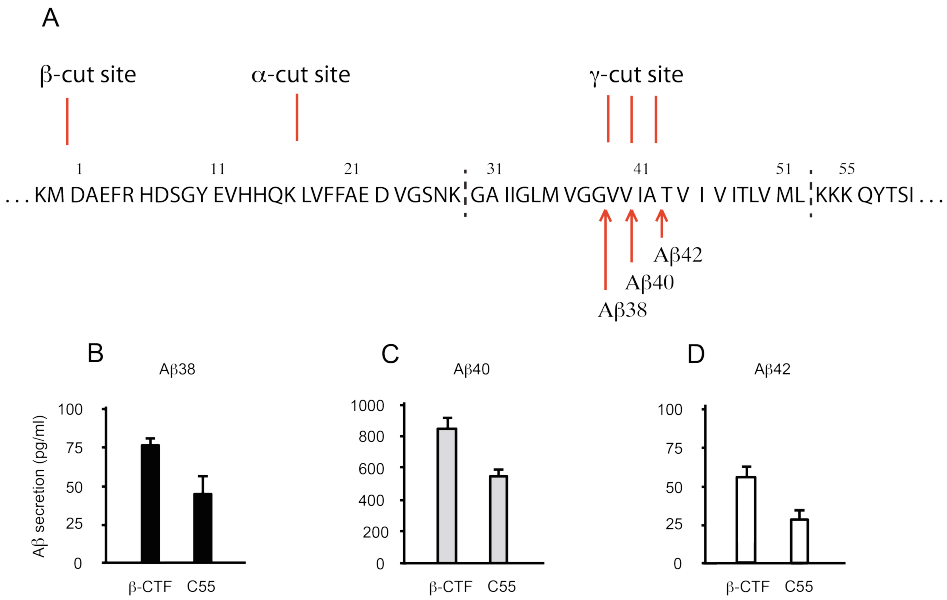

Figure 4-1. Amino acid sequence of β-CTF (including the sequence of C55 peptide) and Aβ secretion from the β-CTF and C55 peptides. (A) Sequence of the extracellular and transmembrane regions of the β-CTF. The β-CTF is produced by β-secretase cleavage to remove the large ectodomain of APP. The first 28 amino acids form extracellular region of the β-CTF and contain the α-secretase cleavage site. The TM domain (denoted by vertical dashed lines) contains the multiple cleavage-site by the γ-secretase complex where Aβ38, Aβ40 and Aβ42 species are generated. Comparison of the levels of Aβ38 (B), Aβ40 (C) and Aβ42 (D) produced by proteolysis of the wild-type β-CTF and C55 peptide is shown.

4.2.2 The extracellular $L^{17}VFFA^{21}$ sequence globally adopts the β-sheet secondary structure in membrane bilayers

The influence of the A21G mutation or deletion of hydrophobic $L^{17}VFFA^{21}$ sequence on processing may originate from a change/loss in the structure of the extracellular sequence of the β-CTF. Polarized FTIR spectroscopy can be used to assess the global secondary structure of membrane reconstituted peptides and proteins. Hydrophobic membrane peptides incorporate into bilayers as TM α-helices. Figure 4-2 A presents the FTIR spectrum of the CO vibration frequency of DMPC: DMPG lipid head groups at 1736 cm^{-1} and the amide I vibration region of wild type C55 ranged from to 1600 cm^{-1} to 1700 cm^{-1}. The FTIR spectrum exhibits both an intense band at 1657 cm^{-1} corresponding to α-helical structure and a weaker band at 1626 cm^{-1} corresponding to β-strand or β-sheet structures. The dichroic ratio (I_{90}/I_0) of the 1657 cm^{-1} band is 3.2 ± 0.2, which is consistent with an average orientation of the TM α-helix of ~20° relative to the bilayer normal. The high dichroic ratio of TM domain served as a way to estimate the reconstitution quality into membrane bilayers. Figure 4-2 B presents the comparison of FTIR spectrum of wild-type C55 (in black) and wild-type C99 or referred as β-CTF (in red). Figure 4-2 C presents the comparison of FTIR spectrum of wild-type C55 (in black) and C43 TM peptide (or referred as APP TM peptide) (Glu22-Val64) corresponding to TM domain and a few residues on the EC and IC sequence (in red). The overlapping of FTIR spectrum exhibits an extra band at 1626 cm^{-1} corresponding to β-strand or β-sheet structures, which can be assigned to the extracellular sequence.

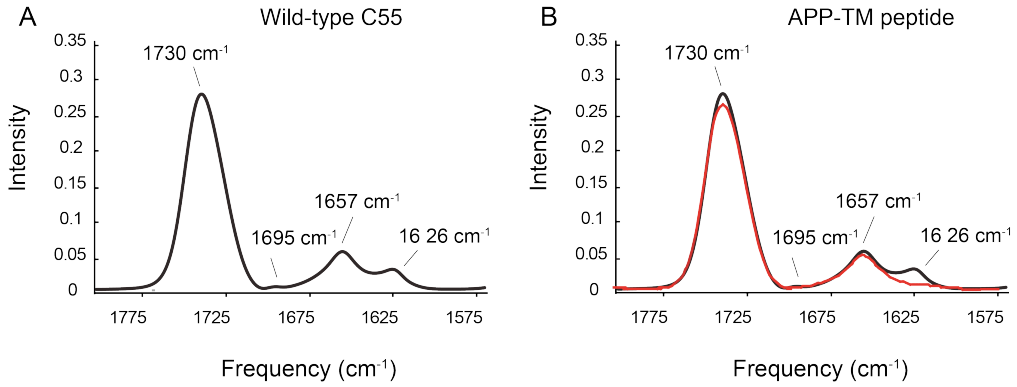

Figure 4-2. FTIR spectrum of wild-type C55 and APP-TM peptides in bilayers. FTIR spectra of wild-type C55 (A) and comparison of wild-type C55 (in black line) and APP-TM (in red line) (B) reconstituted into DMPC: DMPG bilayers. The C55 peptide contains the full extracellular domain of the β-CTF starting at Asp1 and stopping at Lys55. The APP TM peptide starts at Glu22 and stops at Val64. The additional β–sheet peak at 1626 cm^{-1} is attributed to the extracellular sequence of wild-type C55.

4.2.3 The LVFF sequence adopts α-helix in detergent micelles

The determination that the β-structure stretches through the LVFF sequence also argues that this region adopts a different secondary structure in membrane bilayers than in detergent micelles. Previous studies showed that the $K^{16}LVFFA^{21}$ can adopt α–helical structures in LMPG detergent micelles. [64]. Using FTIR spectroscopy, we further characterized the global secondary structures of C55 in LMPG micelles, isotropic bicelles (with q = 0.25), lipid fragments (with higher q values) and bilayers [51]. Figure 4-3 A shows that the extracellular sequence substantially adopts very different secondary structure in detergent and lipid bilayers. In Figure 4-3 B, this β-structural feature can be induced by increasing the bilayer structure as one goes from q=0.25 isotropic bicelles to q=2.0 bicelles with appreciable bilayer character. Q values are defined as the molar ratio of the lipids, e.g. DMPC and DMPG to the short chain lipids, e.g. DHPC. Figure 4-3 C presents that no β-structural feature observed in q=0.25 isotropic bicelles that is observed similar to in the detergent micelle environment. Figure 4-3 D indicates that the shoulder at 1631 cm-1 emerges only with high lipid contents (q=2.0).

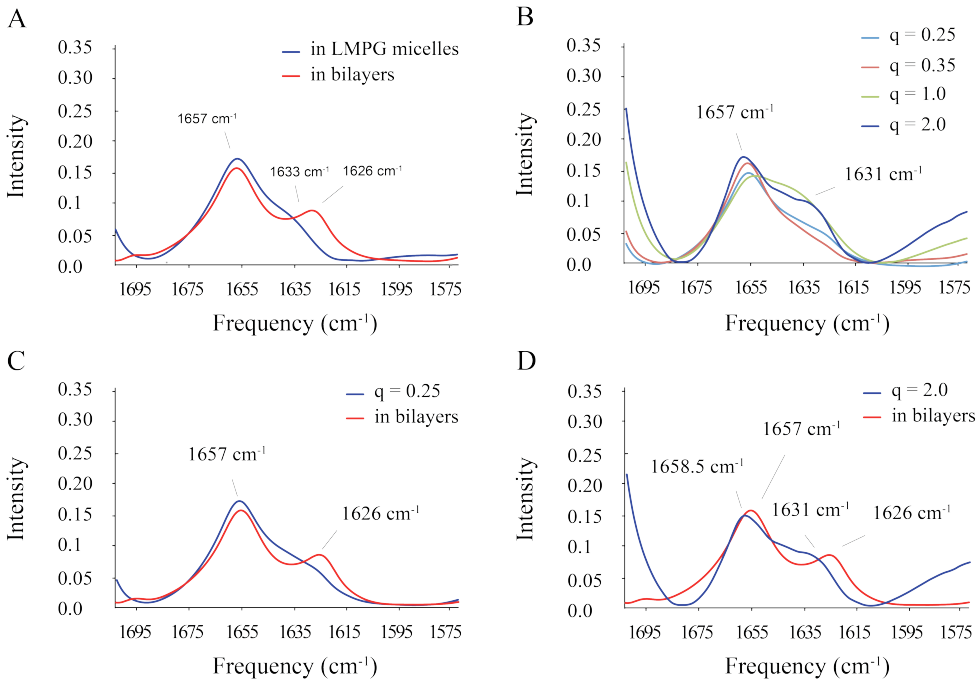

Figure 4-3. FTIR spectra of the wild-type C55 in detergent micelles, bilcelles (q=0.25–2.0) and DMPC: DMPG bilayers. (A) Comparison of FTIR spectra of wild-type C55 reconstituted in bilayers (red) and in LMPG micelles (blue). (B) Comparison of FTIR spectra of wild-type C55 in bicelles (DMPC/DMPG: DHPC) with q values ranging from q = 0.25, 0.35, 1.0 and 2.0. (C) Comparison of FTIR spectra of wild-type C55 in membrane bilayers (red) and in bicelles with q = 0.25 (blue). The distinct peak at 1626 cm^{-1} only presents in the bilayer sample. (D) Comparison of FTIR spectra of wild-type C55 in membrane bilayers (red) and in bicelles with q = 2.0 (blue). The shoulder at 1631 cm^{-1} emerges in the bicelle sample with a high q value (C). The molar ratio of protein: total lipid was 1:50 (with a DMPC: DMPG molar ratio of 10:3) in additional to the short chain lipids.

4.2.4 Extracellular region folds into a well-defined structure that incorporates β-strands in the region of YEV and LVFF.

The C55 peptide incorporates the full extracellular sequence following the site of β -secretase cleavage. Comparison of the FTIR spectrum of C55 with the spectrum of the TM peptide with a truncated extracellular domain used in our previous studies [(20)] argues that the 1626 cm^{-1} band arises from the extracellular region of C55. To establish the specific region that is responsible for this β-structure, we designed a series of alanine mutants within the extracellular region of C55 (in Figure 4-4). In the Aβ peptides, the first ten hydrophilic residues are generally considered to be unstructured [(65)]. We first focus on the sequence of Tyr10 to Val24 with Alanine scanning where Tyr10 – Glu11 is the minor β–cleavage site. Mutation of the Tyr10-Glu11-Val12 sequence to alanine dramatically reduces the intensity of the 1626 cm^{-1} IR band. Similarly, mutations of Lys16 and Phe19-Phe20 to alanine reduce the 1626 cm^{-1} intensity consistent with the disruption or reduction of the β-sheet secondary structure. In contrast, the mutation to alanine of His13-His14-Gln15 and Glu22-Asp23-Val24 do not strongly influence the 1626 cm^{-1} peak position or intensity. These results argue that the extracellular region folds into a defined structure that at least incorporates two β-strands in the region of $Y^{10}EV^{12}$ and $L^{17}VFF^{20}$. The small 1695 cm^{-1} resonance in wild-type protein is often associated with anti-parallel β-sheet. The loss of this peak upon the YEV and LVFF mutations suggests that these sequences adopt an anti-parallel β-sheet fold within inter- or intra-molecular interaction.

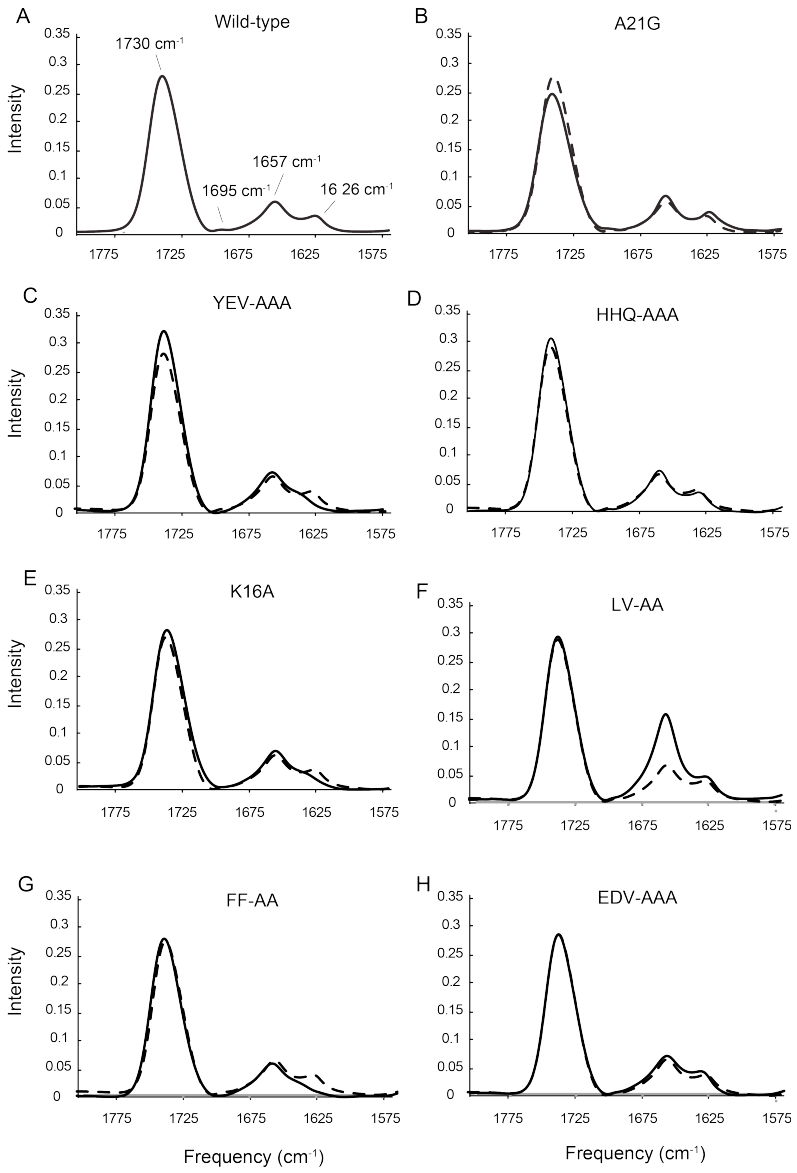

Figure 4-4. FTIR spectra of the wild-type C55 and mutants. Comparison of FTIR spectra of wild-type C55 (A) reconstituted into DMPC: DMPG bilayers with spectra of the C55 protein containing the Flemish A21G (B) and alanine mutations within the extracellular sequence between Tyr10 and Val24: YEV (C), HHQ (D), K (E), LV (F), FF (G) and EDV (H). The molar ratio of the DMPC: DMPG was 10:3, and the molar ratio of C55: total lipid was 1:50. The FTIR spectrum of wild-type is in solid line and mutants are shown in dashed line in (B)-(H).

4.2.5 Selective incorporation of ^{13}C labeled amino acids in LVFF region in the wild-type C55 peptides cause β–sheet peak splitting

Figure 4-5 shows that the β-sheet peak at 1626 $cm^{-1}$of FTIR spectrum splitting with ^{13}C labeled amino acids selectively incorporated into the C55 peptides. To further verify whether a anti-parallel β-structure associated with Leu17-V-F-F-Ala21 sequence, we selectively incorporate ^{13}C labeled amino acids in the β-structure, and transmembrane helix, and monitor the effect of the different reduced mass along with the different position. Phe19 and Phe20 right next to Ala21 have the biggest influence on the β-structure. The incorporation with ^{13}C labeled Phe19 (Figure 4-5 A), and ^{13}C labeled Phe20 (Figure 4-5 B) in wild-type C55 lead to the β-sheet peak split into 1608 cm^{-1} and 1630 cm^{-1} from 1626 cm^{-1}. Concordantly, wild-type peptides with ^{13}C labeled Ile31, ^{13}C labeled Gly37, and ^{13}C labeled Ala42 does not lead to β-sheet peak split.

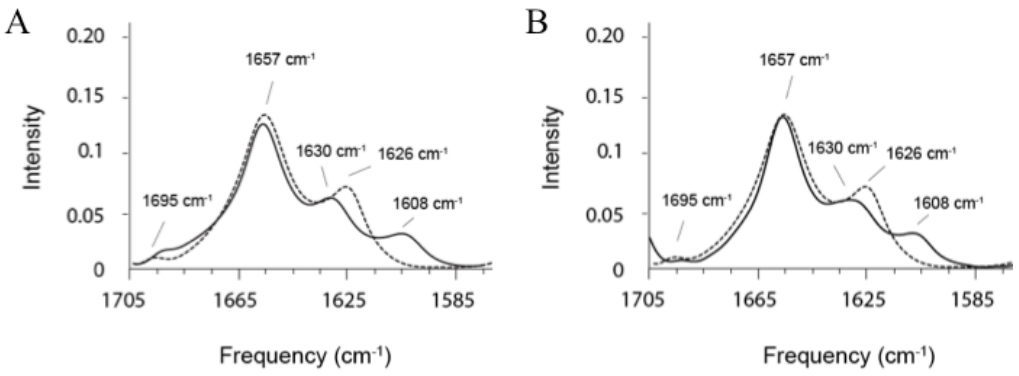

Figure 4-5. FTIR spectra of wild-type and A21G C55 in DMPC: DMPG bilayers with stable isotope editing. FTIR spectra of unlabeled wild-type C55 is presented in dashed lines in panel A and B. Comparison of the FTIR spectrum of unlabeled wild-type C55 with the wild-type C55 containing selectively ^{13}C labeled amino acids (solid lines in A and B). The wild-type C55 is selectively labeled with U-^{13}C Phe19 in (A) and U-^{13}C Phe20 in (C). The lipid molar ratio of the DMPC:DMPG was 10:3, and the molar ratio of peptide to total lipid was 1:50.

4.2.6 Upfield chemical shifts of ^{13}C Cα and C=O indicates the L^{17}VFFA^{21} sequence adopts local β–sheet structure

Solid-state NMR is complementary to FTIR spectroscopy and allows us to probe the local structure in the region of LVFFA. Figure 4-6 presents two-dimensional magic angle spinning (MAS) NMR spectra of C55 obtained with dipolar assisted rotational resonance (DARR). MAS increases spectral resolution of membrane proteins in bilayer environments by averaging the chemical shift anisotropy and dipolar interactions. DARR reintroduces the dipolar interaction between labeled ^{13}C sites [(52)], and is used for resonance assignments and for distance measurements between ^{13}C labels. As with the FTIR studies described above, an advantage of using C55 over C99 (or β-CTF) for structural studies is that the peptide is short enough to synthesize by solid-phase methods, which allows site-specific incorporation of ^{13}C isotope labels.

Uniform ^{13}C labeling of the amino acids allows us to readily assign the spectrum because directly bonded ^{13}C-atoms yield strong cross peaks in the 2D spectrum. Figure 4-6 B presents the carbonyl region of the 2D spectrum of C55 containing ^{13}C-labeled amino acids at Phe19, Val24 and Gly25. The Gly29 C=O resonance is observed at ~175 ppm and the higher frequency of the Gly29 chemical shift is consistent with α-helical secondary structure [(66)].

Figure 4-7 summarizes the backbone chemical shifts of the Cα and C=O resonances between Leu17 and Ala30. The backbone chemical shifts are sensitive to the secondary structure of proteins and the deviation from the averaged values is often used to

predict the propensity of the secondary structure [67]. Here, the Cα and C=O chemical shifts are plotted as differences from the average chemical shifts of these resonances. The deviations to lower chemical shift values for the Cα and C=O resonances (i.e. negative bars) correspond to β-sheet secondary structure. The deviations to higher chemical shift values (i.e. positive bars) correspond to α-helical secondary structure. For the wild-type C55, the Cα and C=O resonances between Leu17 and Ala21 all exhibit negative deviations corresponding to β-structure. The observation of β-structure is consistent with the FTIR results, but contrasts with the α-helical secondary structure by solution NMR structures previously [45, 68]. Gly29 and Ala30 both exhibit positive deviations consistent with the helical TM domain beginning at Lys28. The two residues probed between the $L^{17}VFFA^{21}$ region and the TM domain – Val24 and Gly25 – exhibit negative shifts less than ~ 1 ppm at C=O and Cα of Val25 and Gly25 with exception of ~ 1.5 ppm at Gly25 C=O, suggesting a non α-helical secondary structure (a random coil or β-sheet secondary structure).

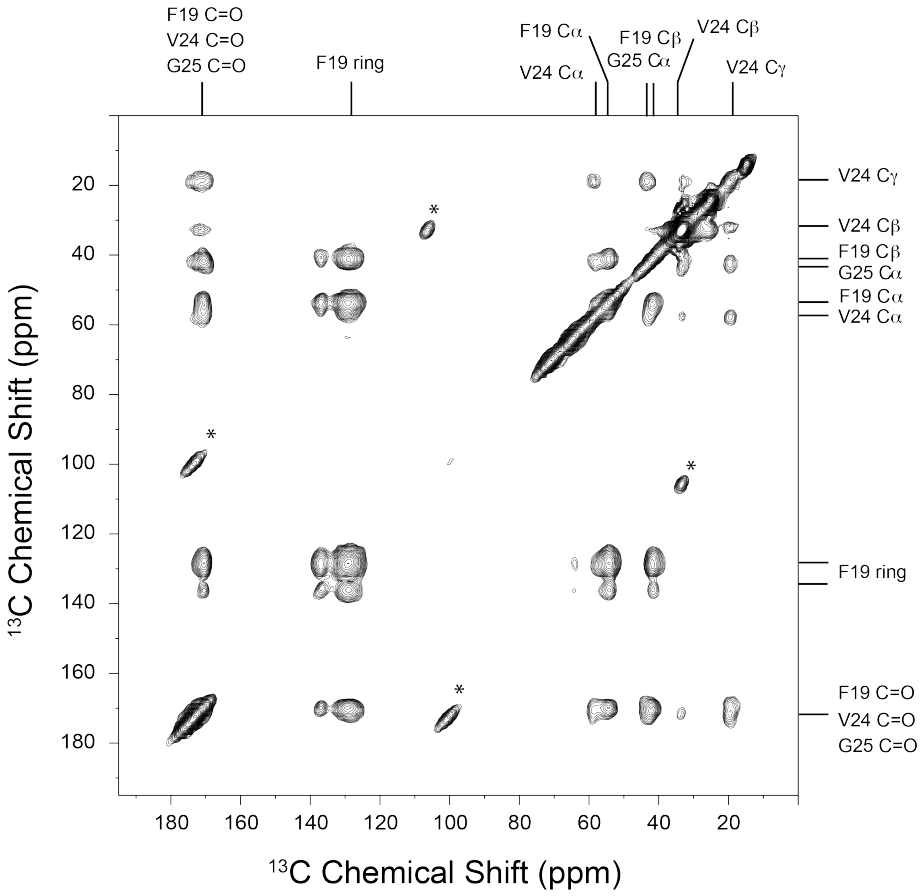

Figure 4-6. 2D DARR spectra of the wild-type C55 in membrane bilayers labeled with U-^{13}C Phe19, Val24, and Gly25. The frequencies of carbonyl and side chain carbon nucleus are assigned mainly based on intra-residual cross peaks with verification of the BMRB statistics of chemical shift value. The complete assignment represents a homogeneous sample preparation and a high-resolution peak distribution of 2D DARR spectrum.

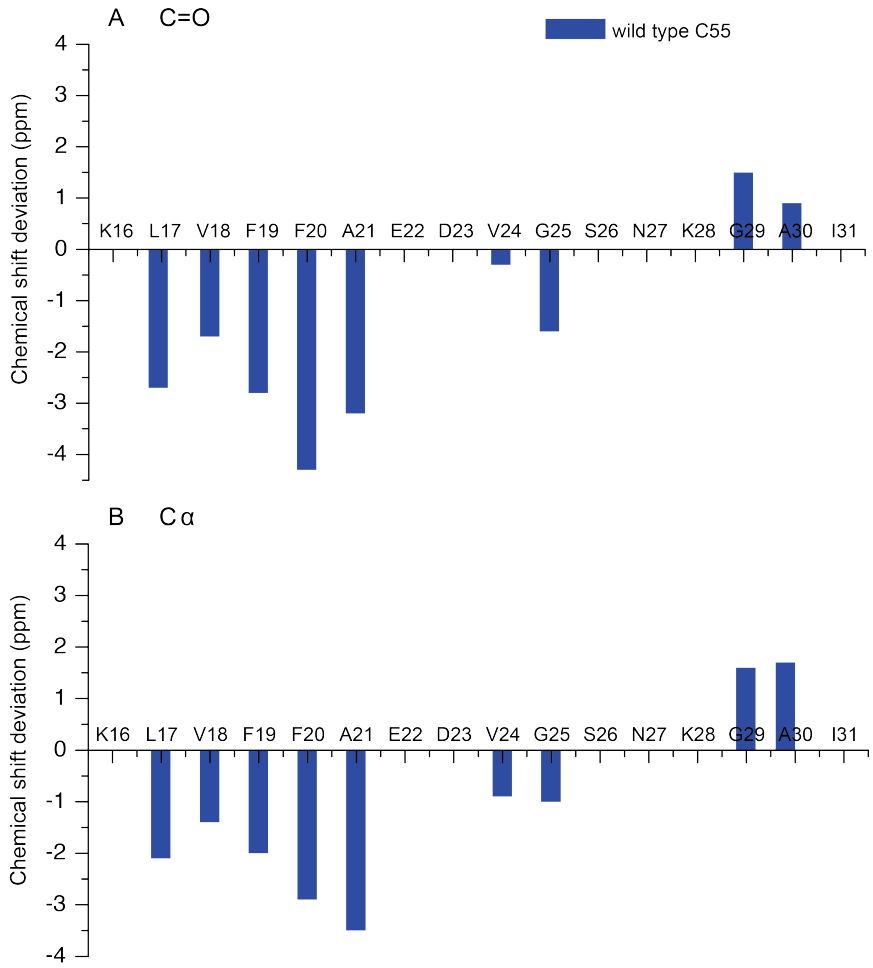

Figure 4-7. Chemical shift deviation of wild-type C55 from average values. The secondary structure propensity predicted from deviation of chemical shifts is focus on three regions, including the hydrophobic sequence of L17-A21, the residues of V24-G25 linking the EC and TM domain and G29-A30, where Gly29 is the starting position of putative TM helix. (A) Carbonyl chemical shifts of deviation from average values. (B) Cα carbon chemical shifts deviation from average values. The average chemical shift values are taken from the BMRB database (http://www.bmrb.wisc.edu/ref_info/ statful.htm). The deviations to lower chemical shift values (i.e. negative bars) correspond to β-sheet secondary structure. The deviations to higher chemical shift values (i.e. positive bars) correspond to α-helical secondary structure. The ratio of peptide to total lipid is 1: 50.

4.2.7 The wild-type C55 can homodimerize through the GxxxG interface but not GxxxA motif in membrane bilayers

Complementary studies involving the mutation of the consecutive $G^{29}xxxG^{33}xxxG^{37}$ motifs support the idea that dimerization of the TM domain of the β-CTF influences processing [21, 23]. Nevertheless, the question of whether the GxxxG motifs are involved in dimerization and how they might change upon mutation has been unclear. Recently, Arseniev and coworkers determined the dimer structure of residues Gln15- Lys53 in DPC detergent micelles [68]. The TM dimer interface in the NMR structure is formed from the $G^{38}xxxA^{42}$ sequence rather than $G^{33}xxxG^{37}$. The GxxxA interface was previously suggested in several studies, e.g. TM dimeric interface in Glycophorin A [21, 25].

In Figure 4-8, we show unambiguously that the TM dimerization of wild-type C55 sequence is mediated by the $G^{33}xxxG^{37}$ interface but not $G^{38}xxxA^{42}$. The strong cross peak between Gly33 Cα and Gly33 C=O observed upon mixing two labeled peptides can only be explained by a well-defined dimer structure. This result is similar to that obtained for the TM region alone in Chapter 3 [20] but different from that in detergent micelles. In Figure 4-8 A, full ^{13}C DARR spectrum is shown where the Gly ^{13}C=O to $^{13}C\alpha$ cross peak mediated by GxxxG contact is in red box and the Ala ^{13}C=O to $^{13}C\beta$ cross peak mediated by GxxxA contact is in blue box. For experiment designing, The DARR experiments have different resolution on the first (2k) and the second dimension (128). The spinning sidebands are aliased and fold back only clearly shown on the second dimension.

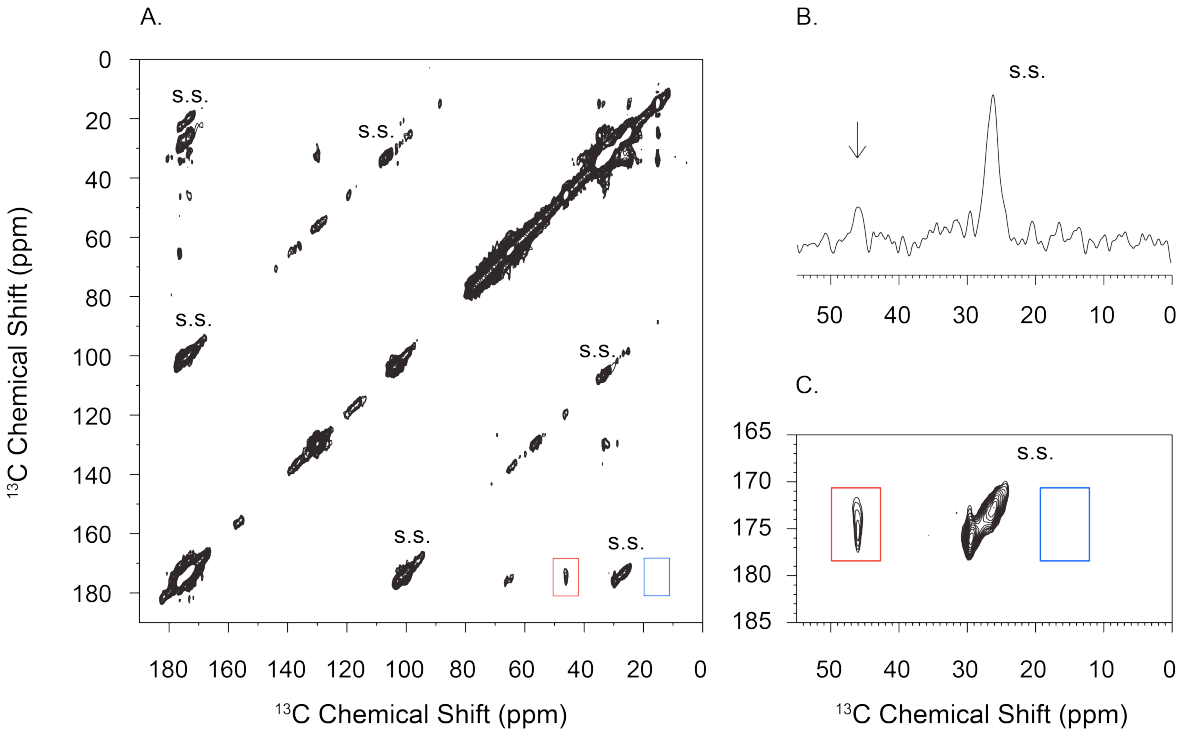

Figure 4-8. 2D DARR NMR spectra of the wild-type in bilayers to test two putative homodimeric interfaces, $G^{29}xxxG^{33}xxxG^{37}$ or $G^{38}xxxA^{42}$ motifs. Two peptides are selectively ^{13}C labeled at Gly33 and Ala42. The first peptide is labeled with ^{13}C=O labeled Ile31, ^{13}C=O labeled Gly33, and ^{13}Cβ labeled Ala42, and the second peptide is labeled with ^{13}Cα labeled Gly33, and ^{13}C=O labeled Ala42. Two wild-type C55 peptides are mixed in equal molar amounts, and reconstituted into POPC: POPS bilayers. The peptide-to-lipid ratio is 1: 50. (A) The DARR spectra of mixed wild-type C55 peptides are shown. Only cross peaks resulting from Gly33 resonances on different peptides (i.e. Gly33 Cα to Gly33 C=O in red box) are observed for both wild-type C55. Cross peaks are not observed between resonances associated with Ala42 on different peptides (i.e Ala42 Cβ to Ala42 C=O, blue box). (B) 1D rows through the Gly33 C=O. (C) 2D carbonyl region of DARR spectrum. S.S. stands for the spinning sideband. Cross peak at ~ 66 ppm, ~ 32 ppm and ~ 25 ppm are assigned to the ^{13}C nature abundance of lipid headgroup and acyl chain.

4.2.8 The molecular modeling of wild-type C55 dimer in membrane bilayers

In Figure 4-9 below, we show that the TM dimerization of wild-type C55 sequence is mediated by the $G^{33}xxxG^{37}$ interface but not $G^{38}xxxA^{42}$ based on the strong cross peak between Gly33 Cα and Gly33 C=O upon mixing two labeled C55 peptides in membrane bilayers. The extracellular anti-parallel β-sheet structure is defined based on the upfield chemical shifts, mutational studies by FTIR spectrum and anti-parallel peak at 1695 cm^{-1}.

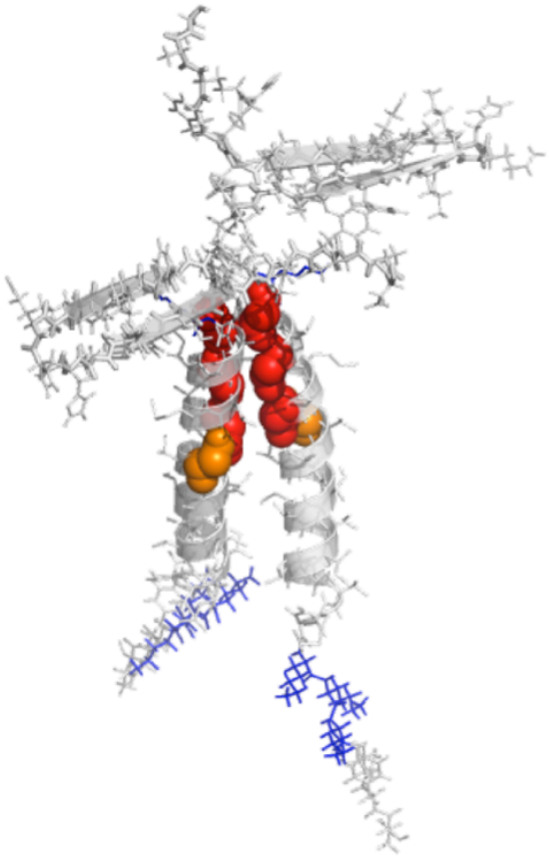

Figure 4-9. Molecular model of wild-type C55 dimer structure. The dimer structures of wild-type C55 are modeled from PyMol software. The structures are constructed based on the global and local secondary structures from FTIR and solid state NMR data. The extracellular sequence is modeled as intra-antiparallel β-sheet registry of $HDSGYE^{11}$ and $K^{16}LVFFAE^{22}$ with a complimentary charge-charge interaction. Glycine residues are labeled as red and orange spheres (e.g. Gly29, Gly33 and Gly37 in red and Gly38 in orange) and three lysine residues in the C-terminal juxtamembrane sequence are shown as blue sticks.

4.3 Discussion

The mutations involved in the extracellular sequence of the β-CTF have a strong influence on intramembranous processing by the γ-secretase complex. Mutations including the deletion of hydrophobic sequence of $L^{17}VFFAED^{23}$ or the clinical single mutation A21G have been shown to alter the interaction with the γ–secretase complex [26]. We asked the question whether the extracellular sequence has a well-defined conformation where the mutations can induce a structural change and lead to different processing. We established the structure of extracellular sequence and TM domain of wild-type C55, e.g. focusing on the $L^{17}VFFA^{21}$ – $V^{24}G^{25}$ – sequence and TM dimerization motifs, e.g. GxxxG and GxxxA interface by using FTIR and NMR spectroscopy, and propose how these structure features are linked to processing of the β-CTF. FTIR and NMR measurements of C55 in membrane bilayers provide evidence that β-strand or sheet secondary structure, rather than helical structure, is adopted in the extracellular region of the β-CTF. The results also emphasize the C55 can form a TM stable homodimer, which is mediated by GxxxG motifs but not GxxxA.

4.3.1 The structure of APP near the region of A21G regulates processing

The Flemish mutation was first described by Hendriks *et al.* [34] and later shown to lead to an increase in Aβ production (~ 2 fold) [33]. Tian *et al.* [26] found that the LVFFAED region in the extracellular domain of the β-CTF was inhibitory to the activity of γ-secretase. They observed that deletion of this seven-residue sequence resulted in a 25-fold increase in secreted Aβ40 compared to a 4-fold increase in total secreted Aβ for the A21G mutant [26]. In contrast, the mutations at Glu22 and Asp23 do not significantly influence Aβ secretion.

4.3.2 FTIR and NMR measurement show LVFFA region in the wild-type C55 peptides is in anti-parallel β-sheet

Our structural studies show that Ala21 is at the edge of the β-sheet fold in the extracellular domain of the β-CTF. The FTIR measurements show that the extracellular sequence of wild-type C55 globally adopts β–structure that is consistent with the observation of downfield (higher frequency) chemical shift values on the LVFFA region by solid state NMR. Alanine scanning on the extracellular sequence indicates that LVFFA is a part of this well-defined anti-parallel β–sheet fold. The measurement also show that Val24 and Gly25 in wild-type C55 are most likely in random coil or β–structure that link the LVFFA sequence and TM helix domain. Based on the structure characterization of EC and TM domain in wild-type C55, we intend to show how the mutations near this region, e.g. A21G influence the well-defined β-fold and correlate it to the increased processing.

4.3.3 The wild-type C55 dimerizes through the GxxxG interface

The observation that the existence of an additional $G^{25}xxxG^{29}$ motif in the extracellular sequence of the β-CTF suggests the possibility of mutations near this region might influence the TM dimerization of the protein. Complementary studies involving the mutation of the consecutive $G^{29}xxxG^{33}xxxG^{37}$ motifs support the idea that dimerization of the TM domain of the β-CTF influences processing [21, 23]. Nevertheless, the question of whether the GxxxG motifs are involved in dimerization and how they might change upon mutation has been unclear. Recently, Arseniev and coworkers determined the dimer structure of residues Gln15- Lys53 in detergent micelles [68]. The dimer interface in the

NMR structure is formed from the $G^{38}xxxA^{42}$ sequence rather than $G^{33}xxxG^{37}$. The GxxxA interface was previously suggested in several studies [21, 25].

In these studies, we show unambiguously that the wild-type sequence is mediated by the $G^{33}xxxG^{37}$ interface. The strong cross peak between Gly33 Cα and Gly33 C=O observed upon mixing two labeled peptides can only be explained by a well-defined dimer structure. This result is similar to that obtained for the TM region alone in Chapter 3 [20]. In Chapter 5, we test whether mutations near this region, e.g. the A21G mutation can change the dimer interface or increases the dimerization strength since A21G will further introduce additional GxxxG motif upstream of extracellular sequence.

4.4 Conclusions

The transition sequence of cluster mutation between α– and β-cleavage site motivated us to examine the structure of Leu17-Val18-Phe19-Phe20-Ala21, -Val24-Gly25- and Gly29-Ala30-Ile31- sequence. We show that in membrane bilayers the extracellular sequence from Leu17 to Ala21 has β-secondary structure and that the transmembrane region is helical starting at Gly29. Val24 and Gly25 region between these two structure domains can serve as transition junction with random coil or β-structure feature. Here, we show that an overall increase in the production of Aβ peptides can be correlated to the structural change. We propose to investigate that the mutation near this cleavage site might influence this junction and influence of the increased processing.

Chapter 5. Structural variation by familial mutations between the α-cleavage site and TM domain

5.1 Introduction

Different from familial mutations near the β-cleavage and γ-cleavage site, the mutations between the α–cut site and TM domain can influence on either the processing with different amounts of Aβ secretion, or influence the mutant Aβ peptides that can result in the different morphology of fibrils or toxicity to neuronal cells. Secondly, this mutational cluster is particularly of interest, since the transitional position from the α–cut site to TM domain could potentially influence the upstream cleavage by α–secretase or the intramembranous proteolysis by the γ–secretase. The genetic mutations including the

Lys16 right before the hydrophobic Leu^{17}-Val-Phe-Phe^{20} sequence and Ala21, Glu22 and Asp23 before the TM sequence, which is near the position of the α-secretase cleavage site at Lys16-Leu17. Studies by Kaden *et al.* [69] show that the K16N mutation can increase Aβ production by inhibiting the secondary α-cleavage of β-CTF.

Interestingly, no clinical mutations have been found in the extracellular hydrophobic Leu^{17}-Val-Phe-Phe^{20} sequence that is right after the α–cut site at Lys^{16} - Leu^{17}. Previous studies by Tian *et al.* [26] suggested that the L17-V18-F19-F20-A21 sequence is a part of an inhibitory motif that modulates γ-secretase processing. Upon deletion of this motif, the catalytic efficiency of γ-secretase increases 42-fold compared to full-length β-CTF. The A21G (Flemish), E22Q (Dutch), E22G (Arctic), E22K (Italian), and D23N (Iowa) mutations [34-37] are several residues below the L^{17}-V-F-F^{20} sequence and have very different effects on APP processing [33] and Aβ peptide degradation [70]. The A21G mutation appears to increase Aβ production by ~2-4 fold but not via a change in α-secretase cleavage [33],[26]. In contrast, mutations at Glu22 and Asp23 do not markedly change the level of total secreted Aβ peptides [26, 33, 38], but rather increase the rate of fibril formation after the Aβ peptides are generated by proteolysis [18].

To understand the diversity of effects within this central cluster of mutations midway between the β- and γ- cleavage sites, we focus here on the A21G Flemish mutation and address how the removal of a single methyl group can have a dramatic influence on Aβ production. Mutations in the G25-S26-N27-K28 region, which is a few residues C-terminal to position 21, also influence Aβ processing. Ren *et al.* [41] found that mutation of Ser26 and Lys28 reduces the secreted Aβ without a corresponding loss of the

AICD cleavage product. More recently, Kukar *et al.* [61] restated that the mutations at Lys28, e.g. K28A or K28Q mutations shifted the major cleavage site upstream by generating more shorter Aβ33 and concomitantly reducing the longer Aβ isoform without changing the production of AICD. Consistently, these results suggest that the transition sequence between the EC and TM domains can have a regulatory effect on the position of γ-cleavage.

5.2 Results

5.2.1 The A21G mutation leads to an increase in Aβ production.

We first addressed whether the A21G or LVFF to AAAA mutations can affect the cleavage by α–secretase. The full-length APP695 DNA constructs for wild-type protein and the A21G and LVFF to AAAA mutants were transfected in CHO cell lines. Figure 5-1 shows that the A21G mutation increases the ratio of soluble βAPP/ αAPP by a factor of 1.2, while the LVFF mutation increases the ratio of soluble βAPP/ αAPP by a factor of 1.3. This observation indicates that the LVFF mutation can better affect the α cleavage, and increase the β cleavage than the A21G mutation. The total Aβ secretion from A21G and LVFF APP mutants both increase compared to wild-type APP. The ratio of Aβ42/40 remains the same for both A21G and LVFF mutants from APP695. The protein overexpression levels were measured by Western blotting. Although the A21G mutation increases both cleavage at the α-cut and γ-cut sites, the influence is stronger on the cleavage within the transmembrane domain by the γ-secretase complex.

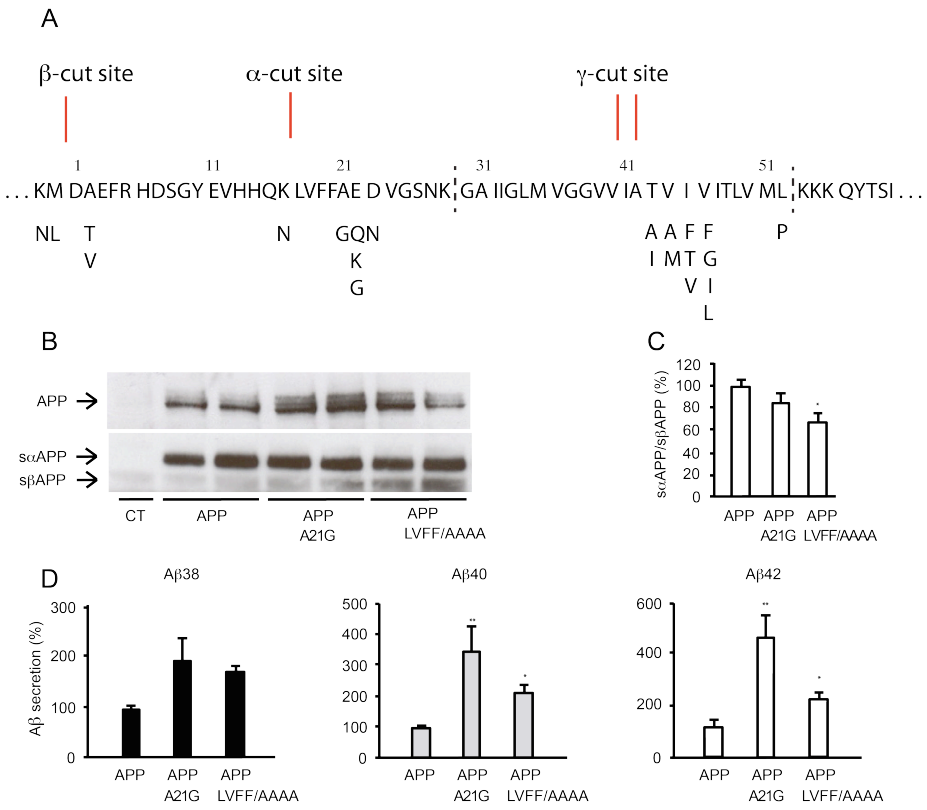

Figure 5-1. Sequential cleavage of APP and Aβ secretion. The top panels show that the production of sαAPP and sβAPP are roughly the same for wild-type and A21G. There is a significant increase in the sαAPP/sβAPP ratio in the LVFF mutant. Aβ peptides produced from proteolysis of wild-type and A21G APP. (A) Amino acid sequence of APP with α-, β– and γ–cleavage site. (B) SDS PAGE showing expression levels of the wild-type and A21G APP and sαAPP and sβAPP fragments. (C) Comparison of the sαAPP/sβAPP ratio from wild-type, the A21G mutant and LVFF to alanine APP mutants. (D) Comparison of the levels of Aβ38, Aβ40 and Aβ42 among wild-type, A21G and LVFF to alanine APP mutants.

We next tested whether the A21G mutation influences the processing of the β-CTF by the γ-secretase complex. Figure 5-2 shows that the total Aβ secretion from A21G β-CTF is ~ 2 fold greater than wild-type β-CTF. The secretion of Aβ38 and Aβ40 from A21G β-CTF increases 1.8 times compared to wild-type β-CTF, while Aβ42 production increases 3.8 times. The data support previous studies that mutation at A21G can increase the cleavage efficiency within the transmembrane domain by the γ-secretase [(26)].

Proteolysis of the wild-type β-CTF results predominantly in the Aβ40 peptide (~ 85%), with smaller amounts of Aβ38 (~ 10%) and Aβ42 (~ 5%). Figure 5-2 presents the amount of each of these secreted Aβ peptides produced by γ-secretase cleavage as a percentage relative to the wild-type peptide. Both the A21G mutation and the LVFF to AAAA mutation increase the total Aβ production. The A21G mutation results in a 1.7-fold increase in Aβ40. A larger increase (4.5-fold) is observed in Aβ40 for the LVFF to AAAA mutation. There is a striking increase (4-fold) in Aβ42 produced relative to wild-type in the A21G mutant. This observation is significant in that Aβ42 is the major component of amyloid plaques.

We also compared the influence of the A21G mutation with the LVFF to AAAA mutation using a shorter version (C55) of the β-CTF. Similarly to our structural studies on the wild-type protein, we used the C55 peptide construct rather than the full-length β-CTF protein to allow selective incorporation of ^{13}C probes for structural studies by solid-phase peptide synthesis. In Figure 4-1, we have showed that C55 can act as a substrate of γ-secretase and is processed in a similar way to β-CTF, producing the same Aβ42/ Aβ40 ratio. In Figure 5-2 C, we show that both the A21G and the LVFF to AAAA mutations increase Aβ secretion. The changes in Aβ38, Aβ40 and Aβ42 secretion using C55 are similar to those using the full-length β-CTF indicating that C55 has the physiologically

relevant structural features that reflect the intramembranous substrate processing on both wild-type and mutants.

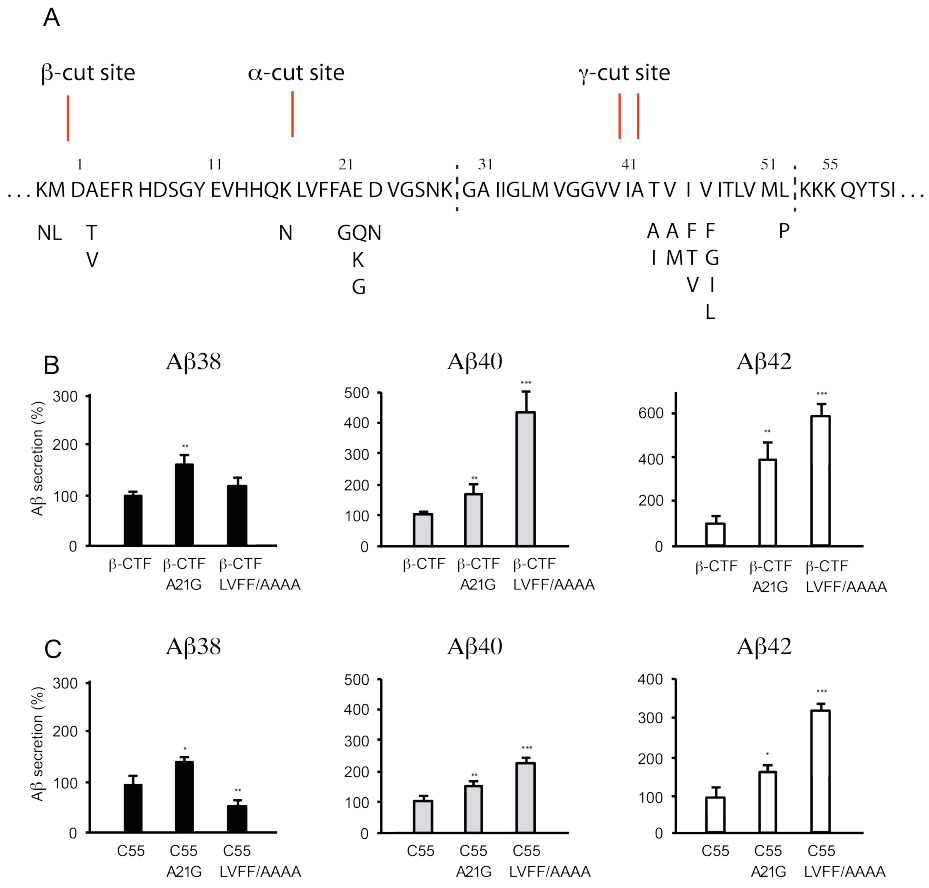

Figure 5-2. Sequence of β-CTF and Aβ secretion of wild-type β-CTF and C55, A21G and LVFF to AAAA mutant. (A) Sequence of the extracellular and transmembrane regions of the β-CTF. The β-CTF is the cleavage product by β-secretase from APP. The first 28 amino acids form extracellular region of the β-CTF and contain the α-secretase cut-site at K^{16}-L^{17} as well as the site of several familial AD mutations. The TM domain (denoted by vertical dashed lines) contains the site of γ-secretase cleavage and an additional cluster of familial AD mutations. (B) Comparison of the levels of Aβ38, Aβ40 and Aβ42 produced by proteolysis of the wild-type β-CTF, A21G and LVFF-to-AAAA mutants. (C) Comparison of the levels of Aβ38, Aβ40 and Aβ42 produced by proteolysis of wild-type C55 and the corresponding A21G and LVFF-to-AAAA mutants of C55.

5.2.2 The $L^{17}VFFA^{21}$ sequence of A21G C55 is globally β-sheet in membrane bilayers

The influence of the A21G mutation on processing may originate from a change in the structure of the extracellular sequence of the β-CTF. Polarized FTIR spectroscopy can be used to assess the global secondary structure of membrane reconstituted peptides and proteins. Hydrophobic membrane peptides incorporate into bilayers as transmembrane α-helices. Previously, Figure 4-4 A and B present the FTIR spectrum of the amide I vibration region of wild type C55 and A21G C55 in bilayers. The FTIR spectrum both exhibits both an intense band at 1657 cm^{-1} corresponding to α-helical structure and a weaker band at 1626 cm^{-1} corresponding to β-strand or β-sheet structure. The dichroic ratio of the helical peak of both is 3.2 ± 0.2, which infers an average orientation of the TM α-helix of ~20° relative to the bilayer normal.

5.2.3 The A21G mutation influences the β-sheet structure in membrane bilayers

The A21G mutation has only a slight influence on the position of the 1626 cm^{-1} band observed in the FTIR spectrum of C55. To further explore whether there are local changes in structure, we compared both FTIR spectra of wild-type and A21G C55 peptides containing specific ^{13}C labels at backbone carbonyl positions within the LVFF sequence. The ^{13}C=O labels with the heavier atom mass serve to shift the amide vibration to lower frequencies. The frequency and intensity of the shifted resonances are sensitive to whether the ^{13}C=O labeled sites fall within parallel or antiparallel β-sheet structure [(71)]. We selected Phe19 and Phe20 mutations at these positions next Ala21 which have a large influence on the 1626 cm^{-1} resonance. In the FTIR spectra of wild-type C55 (Figures 5-3A and C), the incorporation of ^{13}C leads to splitting of the 1626 cm^{-1} band into two components at 1608 cm^{-1} and 1630 cm^{-1}. These shifts are similar to those described for model peptides [(71)] and are consistent with this region of C55 adopting anti-parallel β-sheet structure. In contrast, ^{13}C labeling on F19 and F20 does not cause the β-sheet peak to split

(Figures 5-3 B and D) in the A21G mutant suggesting that the anti-parallel structure observed at positions F19-F20 has been disrupted or twisted, although the rest of the β-sheet structure or content remains intact. These results suggest that Ala21 is at the edge of the β-sheet structure and that mutation can have a strong influence on the adjacent residues.

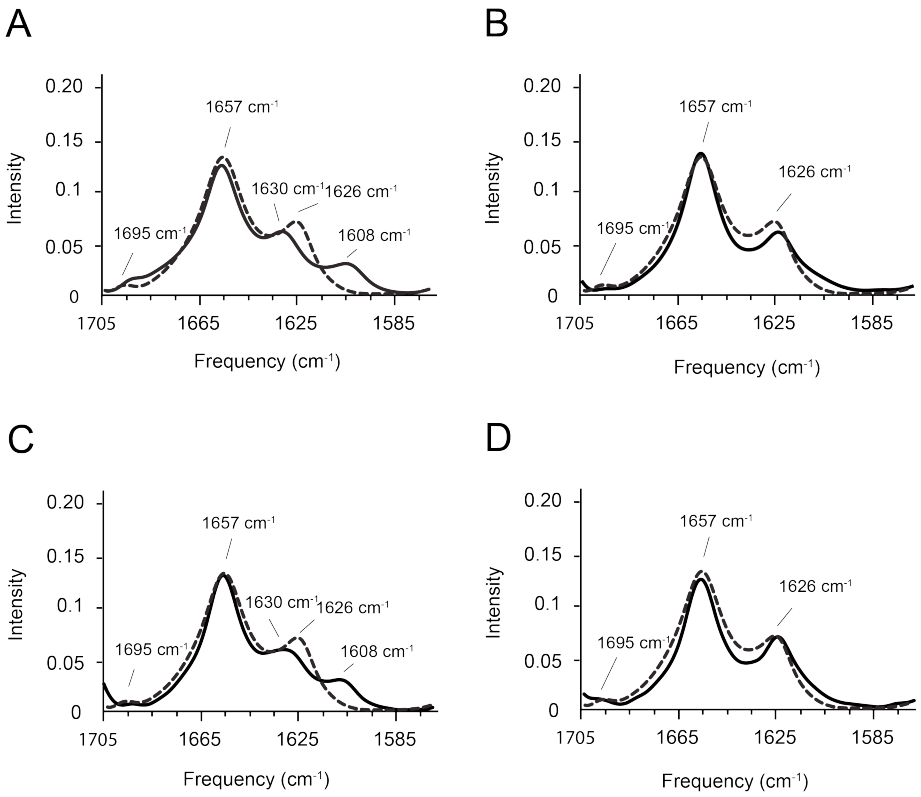

Figure 5-3. FTIR spectra of wild-type and A21G C55 in DMPC: DMPG bilayers with stable isotope editing. FTIR spectra of unlabeled wild-type C55 is presented in dashed lines in panel (A)-(D). Comparison of the FTIR spectrum of unlabeled wild-type C55 with the wild-type C55 containing selectively ^{13}C labeled amino acids (solid lines in A and C), and the A21G C55 containing selectively ^{13}C labeled amino acids (solid lines in B and D). The wild-type C55 is selectively labeled with U-^{13}C Phe19 in (A) and U-^{13}C Phe20 in (C). Similarly, the A21G C55 is selectively labeled with U-^{13}C Phe19 in (B) and U-^{13}C Phe20 in (D). The molar ratio of the DMPC:DMPG was 10:3, and the molar ratio of peptide to total lipid was 1:50.

5.2.4 The A21G mutation reduces the propensity of local β-sheet structures in membrane bilayers on Phe19 and Phe20

Solid-state NMR is complementary to FTIR spectroscopy and allows us to probe the local secondary structure in the region of Ala21. Figure 5-4 presents two-dimensional magic angle spinning (MAS) NMR spectra of C55 obtained with dipolar assisted rotational resonance (DARR). MAS increases spectral resolution of membrane proteins in bilayer environments by averaging the chemical shift anisotropy and dipolar interactions. DARR reintroduces the dipolar interaction between labeled ^{13}C sites [52]. As with the FTIR studies described above, an advantage of using C55 over C99 for structural studies is that the peptide is short enough to synthesize by solid-phase methods, which allows site-specific incorporation of ^{13}C isotope labels. Figures 5-4 A present the full spectra and selected regions of the 2D spectra in which the wild-type and A21G peptides in bilayers are overlaid. Uniform ^{13}C labeling of the amino acids allows us to readily assign the spectrum because directly bonded ^{13}C-atoms yield strong cross peaks in the 2D spectrum. Figures 5-4 B shows the region of aliphatic carbons of side chains of wild-type C55 overlaid with A21G C55 in membrane bilayers. Interestingly, the Val24 Cβ of A21G C55 shifts ~ 4 ppm to lower frequencies with a more intense cross peak (e.g. from Cβ and C=O) that implies a transition from random-coil or β–structure to more rigid or α-helical structure upon mutation. The shifting to lower frequencies values of Cβ (i.e. negative bars) corresponds to higher α-helical secondary structure propensity. Cross peak from Val24 Cα and Gly25 Cα observed in wild-type C55 is missing (or with much lower intensity) upon A21G mutation which also implies a local structure change from extended to more rigid conformation in this region. To further identify this observation, a series of ^{13}C labeled amino acids are incorporated into both sequence of wild-type C55 and A21G C55 for comparison of a local structure rearrangement.

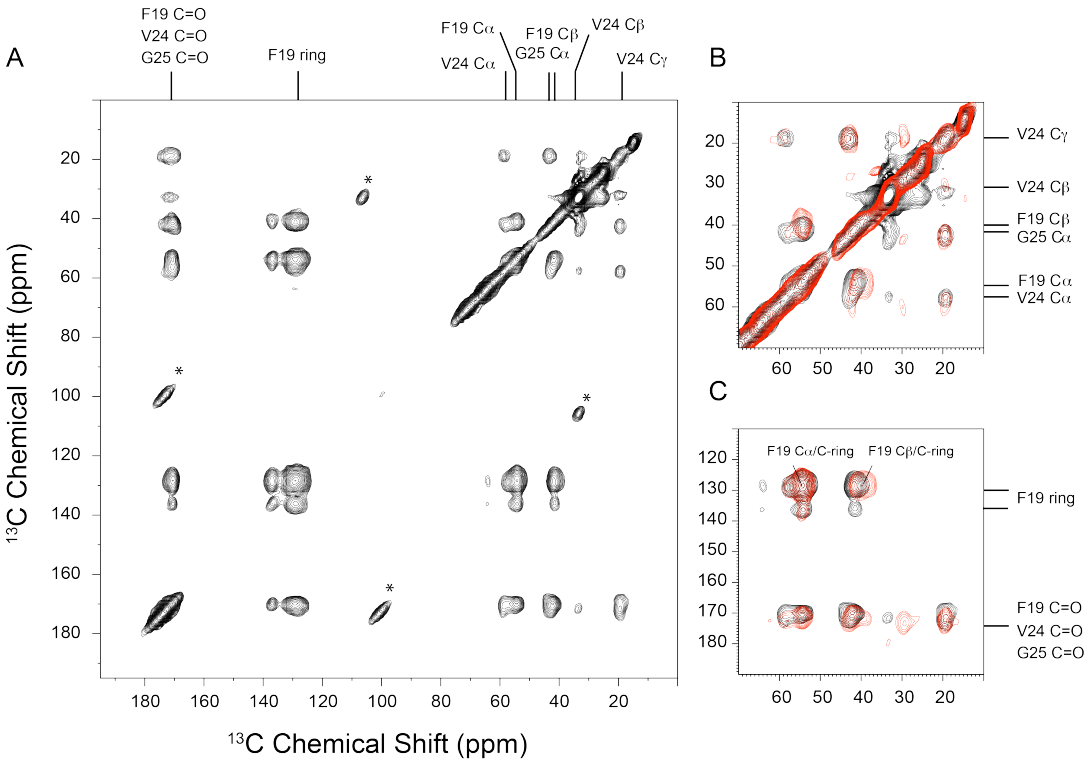

Figure 5-4. 2D DARR spectrum of wild-type C55 and A21G mutant in membrane bilayers. (A) Overlap of the 2D DARR spectrum of wild-type C55 (black) and the A21G mutant (red) with U-^{13}C Phe19, Val24, and Gly25. (B) Overlap of the aliphatic sidechain of wild-type C55 (black) and the A21G mutant (red) with uniformly-^{13}C Phe20, and Gly29. (C) Overlap of the carbonyl region of wild-type C55 (black) and the A21G mutant (red)

Figure 5-5 A presents the carbonyl region of the 2D spectrum of C55 containing ^{13}C-labeled amino acids at Phe19, Val24 and Gly25. The C=O resonances of Phe19 and Gly25 both contribute to the shoulder observed in the 1D spectrum (top of panel A) and shift to higher frequency in the A21G mutant. Figure 5-7 B presents the carbonyl region of the 2D spectrum of C55 labeled at Phe20 and Gly29. In this case, the C=O resonance of Phe20 makes the major contribution to the low frequency shoulder at ~170 ppm, which shifts to higher frequency in the A21G mutant. The Gly29 C=O resonance is observed at ~175 ppm and does not change in the A21G mutant. The higher frequency of the Gly29 chemical shift is consistent with α-helical secondary structure, while the change of the Phe19, Phe20 and Gly25 chemical shifts to higher frequency is consistent with a decrease in β-structure and increase in α-helical structure [(66)].

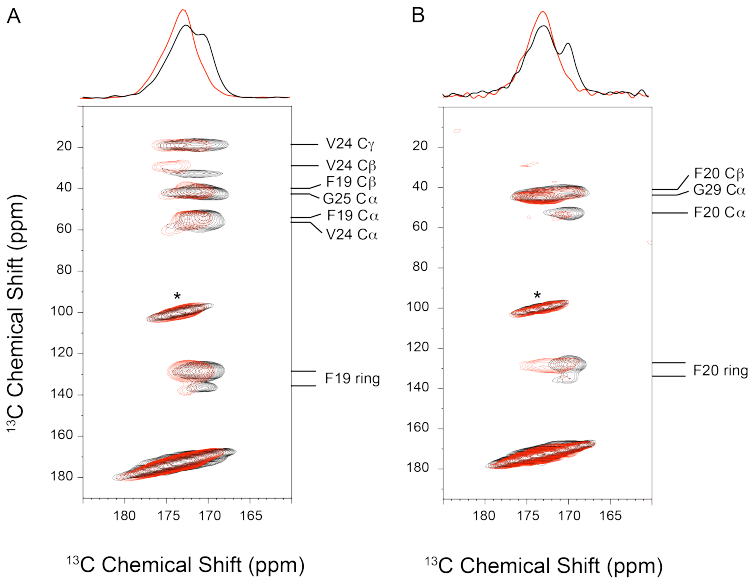

Figure 5-5. Carbonyl region of 2D DARR spectrum of wild-type C55, and A21G labeled with Phe19 and Phe20. (A) Overlap of the carbonyl region of wild-type C55 (black) and the A21G mutant (red) with U-^{13}C Phe19, Val24, and Gly25. The 1D CP spectra of carbonyl region are shown at the top of the 2D plot. (B) Overlap of the carbonyl region of wild-type C55 (black) and the A21G mutant (red) with uniformly-^{13}C Phe20, and Gly29. The 1D CP spectra of carbonyl region are shown at the top of the 2D plot.

Figure 5-6 A and B summarizes the chemical shifts of the Cα and C=O resonances between Leu17 and Ile31 of wild-type (in black) and A21G C55 (in red). The chemical shifts are plotted as differences from the average chemical shifts of these resonances. The deviations to lower chemical shift values of Cα and C=O (i.e. negative bars) correspond to β-sheet secondary structure. The deviations to higher chemical shift values of Cα and C=O (i.e. positive bars) correspond to α-helical secondary structure. For wild-type C55, the Cα and C=O resonances between Leu17 and Ala21 all exhibit negative deviations corresponding to β-strand or sheet structure. The observation of β-structure is consistent with the FTIR results, but contrasts with solution NMR structures previously determined of this region [45, 68]. Mutation to A21G results in less negative deviations of both the Cα and C=O chemical shifts (in red bar) suggesting that there is a reduction in β-structure. Gly29 and Ala30 both exhibit positive deviations consistent with the helical TM domain beginning at Lys28. Mutation to A21G does not alter these latter chemical shifts in TM domains. The two residues probed between the LVFF region and the TM domain – Val24 and Gly25 – exhibit negative shifts in wild-type C55 and positive shifts in the A21G mutant, suggesting a change in the local secondary structure from β-strand or random coil to α-helix in this region that is consistent with the observation of aliphatic side chain in Figure 5-6 B and C.

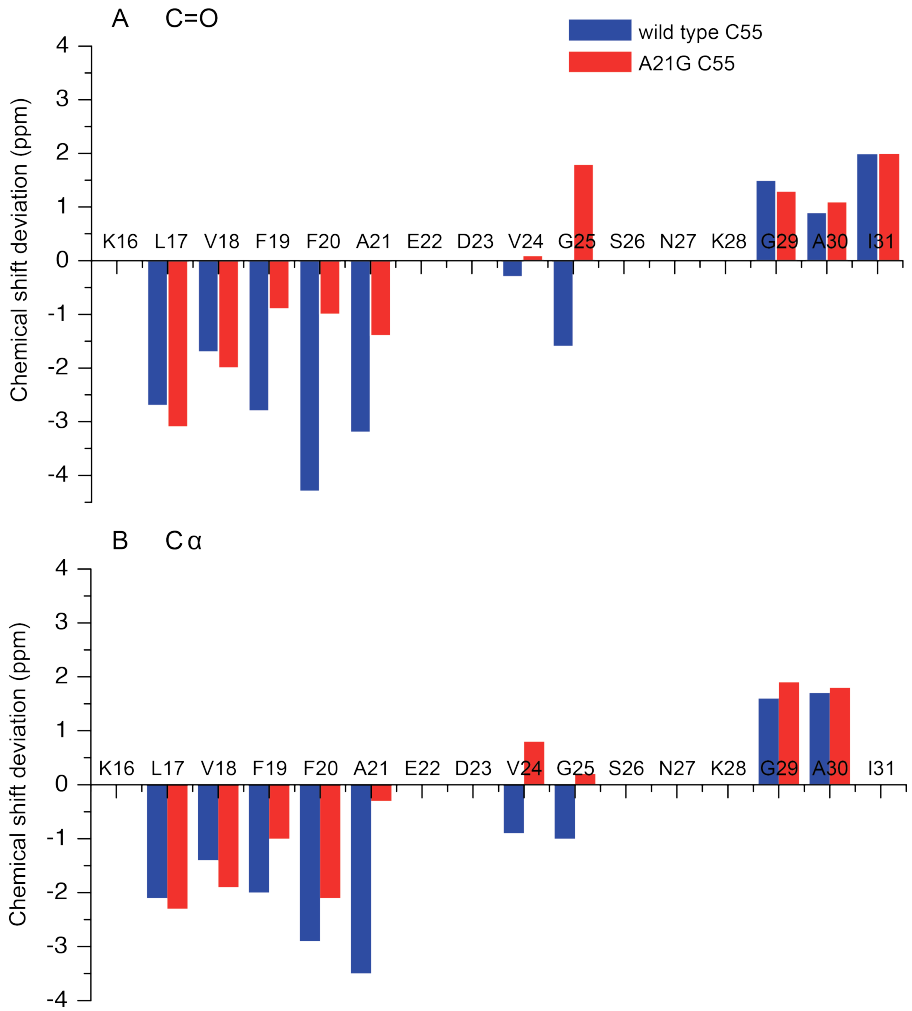

Figure 5-6. Chemical shift deviation of wild-type C55 and A21G mutant from average values (A) ^{13}Carbonyl chemical shifts deviation from average values. (B) ^{13}Cα carbon chemical shifts deviation from average values. The average chemical shift values are taken from the BMRB database (http://www.bmrb.wisc.edu/ref_info/statful.htm). The deviations to lower chemical shift values (i.e. negative bars) correspond to β-sheet secondary structure. The deviations to higher chemical shift values (i.e. positive bars) correspond to α-helical secondary structure.

5.2.5 The A21G mutation increases the helical character of the VGSNK sequence

The conclusion that the region between Gly25 and Gly29 increases in helical secondary structure in the A21G mutant is supported by DARR measurements of dipolar couplings between these two residues. Figure 5-7 presents DARR NMR spectra of the wild-type (black) and A21G C55 (red) isotopically labeled at Gly25 (^{13}C=O) and Gly29 (^{13}Cα). The distance between the ^{13}C=O Gly25 and ^{13}Cα Gly29 carbons is ~5.3 Å when this region adopts α-helical secondary structure, but considerably longer when this sequence is extended. The 5.3 Å distance is marginally within the ~6 Å distance range of the DARR experiment. Comparison of the two spectra shows the appearance of the cross peak (indicated by the arrow) correlating the ^{13}C=O Gly25 and ^{13}Cα Gly29 resonances in the A21G mutant. The cross peak intensities were normalized on the basis of the intra-residue cross peak intensity in U-^{13}C Leu17, also present in the sample. Taken together, the appearance of the cross peak in A21G C55 is consistent with the downfield (higher frequency) chemical shifts (higher frequency) of Gly25 C=O and suggest that Gly25 CO – Gly29 Cα folding into a α-helical structure upon mutation. The upfield chemical shift of Gly25 Cα argues that the extended TM helix starts from Gly25 but not Val24.

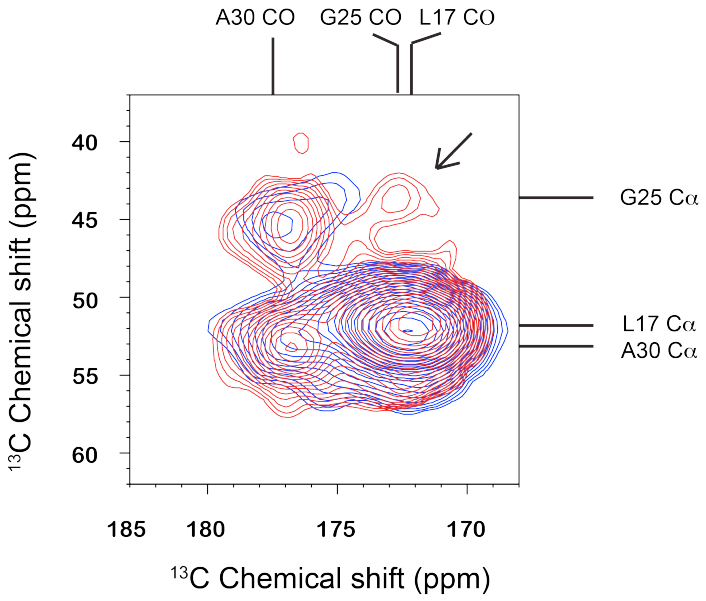

Figure 5-7. The carbonyl-Cα region of 2D DARR spectrum of wild-type C55, and A21G mutant for interhelical contacts. 2D DARR NMR spectra showing intra-helical contacts between Gly25 and Gly29 induced with the A21G mutation. The spectra of wild-type C55 (blue) and A21G C55 (red) in DMPC: DMPG bilayers are shown. The peptides are labeled with ^{13}C=O labeled Gly25 and ^{13}Cα labeled Gly29. The inter-residue cross peak between the Gly25 C=O and Gly29 Cα indicates the formation of helical secondary structure in the A21G peptide (arrow). Additional labels are observed from ^{13}C labeled Leu17 and U-^{13}C-labeled Ala31. The cross peak from the intra-residual ^{13}C carbonyl and ^{13}Cα of Leu17 is used to normalize two spectrum. The ratio of peptide to total lipid is 1: 50. The carbonyl-Cα cross peak regions show the overlapping of intra-residue cross peaks from Leu17 and Ala30 plus the inter-residue cross peaks from Gly29 Cα to Gly25 and Ala30 carbonyl.

5.2.6 Both dimerization of wild-type and A21G C55 is mediated by a GxxxG interface

In membrane proteins glycines are abundant in TM helices, and the GxxxG sequence is well known to be a dimerization motif [72]. The TM region of APP is unusual in containing three consecutive GxxxG motifs. The A21G mutation generates a fourth consecutive GxxxG motif in the extracellular sequence. Observation that the helical secondary structure increases in the region between Gly25 and Gly29 in the A21G mutant raises the possibility that the helical $G^{25}xxxG^{29}$ motif can further stabilize TM dimer of C55.

Previously, 2D DARR NMR experiments were designed to test if either of these dimer interfaces exists in wild-type C55 (in Figure 4-8). These experiments involve co-mixing of two different peptides and cross peaks in the 2D spectra are only observed between heterodimers (e.g. two different ^{13}C labeled C55 peptides), which at most can represent 50% of the total population of dimers. Similarly, ^{13}C labels were selectively incorporated at Gly33 and Ala42 in two A21G C55 peptides. The first peptide is labeled with ^{13}C=O Gly33 and $^{13}C\beta$ Ala42, and the second peptide is labeled with $^{13}C\alpha$ Gly33 and ^{13}C=O Ala42. In a complex of the two peptides, the Gly33 residues would be closely packed if the $G^{33}xxxG^{37}$ motif lines the dimer interface, whereas the Ala42 residues would be in close proximity if the $G^{38}xxxA^{42}$ motif mediates dimerization.

Two A21G C55 peptides were reconstituted into POPC: POPS membranes in equimolar amounts. A parallel reconstitution was carried out with two A21G C55 peptides. Figure 5-8 A presents the full DARR spectrum of wild-type C55 (in black; the same as in Figure 4-8 A) overlaid with the spectrum of the A21G mutant (red). In both the wild-type and A21G C55 peptides, cross peaks are observed between Gly33 ($^{13}C\alpha$)-Gly33 (^{13}C=O) (in red box), but not between Ala42 ($^{13}C\beta$) - Ala42 (^{13}C=O) labels (in

blue). No intensity was observed at this position in DARR spectra of the single peptides containing the ^{13}C=O Gly33 and ^{13}Cβ Ala42 labels or the ^{13}Cα Gly33 and ^{13}C=O Ala42 labels. The cross peak from Gly33 (^{13}Cα)-Gly33 (^{13}C=O) was only observed when the two peptides were mixed. These results indicate that in membrane bilayers both wild-type and A21G C55 associate via the GxxxG motif in the TM domain, rather than the GxxxA motif observed in detergent micelles.

The appearance of the Gly33 (^{13}Cα) -Gly33 (^{13}C=O) cross peaks provides a qualitative measure of dimerization. The intensity of the cross peak can be related to inter-nuclear distance, or in the case of a monomer-dimer equilibrium to the amount of dimeric peptide in the same experimental conditions. Figure 5-8 B presents rows from the 2D DARR spectra illustrating the intensity difference in the Gly33-Gly33 cross peak between the wild-type and A21G peptides. The cross peak intensity goes up ~1.4 fold suggesting a corresponding shift from monomer to dimer in the A21G mutant of C55. DARR spectrum have different resolution on the direct (2k) and indirect dimension (128). The spinning sidebands are aliased and fold back only clearly shown on the second dimension.

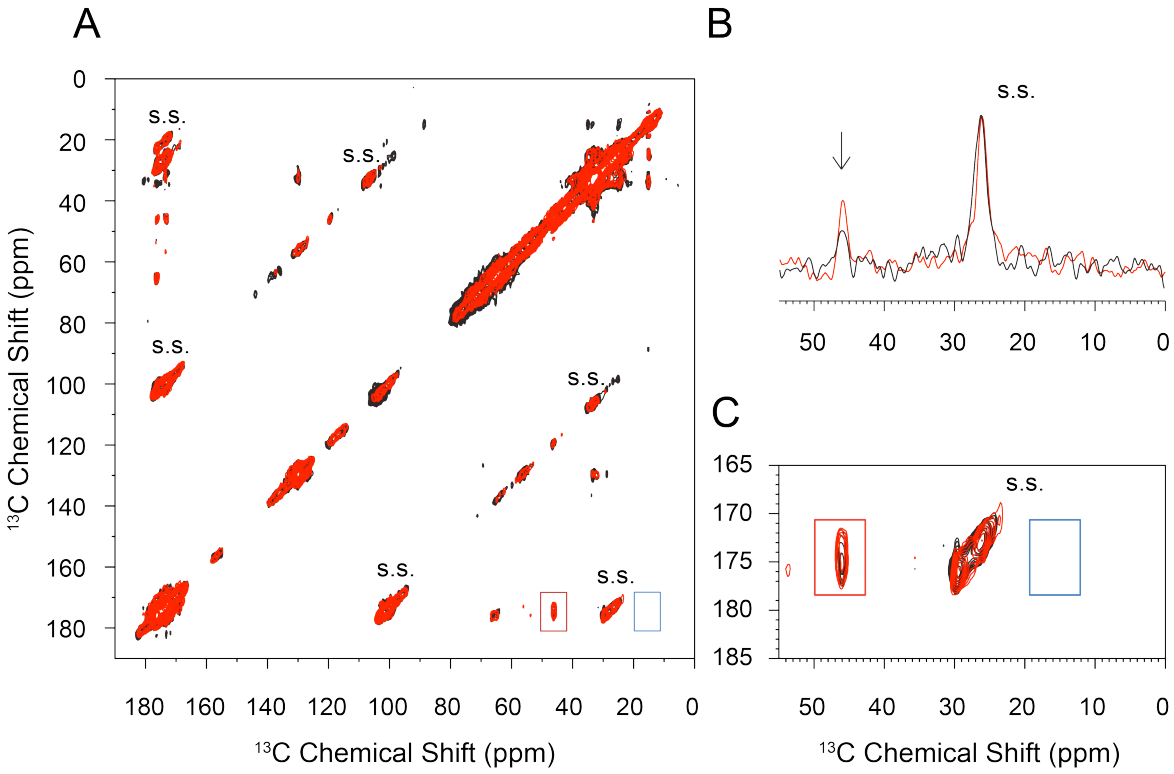

Figure 5-8. 2D DARR NMR spectra of the wild-type and A21G C55 in bilayers to test two putative homodimeric interfaces, $G^{29}xxxG^{33}xxxG^{37}$ or $G^{38}xxxA^{42}$ motifs. Two peptides are selectively ^{13}C labeled at Gly33 and Ala42. The first peptide is labeled with ^{13}C C=O labeled Ile31, ^{13}C C=O labeled Gly33, and ^{13}C Cβ labeled Ala42, and the second peptide is labeled with ^{13}C Cα labeled Gly33, and ^{13}C C=O labeled Ala42. Two wild-type C55 peptides are mixed in equal molar amounts, and reconstituted into POPC: POPS bilayers. The peptide-to-lipid ratio is 1: 50. (A) The DARR spectra of mixed wild-type C55 peptides (in black) and A21G C55 (in red) are shown. Only cross peaks resulting from Gly33 resonances on different peptides (i.e. Gly33 Cα to Gly33 carbonyl in red box) are observed for both wild-type C55. Cross peaks are not observed between resonances associated with Ala42 on different peptides (i.e Ala42 Cβ to Ala42 carbonyl, blue box). (B) 1D rows through the Gly33 carbonyls. (C) 2D carbonyl region of DARR spectrum. S.S. stands for the spinning sideband. Cross peak at ~ 66 ppm, ~ 32 ppm and ~ 25 ppm are assigned to the ^{13}C nature abundance of lipid head group and acyl chain.

5.3 Discussion

The A21G mutation involves the loss of a single methyl group in the extracellular sequence of the APP protein, but has a strong influence on intramembranous processing by the γ-secretase complex. We address how the A21G Flemish mutation alters the structure of the extracellular region and TM domain using FTIR and NMR spectroscopy, and propose how these changes are linked to processing of the β-CTF. FTIR and NMR measurements of wild-type C55 in membrane bilayers (in Chapter 4) provide evidence that β-strand or sheet secondary structure, rather than helical structure, is adopted in the extracellular region of the β-CTF. The A21G mutation influences both the upstream LVFF sequence, particularly Phe19 and Phe20, the downstream $G^{25}SNKG^{29}$ sequence and TM dimerization. These data emphasize the ability of glycine to destabilize β-sheet structure [(73)] and to stabilize TM dimers through GxxxG motifs [(72)].

5.3.1 The structure of APP near the region of A21G regulates processing

The genetic Flemish mutation (A21G) was first described by Hendriks *et al.* [(34)] and later shown to lead to an increase in Aβ production (1.3-2 fold) [(33)]. Tian *et al.* [(26)] found that the LVFFAED region in the extracellular domain of the β-CTF was inhibitory to the activity of γ-secretase. They observed that deletion of this seven-residue sequence resulted in a 25-fold increase in secreted Aβ40 compared to a 4-fold increase in total secreted Aβ for the A21G mutant [(26)]. In contrast, the mutations at Glu22 and Asp23 do not influence Aβ secretion. The different ratio of α–CTF/ β-CTF between the wild-type and A21G indicates the α–or β-cleavage can influence the Aβ secretion from full-length APP (Figure 5-1). To monitor the Aβ secretion directly released from the γ–cleavage, DNA construct of β-CTF are transfected into CHO cell lines and the secreted peptides in medium are measured. To more directly test the role of the hydrophobic LVFF sequence

in regulating Aβ secretion, we substituted LVFF to Alanines with a smaller side chain and found that the mutation increases Aβ secretion (Aβ40 and Aβ42) ~4.5-fold from β-CTF, considerably less than the increase observed when the sequence is deleted, but much greater than the ~1.7 fold increase due to the A21G mutation (in Figure 5-2). Although both A21G and LVFF to AAAA mutations increase the processing from full-length APP and β-CTF, the total secretion and Aβ42/Aβ40 ratio are essentially different. The Aβ production difference between full-length APP and β-CTF is known for its distinct sorting pathways under differentially post-translational modification in the extracellular sequence *(74)*.

Our studies show that Ala21 is at the edge of the β-sheet fold in the extracellular domain of the β-CTF. The FTIR measurements show only modest changes in the 1626 cm^{-1} band upon mutation of Ala21 to glycine. In contrast, the A21G mutation results in large changes in the chemical shifts at Phe19, Phe20 and Gly25 consistent with unraveling of the β-sheet structure at the end of the LVFF sequence and the formation of helical secondary structure in the $G^{25}SNKG^{29}$ sequence. Mutation of Ala21, but not the adjacent Glu22 and Asp23 residues, induces structural changes in the hydrophobic LVFF sequence and TM-JM junction sequences, VGSNK. For example, solid-state NMR measurements of the Dutch (E22Q) and Iowa (D23N) mutants containing ^{13}C=O labeled Gly25 do not exhibit the large chemical shift change as observed in the A21G mutant (in Figure 5-8 below). These changes are consistent with the substitution of Ala21 with hydrophobic residues (Leu and Phe), which reduce Aβ secretion, and charged residues (Glu and Lys), which overall tend to increase Aβ secretion (the detailed discussion is shown in Figure 5-9). Taken together, these results link how the β-structure change of LVFFA can influence the intramembranous γ–cleavage.

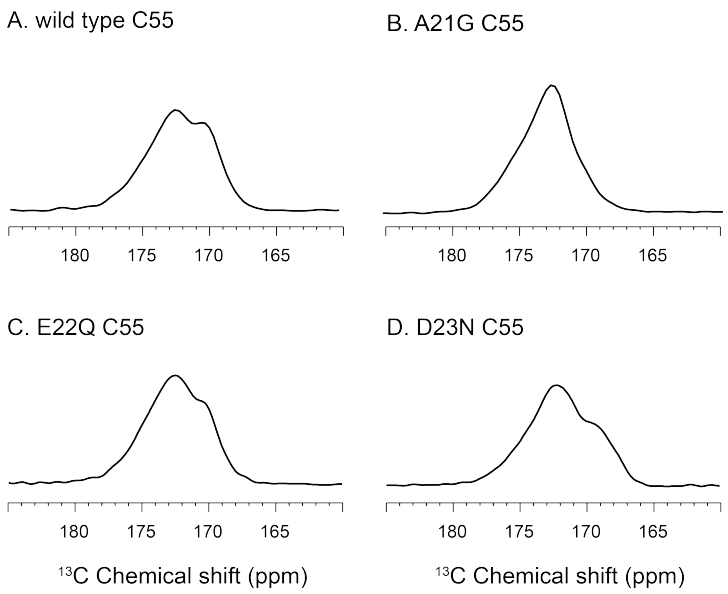

Figure 5-9. One-dimensional MAS CP NMR spectra wild-type C55 and C55 with the A21G, E22Q and D23N mutations. The region of the ^{13}C carbonyl resonances is shown for comparison. In each case, the C55 peptide was labeled at U-^{13}C Phe19, Val24, and Gly25. The shoulder observed in wild-type C55 at ~170 ppm has contributions from the C=O resonances of Phe19 and Gly25, which both shift to ~173 ppm in the A21G mutant. In contrast, these resonances do not change appreciably in the E22Q or D23N mutants.

5.3.2 Both wild-type and A21G C55 dimerize through the GxxxG interface

The observation that the A21G mutation introduces an additional extracellular GxxxG motif into the β-CTF and that the $G^{25}xxxG^{29}$ sequence becomes more helical suggests that the A21G mutation influences dimerization of the TM domain of the protein. Complementary studies involving the mutation of the consecutive $G^{29}xxxG^{33}xxxG^{37}$ motifs support the idea that dimerization of the TM domain of the β-CTF influences processing [21, 23]. Nevertheless, the question of whether the GxxxG motifs are involved in dimerization and how they might change upon mutation has not been conclusive. Recently, Arseniev and coworkers determined the dimer structure of residues Gln15-Lys53 in detergent micelles [68]. The dimer interface in the solution NMR structure is formed from the $G^{38}xxxA^{42}$ sequence rather than $G^{29}xxxG^{33}xxxG^{37}$. The GxxxA interface was previously suggested in several studies [21, 25].

In our structure data, we show clearly that the A21G C55 is mediated by the $G^{33}xxxG^{37}$ interface but not $G^{38}xxxA^{42}$ motif. The strong cross peak between Gly33 Cα and Gly33 C=O observed upon mixing two labeled peptides can only be explained by a well-defined dimer structure. This result is similar to that obtained for the wild-type TM region alone (in Chapter 3) and C55 (in Chapter 4) where the $G^{29}xxxG^{33}xxxG^{37}$ motif mediates the TM homodimerization [20]. The observation that the A21G mutation does not change the dimer interface and increases the dimerization strength with the stronger cross peak implies the large influence of the mutation on processing is associated with the structural changes in the extracellular domain. Coincidently, these results support the conclusions of Tian *et al.* [26] that the LVFFAED sequence is inhibitory.

5.3.3 Extension of β-structure character by Ala21 mutation leads to the decreased total secretion of Aβ peptides

In Figure 5-9, we highlighted the critical position of Ala21 between the hydrophobic $L^{17}VFF^{20}$ sequence, which results in an increase in Aβ production upon mutation, and the charged Glu22–Asp23 sequence, which does not result in large changes in Aβ secretion upon mutation. Ala21 is mutated to hydrophobic residues (Leu and Phe) or charged residues (Glu and Lys). The mutation of Ala21 to Leu or Phe reduces Aβ40 and Aβ42 production consistent with the hydrophobic character of these residues inhibiting the γ-secretase complex activity. In contrast, substitution of Ala21 with Glu similar to the downstream ED sequence, does not significantly affect Aβ40 secretion, although increases Aβ42 and decreases Aβ38 secretion. This is consistent with the observation that the familial Dutch (E22Q) and Iowa mutations (D23N) largely do not influence APP processing. More substantial changes are observed upon substitution of Ala21 with lysine (A21K), which increases Aβ40 secretion (~ 1.2 times) and results in larger increases in Aβ38 (~ 1.7 times) and Aβ42 secretion (~ 1.7 times).

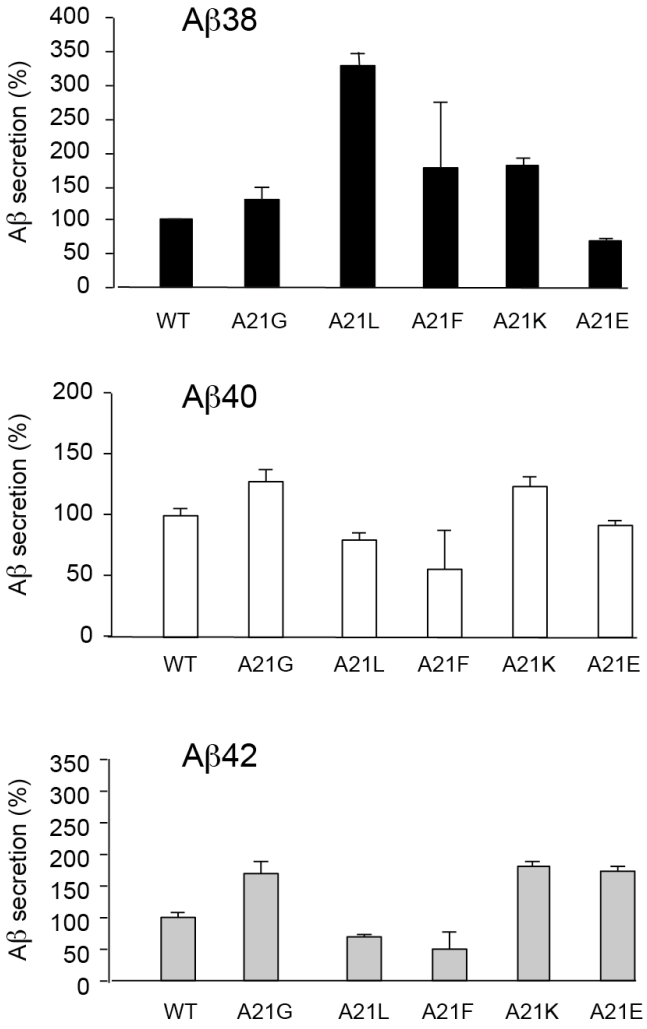

Figure 5-10. Influence of Aβ processing upon substitution of Ala21 with hydrophobic and charged residues. The A21F and A21L mutations, which replace Ala21 with a hydrophobic residue extend the upstream $L^{17}VFF^{20}$ hydrophobic sequence, reduce Aβ40 and Aβ42 production. The A21E mutation replaces Ala21 with a residue identical to the following Glu22. A21E largely does not affect Aβ40 secretion, although increases Aβ42 and decreases Aβ38 secretion. A21K slightly increases Aβ40 secretion and results in larger increases in Aβ38 and Aβ42.

5.4 Conclusions

Proteolysis of the β C-terminal fragment (β-CTF) of the amyloid precursor protein generates the amyloid β (Aβ) peptides associated with Alzheimer's disease. Familial mutations in the extracellular sequence of the β-CTF, such as the A21G Flemish mutation, can influence intramembraneous cleavage by γ-secretase and increase Aβ peptide secretion. We address how the Flemish mutation alters the structure of C55, the first 55-residues of the β-CTF, using solid-state NMR and Fourier transform infrared spectroscopy. We show that in membrane bilayers the extracellular sequence from Leu17 to Ala21 has β-secondary structure and that the transmembrane region is helical starting at Gly29. The familial A21G mutation reduces the β-structure near the site of the mutation and increases α-helical structure in the region from Gly25 to Gly29 at the junction between the extracellular and transmembrane domains. These changes are correlated with an overall increase in the production of Aβ peptides.

Chapter 6. Structural variation caused by adding cholesterol into lipids

6.1 Introduction

As with the A21G mutation, the presence of cholesterol and cholesterol-rich domains is linked to Aβ secretion by influencing the cellular events of β-secretase cleavage, γ-secretase activity and the level of secreted Aβ [(45)]. Depletion of cholesterol inhibits the γ-secretase activity and Aβ secretion, while addition of cholesterol enhances the processing of γ-secretase [(46, 47)]. The influence of cholesterol can be in many aspects.

For instance, γ-secretase is found in lipid-raft microdomain and cholesterol can interact with β-CTF [(63)].

Previous structure studies in detergent/lipids mixtures by Barret P. *et al.* proposed that a cholesterol-binding site was identified in the juxtamermbrane region of β-CTF between the extracellular and transmembrane domains [(63)]. Residues that appear sensitive to cholesterol binding include Phe20, Glu22 and Gly33. Phe20 is the last residue in the $L^{17}VFF^{20}$ sequence. Glu22 is a site of familial mutation that is adjacent to Ala21 and Asp23, also sites of FAD mutations. Gly33 is part of the GxxxG sequence close to the N-terminus of TM domain that has been implicated in mediating TM helix dimerization of the β-CTF in membrane bilayers.

In my study, I target the structural changes in the extracellular domain of the β-CTF arising from the A21G mutation and compare the changes with those caused by incorporating cholesterol into model membranes. Fourier transform infrared (FTIR) and solid-state NMR measurements are made on C55, corresponding to the first 55 residues of the β-CTF, which includes the extracellular and transmembrane regions of the protein. Peptides are reconstituted into in three different model membrane bilayers, e.g. saturated C14 acyl chain lipid (DMPC: DMPG), single unsaturated C18 acyl chain lipid (POPC: POPS) (i.e. unsaturated C18 acyl chain lipid is enriched in neuronal and CHO cells reported by *Spector et al*.) and POPC: POPS: Cholesterol (i.e. 28.5 molar % of cholesterol is used in our structure studies that is comparable to cholesterol composition in neuronal cell membranes according to *R. O. Calderon et al., 1995* [(75)]). In Chapter 4 and Chapter 5, we show that the transmembrane region in wild-type C55 is helical through Gly29 and that the extracellular sequence at least from Leu17-Ala21 has β-type structure. Upon the A21G mutation, the transmembrane domain extends one helical turn up to Gly25 in DMPC: DMPG bilayers, and the β-structure in the extracellular sequence from Leu17-Gly21 is reduced. Here, we show that the influence of the incorporation of cholesterol into bilayers on structure and processing is similar to that caused by the A21G mutation.

6.2 Results

6.2.1 Cholesterol-rich bilayers increase the helicity of the transmembrane domain of wild-type C55

Both familial mutations and cellular environmental factors are known to influence the Aβ generation. For example, a higher concentration of serum cholesterol has been statistically observed as a risk factor for Alzheimer's disease [42]. Hypercholesterolemia leads to an increase in Aβ deposition and intraneuronal accumulation of toxic Aβ oligomers in transgenic mice [43, 44]. Solution NMR studies suggest that cholesterol interacts with the β-CTF in the juxtamembrane boundary between the extracellular and TM domains in micelles or detergent/lipid mixtures [63]. On the basis of our previous observations in the A21G mutation (in Chapter 5), we investigated the possibility that cholesterol may influence the structure of the extracellular region and TM domain of the β-CTF.

Figure 6-1 presents FTIR and solid-state NMR measurements of ^{13}C-labeled C55 peptides reconstituted in POPC: POPS bilayers with and without cholesterol added. In the amide I region of the FTIR spectra, there is an obvious increase in the 1657 cm^{-1} band relative to the 1626 cm^{-1} band upon the addition of cholesterol, i.e. an integration ratio of the deconvoluted peak at 1657 cm^{-1} to the peak at 1626 cm^{-1} is 2.4 to 1 in POPC (A) and POPC: POPS (B) to 3.2: 1 in POPC: POPS: cholesterol (C). This raises the possibility that addition of cholesterol can induce the extended TM helix formation and/or reduced β–structure observed as that in A21G mutation. In the NMR spectra of C55, the addition of cholesterol to POPC: POPS bilayers results in a downfield (higher frequency) shift and broadening of the C=O resonance of Gly25 without influencing the carbonyl chemical shift of Phe19. This observation is consistent with a shift to more helical structure in the

region of Gly25 and adding cholesterol has marginal effect on the extracellular β–sheet structure.

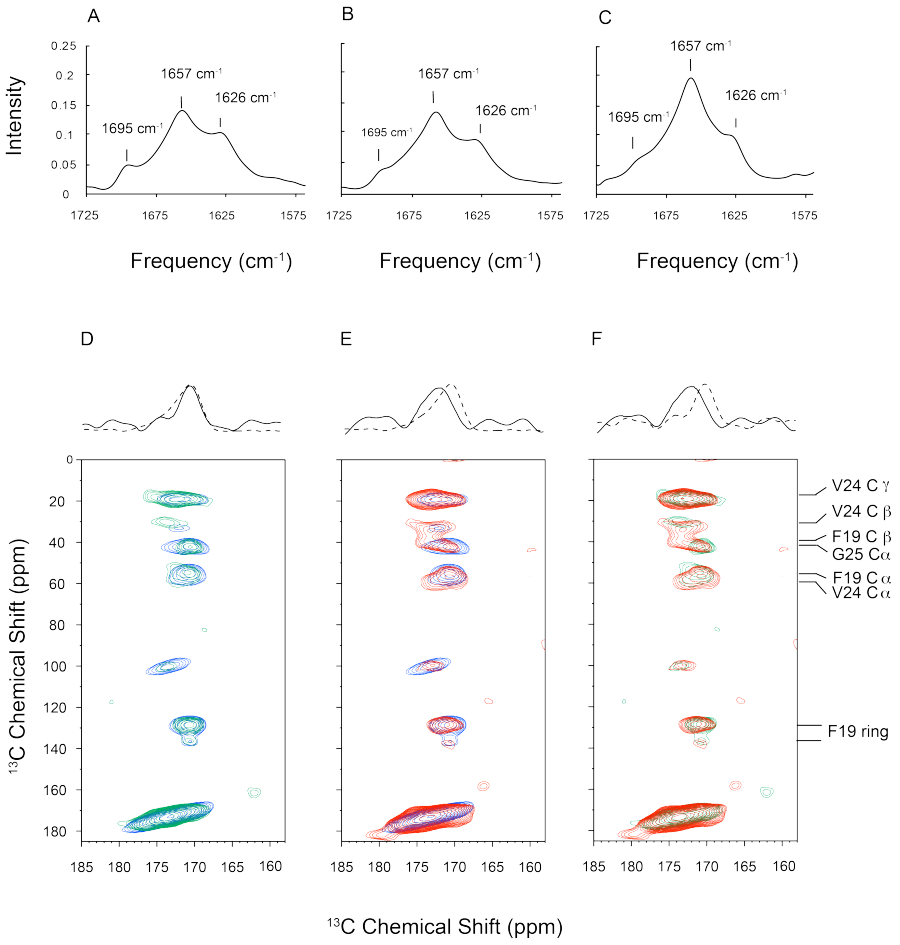

Figure 6-1. FTIR measurements and NMR spectrum have been undertaken of C55 reconstituted in membrane bilayers with and without added cholesterol. Comparison of polarized FTIR spectra of wild-type C55 reconstituted into POPC (A), POPC: POPS (B) and POPC: POPS: cholesterol (C). The spectrum in the amide I stretching region are shown after subtraction of the corresponding lipid backgrounds. The molar ratio of POPC: POPS was 10:3, the molar ratio of POPC: POPS: cholesterol was 10:3:5.2. The molar ratio of C55: total lipid was 1:50. (D-F) NMR spectra of the carbonyl region of C55 labeled with U-^{13}C Phe19, Val24, and Gly25 in three different lipid compositions. (D) Spectra of C55 in POPC (blue) and POPC: POPS (green) are overlapped. On top of the 2D spectrum are the overlapped 1D rows through Gly25 (solid line, POPC: POPS; dashed line, POPC). (E) Spectra of C55 in POPC (blue) and POPC: POPS: cholesterol (red) are overlapped. On top of the 2D spectrum are the overlapped 1D rows through Gly25 (solid line, POPC: POPS: cholesterol; dashed line, POPC). (F) Spectra of C55 in POPC: POPS (green) and POPC: POPS: cholesterol (red) are overlapped. On top of the 2D spectrum are the overlapped 1D rows through Gly25 (solid line, POPC: POPS: cholesterol; dashed line, POPC: POPS). The NMR spectra highlight the downfield (higher frequency) carbonyl chemical shifts of Gly25 upon addition of cholesterol.

6.2.2 Increased helical secondary structure induced by adding cholesterol is supported by intra-helical DARR NMR measurement

Figure 6-2 presents the DARR spectra of wild-type C55 reconstituted in POPC: POPS (blue) and in POPC: POPS: cholesterol (red) bilayers. The peptides are labeled with ^{13}C=O labeled Gly25 and $^{13}C\alpha$ labeled Gly29 for wild-type and A21G C55. In Figure 6-2 A, the cross peak between the Gly25 carbonyl and Gly29 Cα carbon is only observed in the wild-type C55 in POPC: POPS: cholesterol. The appearance of the Gly25-Gly29 cross peak in the A21G mutant (in Figure 5-10) or the addition of cholesterol indicates that both conditions induce more TM helical structure of the C55 peptide.

The observation that both the A21G mutant and cholesterol both result in a Gly25-Gly29 cross peak raises the question whether these two different mechanism can act synergistically. Figure 6-2 B presents 2D DARR NMR spectra of the wild-type (blue) and A21G C55 (red) peptide in POPC: POPS: cholesterol bilayers also using the same ^{13}C labeling scheme. The frequency of Gly29 Cα shifts ~ 1.6 ppm to higher frequency (in red line) relatively to that of wild-type C55 (in black line). The intensity of the cross peak of the A21G mutant is ~1.5-fold higher in the cholesterol containing membranes consistent with a synergistic effect.

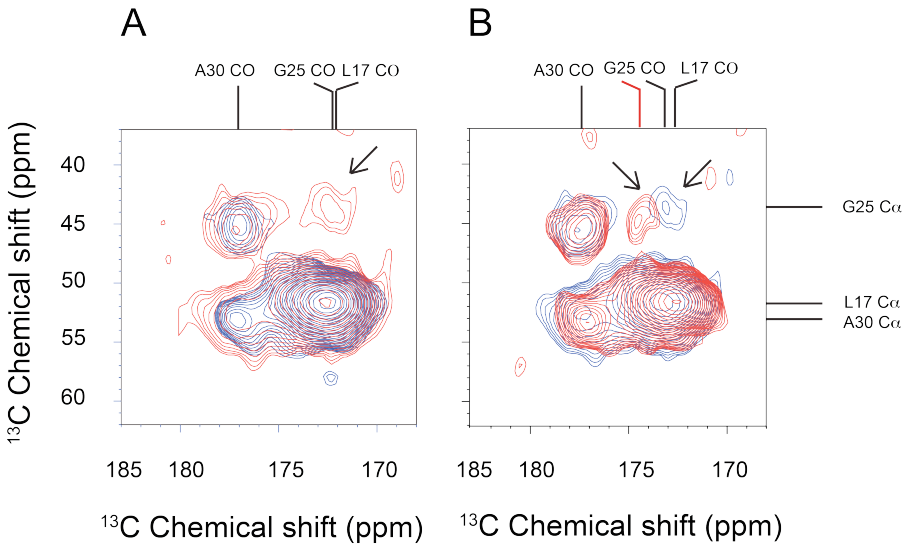

Figure 6-2. Carbonyl and Cα region of 2D DARR NMR spectra showing the intra-helical contacts between Gly25 C=O and Gly29 Cα in POPC: POPS and POPC: POPS: cholesterol lipid bilayers. The peptides are labeled with ^{13}C=O labeled Gly25 and ^{13}Cα labeled Gly29. The inter-residue cross peak between the Gly25 C=O and Gly29 Cα indicates the formation of helical secondary structure induced by the addition of cholesterol or A21G mutation (arrow). Additional labels are observed from 1,2 -^{13}C labeled Leu17 and U-^{13}C-labeled Ala31. The ratio of peptide to total lipid is 1: 50. (A) DARR spectrum of wild-type C55 in POPC: POPS (blue) and wild-type C55 in POPC: POPS: cholesterol (red). The cross peak from Gly25 carbonyl and Gly29 Cα is only observed in the wild-type C55 in POPC: POPS: cholesterol lipid bilayers. (B) 2D DARR NMR spectra of the wild-type (blue) and A21G C55 (red) peptide in POPC: POPS: cholesterol bilayers using the same ^{13}C labeling scheme as in (A). The carbonyl-to-Cα cross peak regions show the overlapping of intra-residue cross peaks from Leu17 and Ala31 plus the inter-residue cross peaks from Gly29 Cα to Gly25 and Ala31 carbonyls. The cross peak from G29 Cα to Gly25 carbonyl is observed on both the wild-type and A21G C55.

6.2.3 Adding cholesterol enhances the TM dimerization of wild-type and A21G C55 peptides in bilayers

We also investigated whether the addition of cholesterol influences the monomer-dimer equilibrium of the wild-type or A21G C55 peptides. Figure 6-3 presents a comparison of inter-helical Gly33-Gly33 dimer contacts in POPC: POPS membranes with and without adding cholesterol. Rows through the Gly33-Gly33 contact from 2D DARR spectra are shown for wild-type C55 (A and B) and the A21G mutant (C and D) reconstituted into bilayers. The cross peak at 46.2 ppm corresponds to the interhelical Gly33 (^{13}Cα) -Gly33 (^{13}C=O) cross peak. The cross peak intensity from wild-type C55 in POPC: POPS: Cholesterol in Figure 6-3 B is approximately the same (relative to the MAS Gly33 ^{13}C=O spinning sideband denoted by * that is used as an internal standard) as that for the A21G peptide in POPC: POPS membranes in Figure 6-3 C, indicating that the monomer-dimer equilibrium is approximately the same. When the A21G mutant is incorporated into POPC: POPS: cholesterol membranes (Figure 6-3 F), the cross peak intensity increases ~2-fold consistent with a shift to more dimer. Adding cholesterol on both cases (e.g. Figure 6-3 A to B and C to D) shows the same trend on the increasing intensity of the interhelical Gly33 (^{13}Cα) -Gly33 (^{13}C=O) cross peak suggesting more dimer formation in bilayers. 20 datasets are collected (with ns = 128 for each experiment). Signals (FID, free induction decay) are averaged and processed. The signal to noise ratios (S/N) for interhelical cross peaks are 4.6 (in Figure 6-3 A), 5.8 (in Figure 6-3 B), 7.2 (in Figure 6-3 C), 7.9 (in Figure 6-3 D), respectively.

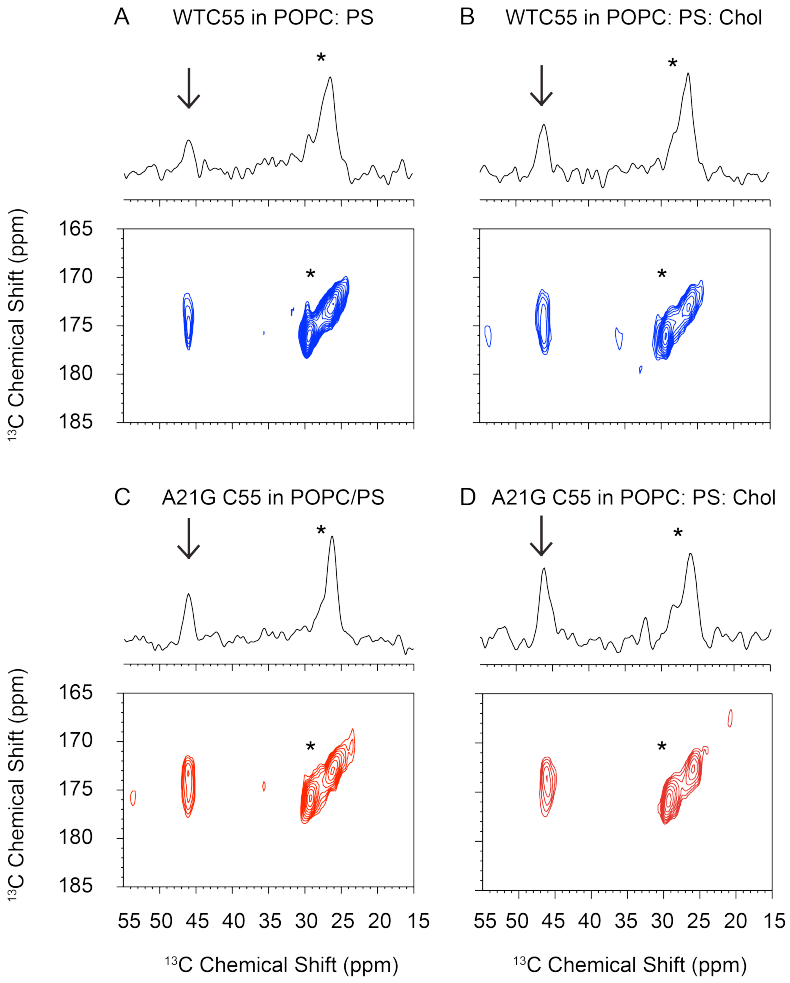

Figure 6-3: 2D DARR spectrum of wild-type C55 and A21G mutant for interhelical contacts in different bilayers. 2D DARR NMR spectra of the wild-type (A and B) and A21G C55 (C and D) in bilayers to test two putative homodimeric interfaces, $G^{29}xxxG^{33}xxxG^{37}$ or $G^{38}xxxA^{42}$ motifs. Two peptides are selectively ^{13}C labeled at Gly33 and Ala42. The first peptide is labeled with 1 -^{13}C labeled Ile31, 1-^{13}C labeled Gly33, and 3-^{13}C labeled Ala42, and the second peptide is labeled with 2-^{13}C labeled Gly33, and 1-^{13}C labeled Ala42. Two wild-type or A21G C55 peptides are mixed in equal molar amounts, and reconstituted into POPC: POPS (A and C) and POPC: POPS: cholesterol (B and D) bilayers. For both wild-type and A21G, only cross peaks resulting from Gly33 - Gly33 contact (i.e. Gly33 Cα to Gly33 carbonyl) are observed. Cross peaks are not observed between resonances associated with Ala42 (i.e Ala42 Cα to Ala42 carbonyl. 1D slices through Gly33 CO are presented on upper panel for each 2D DARR spectra and the cross peaks are indicated with arrows. The A21G C55 in POPC: POPS: cholesterol.

6.3 Discussion

6.3.1 The A21G mutation and cholesterol both increase Aβ production in a similar fashion

Many cellular factors appear to influence the processing of APP, the overall level of secreted Aβ peptides, and the Aβ42/ Aβ40 ratio. The presence of cholesterol and cholesterol-rich domains is linked to γ-secretase activity and the level of secreted Aβ [45]. Depletion of cholesterol inhibits γ-secretase and Aβ secretion, while addition of cholesterol enhances γ-secretase activity [46, 47]. Using γ-secretase functionally reconstituted into proteoliposomes, Selkoe and coworkers [48] found that the optimal cholesterol concentration for Aβ42 production was the same as that for Aβ40. This implies that cholesterol does not influence the Aβ42/ Aβ40 ratio which is similar to the effect observed for A21G APP mutant (Figure 5-1 D).

6.3.2 Cholesterol and the A21G mutation both increase TM helix and dimerization

Spingolipid or cholesterol-rich liquid ordered lipid, also known as lipid raft [49], have been proposed to be involved in several cellular functions or events, e.g. protein trafficking associated to Caveolae and protein-protein association in membrane bilayers [76]. In previous studies by Hecimovic *et al.* [77] showed that the accumulation of cholesterol in Neiman Pick type C (NPC) cells promotes the aggregation of APP or β-CTF in lipid ordered domains (raft) where the secreted Aβ peptides occurs. Here, we start to investigat whether a high concentration of cholesterol added into POPC: POPS model bilayers even without the formation of liquid ordered domain could influence the structure of β-CTF. FTIR and NMR measurements with and without cholesterol indicate an increase in α-helical secondary structure. Cholesterol increases the thickness of the bilayer [78] by 10 % (i.e. ~ 3 Å) and we infer that this induces an increase in the helical structure between Gly25 and Gly29, in a fashion similar to that of A21G mutation. The

result of both the A21G mutation and increase of cholesterol is similar, an increase in Aβ production.

Together the results on the A21G and cholesterol point to a simple model in which structural changes in the extracellular sequence (LVFFAEDVGSNK) sequence lead to a reduction of inhibitory interactions. The large influence of the A21G mutation appears to be on the adjacent Phe19 and Phe20 residues. The increase in helical secondary structure induced by either the A21G mutation or by an increase in cholesterol may increase dimerization.

6.4 Conclusions

Similar to the familial A21G mutation, which reduces the β-structure near the site of the mutation and increases α-helical structure in the region from Gly25 to Gly29 at the junction between the extracellular and transmembrane domains, the changes in the structure of C55 upon incorporation of cholesterol into model membranes can also extend the TM helix and promote the formation of stronger C55 homodimer. The influence of the A21G mutation on structure and processing is similar to that caused by the membrane incorporation of cholesterol suggesting a common link between familial mutations and the cellular environment.

Chapter 7. Structural variation by familial mutations near the γ-cut site

7.1 Introduction

The amyloid deposition of β-amyloid peptides (Aβ) in the brain is a prominent feature of Alzheimer's disease (AD) and is caused by proteolysis of the amyloid precursor protein (APP) via a sequential two-step process. Cleavage of APP by α- or β-secretase near the boundary between ectodomain and extracellular juxtamembrane (JM) sequence causes shedding of the ectodomain, and is required for the second cleavage within the transmembrane (TM) helix of α- and β-CTF [(6)]. The γ-secretase complex catalyzes the second cleavage within the transmembrane domain, which leads to the formation of the

Aβ peptides with different lengths ranging from 38 to 42 amino acids. The Aβ40, cleavage at Val40 – Ile41, is the most prevalent Aβ peptide. However, Aβ42 has a higher propensity to form aggregates than the shorter isoforms and is the most toxic peptide generated from γ-cleavage [8]. Aβ42 is also the principal component of amyloid plaques in AD patients [27].

Familial AD mutations are found in the γ-secretase complex and the APP substrate. The mutations identified in APP were found to cluster in the extracellular region and transmembrane sequence of the protein. These mutations in the extracellular region included the A21G Flemish, E22Q Dutch, E22G Arctic, E22K Italian, and D23N Iowa mutations [34-37] between the α-cut site and TM domain, and the KM670/671NL Swedish (670/671 in APP numbering corresponding to the first two residues before the Aβ sequence), A2T, and A2V near the β-cut site. More recently, two additional mutations, the H6R English [79] and D7N Tottori mutations [80], have been found in the N terminus of Aβ that also cause early onset familial AD. These mutations accelerate fibril formation [81]. A second group of amino acids occurs between the cleavage site (Ala42) that releases the Aβ42 peptide and the cytoplasmic end (Leu52) of the TM domain. These include the T43A Iranian [82], T43I Austrian [83], V44M French [84], V44A German [85], I45V Florida [86], V46I London [87], V46L Indiana [88], V46G [89] and L52P Australian [90] mutations. Mutations downstream the γ-cut sites generate the wild-type Aβ peptides with affecting the processing by the γ–secretase complex.

Within the genetic autosomal mutation, both wild-type and familial mutation are overexpressed as heterozygotes. The mixture of wild-type and Aβ mutant can show very

different neuronal toxicity, e.g. only can K16N form highly toxic heteromeric oligomers mixed with wild-type Aβ peptides [69]. On the other hand, the dimerization analysis by Gorman *et al* [25] show that wild-type TM peptides can interact with V46G mutant peptides in a similar manner to the FRET measurement of self-association. Their results suggest that hetero-dimer can associate and might contribute to the AD pathology.

In this thesis, I mainly focus on the Austrian T43I mutation, which is located in the cluster of TM mutations. T43I causes the largest increase in the Aβ42/Aβ40 ratio [83]. Thr43 is one amino acid downstream of the γ-cleavage site that generates the Aβ42 peptide. This site is roughly midway between the extracellular and intracellular boundaries. On the extracellular side of Thr43, there are several GxxxG motifs within the TM domain that mediates dimerization in membrane bilayers [20]. On the intracellular side of Thr43, is a cluster of β-branched amino acids (Val44, I45, V46) whose mutation results in early onset AD. Gorman *et al.* [25] measured the influence of three FAD mutations (T43I, V46G and V46F) on the monomer-dimer equilibrium in the context of TM peptides. They found a positive correlation between the higher dissociation constant for the dimer (Kd) and the higher Aβ42/40 ratio observed in AD patients, suggesting that processing of the β-CTF monomer results in an increase in Aβ42/ Aβ40 with largely decreased Aβ40.

In our studies, we characterize the influence of the T43I mutation on the structure of C55, a 55-residue peptide corresponding to the extracellular, TM regions and a few charged residues in the C-terminus of the β-CTF. Structural measurements using FTIR

and solid-state NMR spectroscopy are carried out in both detergent micelles and in membrane bilayers. Structural changes are probed both upstream and downstream of the point of mutation. FTIR measurements reveal an increase in β-sheet structure associated with the folding of the extracellular sequence of the β-CTF. The structural changes in the extracellular region of C55 upon mutation within the TM domain are consistent with previous studies showing that this mutation leads to a shift of the TM dimer to monomer. Solution NMR studies show that mutation of Thr43 leads to changes in the chemical shifts of Gly37 and Gly38 within the TM domain. These glycines are involved in TM dimerization. Solid-state NMR measurements reveal a local change at Ile45, C terminal to the mutation site. Large shifts in the carbonyl and Cα carbon resonances of Ile45 are consistent with an increase in local helical structure upon mutation. Taken together, the Thr43 mutation can influence the secondary structure and dimerization of C55 proteins that can be correlated to the higher Aβ42/ Aβ40ratio in AD pathology.

7.2 Results

7.2.1 Mutations at Thr43 change the secretion and ratio of Aβ42 to Aβ40 from APP

There are two clinical mutations at Thr43 that have been described in the literature, the T43A Iranian [82] and T43I Austrian mutation [91]. This replacement introduces different size and polarity of side chains at position 43. To better understand the dependence of amino acid type at position 43 on processing, we analyzed the distribution profile of secreted Aβ38, Aβ40 and Aβ42 produced by processing of a series of Thr43 mutants on β-CTF.

Figure 7-1 A summarizes the distribution of Aβ38, Aβ40 and Aβ42 peptides produced by γ-secretase cleavage. The overall production of Aβ peptides, i.e. the predominant Aβ40 species is generally decreased by substitution of Thr43. The familial Thr43 mutations, T43I and T43A, exhibit decreases of total Aβ production by ~ 65% and 45%, respectively. Mutation of T43I and T43V dramatically decreases the level of Aβ40 and increases Aβ42. The Aβ42/ Aβ40 ratio is highest for T43I (in figure 7-1B).

Among these mutations, serine and valine are the most similar amino acids to threonine. Both have similar molecular volumes. Serine has a β-hydroxyl group, while valine has a β-methyl group. The T43S mutation results in a similar loss of total Aβ production (~50%) as observed for T43I but T43A, and has almost no effect on the Aβ42/ Aβ40 ratio. The T43V mutation, another class of β–branched amino acid like isoleucine closely resembles T43I in total production and has the second highest increase in the Aβ42/Aβ40 ratio. Together these results suggest that loss of the β-hydroxyl group of Thr43 has a crucial influence on the Aβ42/ Aβ40 ratio by decreasing the secretion of Aβ40 with an concomitantly increasing secreted Aβ38.

Of the amino acids tested, glycine and phenylalanine are structurally the most different from threonine. Aβ production is blocked by the T43F mutation, which places a large hydrophobic residue at position 43. T43G exhibits a striking increase in Aβ38 relative to Aβ40 and Aβ42. An increase in Aβ38 is generally observed upon mutation of Thr43 to most amino acids.

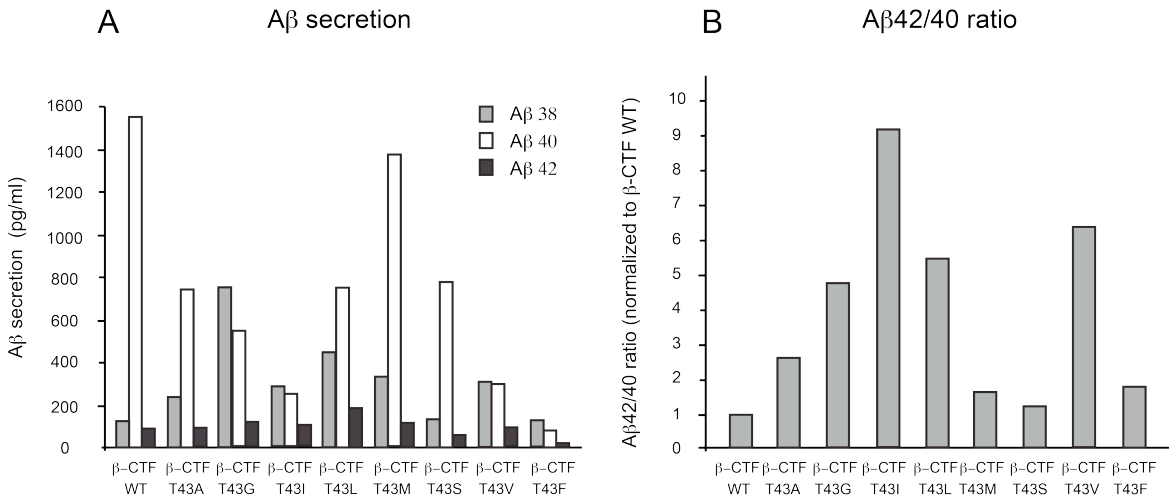

Figure 7-1. Aβ42 and Aβ40 secretion from β-CTF mutant in CHO cell lines. Aβ42 and Aβ40 secretion (A) and the ratio of Aβ42/ Aβ40 secretion (B) are shown here for comparison.

7.2.2 Comparison of wild-type C55 and Thr43 mutants reveal global changes in structure

To characterize the structural differences associated with various Thr43 mutants, we undertook FTIR spectroscopy. Figure 7-2 presents FTIR spectra of wild-type C55 and C55 with a series of Thr43 mutations. The peptides were reconstituted into DMPC: DMPG membrane bilayers. The amide region of the spectrum shows two intense distinct peaks at 1657 cm^{-1} and 1626 cm^{-1} with small peak at 1695 cm^{-1}. The band at 1657 cm^{-1} is characteristic of α-helical global secondary structure, while the band at 1626 cm^{-1} band is characteristic of β-sheet secondary structure. The small 1695 cm^{-1} band is often associated with anti-parallel β-sheet. We have assigned the β-structure in C55 to the extracellular sequence between Tyr10 and Ala21 (in Chapter 3 and 4). Upon mutation of Thr43, except T43V mutant, there is a general increase in resolution and an increase in intensity of the 1626 cm^{-1} band. These changes indicate that mutations in the TM domain have an influence on the extracellular region, and suggest that the TM mutations induce a global change in structure.

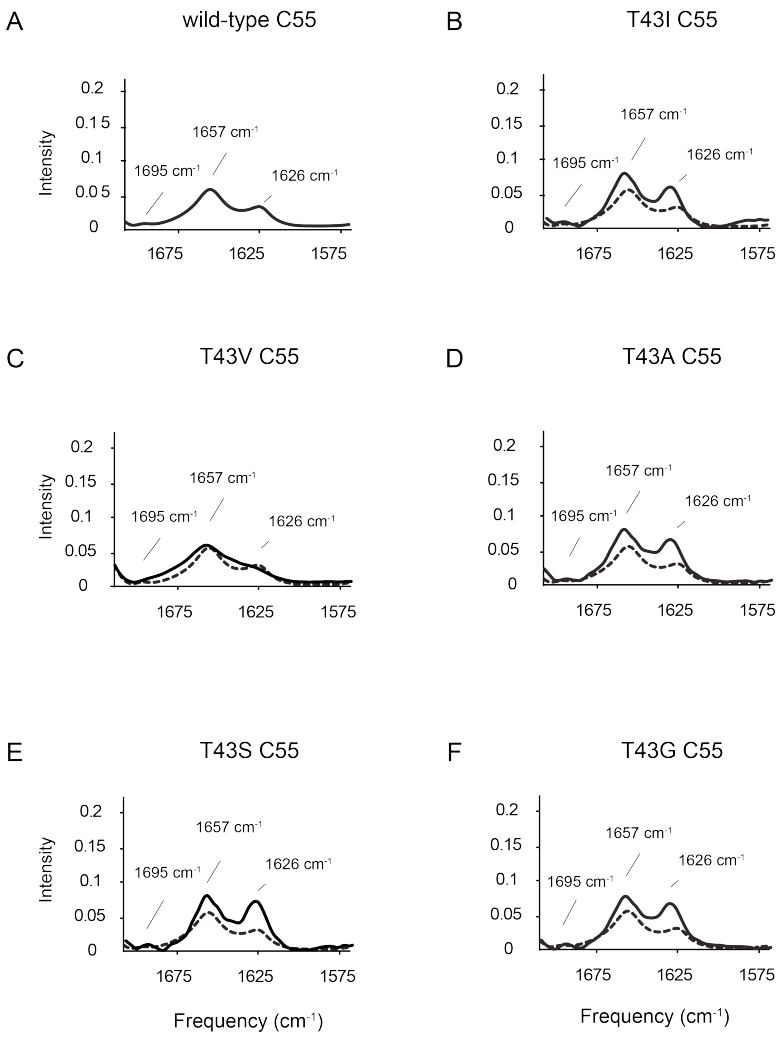

Figure 7-2. FTIR spectrum of wild-type C55 and T43I C55 mutant in bilayers. The spectrum of wild-type C55 is in solid line and the spectrum of mutants are in solid line in (B)-(F). Two major peaks are observed in the amide I region corresponding to TM helix and extracellular β–sheet with a small peak at 1695 cm^{-}. T43I, T43A, T43S and T43G mutant show more distinct peaks at helix and β–sheet peak.

To assess the global structure of C55, we undertook solution NMR studies in detergent micelles. Recently, the groups of Sanders [45, 63] and Arseniev [68] have published solution structures of the β-CTF. Sanders and coworkers [45, 63] have determined a structure of the full β-CTF molecule (residues 1-99), while Arseniev and coworkers [68] have determined a structure of a truncated β-CTF (residues Gln15 – Lys53) in DPC micelles. Figure 7-3 presents the 2D ^{15}N TROSY HSQC spectrum of wild-type C55 in DPC micelles. The spectrum is relatively well resolved; roughly one resonance of equal intensity is visible for each backbone and side chain NH group. The assignments were made on the basis of a series of three-dimensional NMR experiments (and by comparison with assignments of full β-CTF and shorter TM fragments previously). 78% of wild-type C55 proteins in DPC micelles are sequentially assigned. Assigned residues are shown in red on the sequence (in Figure 7-3).

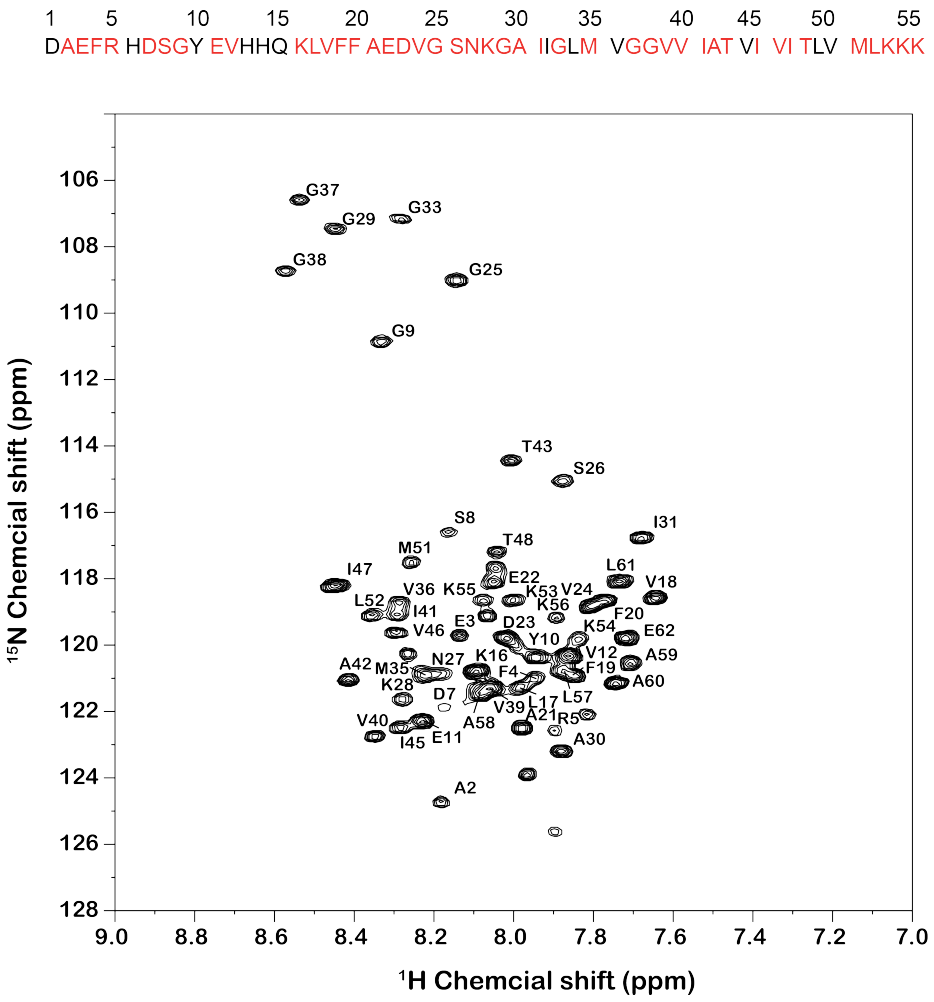

Figure 7-3. 2D ^{15}N, ^{1}H TROSY HSQC spectrum of wild-type C55 in DPC micelles. β-CTF sequence is shown on the top panel. The residues in red are sequentially assigned. 78 % of intrinsic C55 residues are assigned.

Figure 7-4 presents the region of the 2D TROSY HSQC spectra of wild-type C55 and various Thr43 mutants. The region of the glycine resonances is shown for clarity. The striking observation is that the mutations all influence the resonances corresponding to Gly37 and Gly38 within the TM sequence. As a result, the FTIR and solution NMR measurements both argue that mutation of Thr43 globally causes a change in the structure of C55 upstream of the site of mutation.

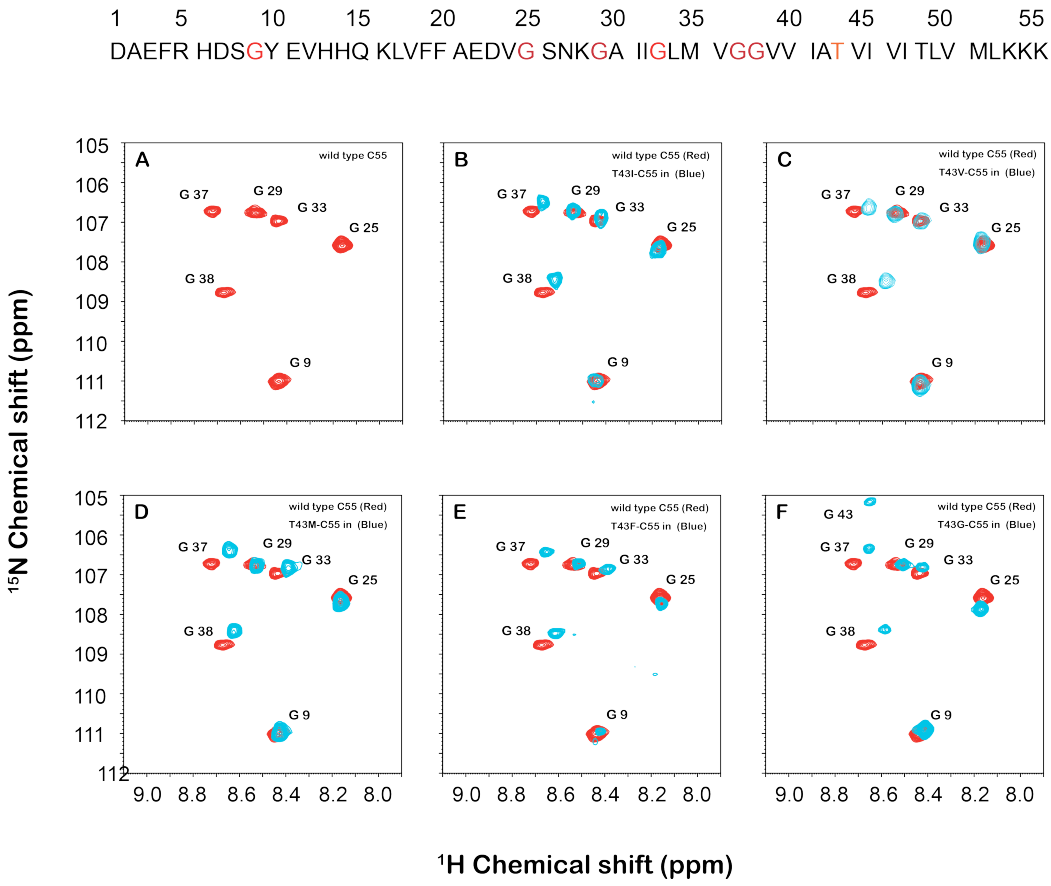

Figure 7-4. Glycine region of 2D ^{15}N, ^{1}H TROSY HSQC spectrum of wild-type C55 and Thr43 mutants in detergent micelles. The comparison between the wild-type and T43I mutants show that Gly37 and Gly38 shift more significantly.

7.2.3 The T43I mutation induces local structural changes in the TM domain of the β-CTF in bilayers.

In order to characterize the local structure surrounding Thr43 in membrane bilayers, solid-state NMR experiments were undertaken on C43 peptides (residues 22 – 66, or APP TM peptide in Chapter 3) incorporating the TM region of the β-CTF. This sequence was previously used in our solid-state NMR studies of TM dimerization [(20)]. In these studies, we observed interhelical NMR contacts between Gly29, Gly33 and Gly37. These three glycines comprise two consecutive GxxxG motifs within the TM sequence.

In an earlier study, Gorman *et al.* [(25)] proposed a comprehensive model for the influence of the TM cluster mutations. In their studies (also on TM peptides), they showed that mutation of Thr43 shifts the structure of the TM dimer toward monomer. Here, we directly test this structural model by measuring interhelical interactions between Gly37 in the C terminal GxxxG motif between the wild-type and T43I mutant.

Figure 7-5 presents solid-state DARR NMR measurements of GxxxG contacts. The measurements involve reconstitution of two TM peptides in DMPC:DMPG bilayers with different ^{13}C-labeling schemes. One peptide is labeled at the backbone carbonyl of Gly37 with ^{13}C, while the second peptide is labeled at the backbone Ca carbon of Gly37 with ^{13}C. Close proximity (< 6 Å) of these ^{13}C labels is manifested as a cross peak in the 2D NMR spectrum. Figure 7-5a shows the region of the 2D spectrum in which the cross peak between the Ca carbon at 45 ppm and the C=O carbon at 175 ppm is observed in the wild-type TM peptide (blue spectrum). In contrast to the wild-type sequence,

incorporation of the same ^{13}C labeling scheme into peptides containing the T43I mutation does not result in an interhelical cross peak (red spectrum). Other stronger peaks are originated from uniformly ^{13}C labeled amino acids on the sequence (i.e. U-^{13}C Ala42, U-^{13}C Val44 and U-^{13}C Ile45 in one T43I mutant peptide as an example). These measurements show that we lose the dimer contact between TM helices previously observed by Sato *et al.* [20]. This observation is also in line with that of GxxxG intra-helical contact of wild-type and A21G C55 but not GxxxA motif. A possible shift of the TM dimer to monomer is consistent with the results of Gorman *et al.* [25].

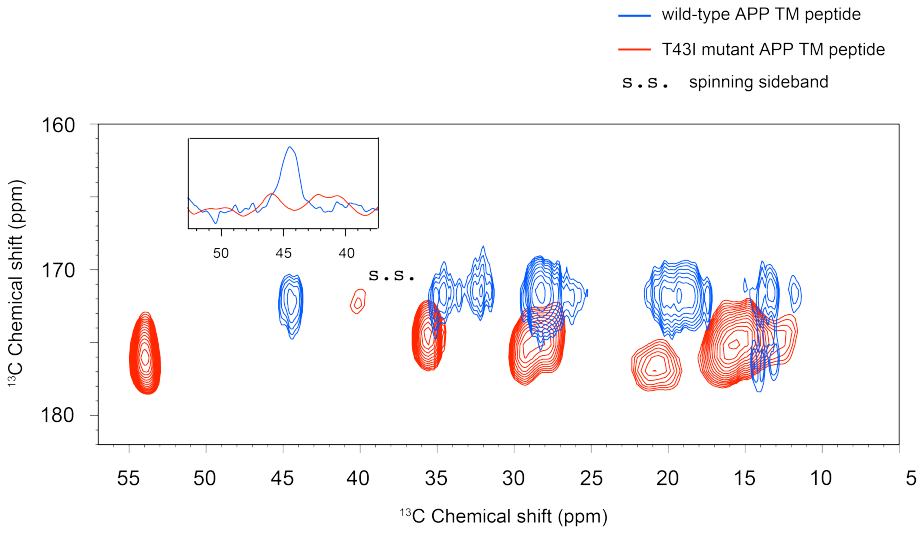

Figure 7-5. 2D DARR spectrum of wild-type APP TM peptide and T43I mutant for interhelical contacts in bilayers. Gly37 ^{13}C=O and Cly37 ^{13}Cα are labeled in two TM peptides. Equal molar of peptides are mixed. Gly Cα region of 1D CP spectrum is boxed and show that only a cross peak from Gly37 ^{13}C=O and Cly37 ^{13}Cα is observed in wild-type APP TM peptides (blue lines) but no T43I mutant peptides. Other stronger peaks are originated from intra-residual contacts of uniformly ^{13}C amino acids on the sequence (i.e. U-^{13}C Ala42, U-^{13}C Val44 and U-^{13}C Ile45 in T43I mutant).

Solid-state NMR spectroscopy also allows us to measure the backbone ^{13}C chemical shifts (i.e. C=O and Cα) along the TM sequence that are sensitive to the secondary structures of the peptide. In Figure 7-6, we summarize the ^{13}C chemical shifts deviation from the averaged values (http://www.bmrb.wisc.edu/ref_info/ statful.htm) of nearby amino acids on the N terminal and C terminal side of Thr43. For amino acids other than glycine, ^{13}C=O chemical shifts greater than ~177 ppm are characteristic of α-helical secondary structure. For glycine, chemical shifts associated with a helical conformation are typically observed between ~174 and 175 ppm. Here, the Cα and C=O chemical shifts are plotted as differences from the average chemical shifts of these resonances. The deviations to higher chemical shift values (i.e. positive bars) correspond to α-helical secondary structure. The backbone chemical shifts of T43I mutant globally show a typical α–helical propensity. The measured chemical shifts for the TM residues of the wild-type sequence are consistent with TM helix, with the notable exception of Ile45 (negative value of ~ 1.5 ppm) and Ala42 (negative value of ~ 0.4 ppm). The observed negative chemical shift deviation is markedly different from that typically observed for a residue within a TM helix, suggesting a possible loss of backbone hydrogen bonding of the Ile45 C=O group. The T43I mutation results in a shift of the ^{13}C=O resonance by 2.5 ppm to positive deviation, suggesting restoration of backbone hydrogen bonding of the Ile45 C=O upon mutation. The chemical shift comparison of Val40 between wild-type and the T43I mutation also shows a negative deviation of ~ 2 ppm with a large positive difference on the chemical shift of Cα. The chemical shift comparison of Gly38 between the wild-type and the T43I mutation also shows a negative deviation of ~ 1 ppm. These observations are particularly of interesting since the position of Val40 is the γ-cleavage

site that releases the Aβ40. The position of Ile45 and Gly38 is the cut-site that generate the upstream and downstream cleavage product of Aβ42 (i.e. the progressive cleavage pathway of Aβ38 - Aβ42 - Aβ45 - Aβ48). The carbonyl chemical shift deviation represents the accessibility of exposed carbonyl on the sequence.

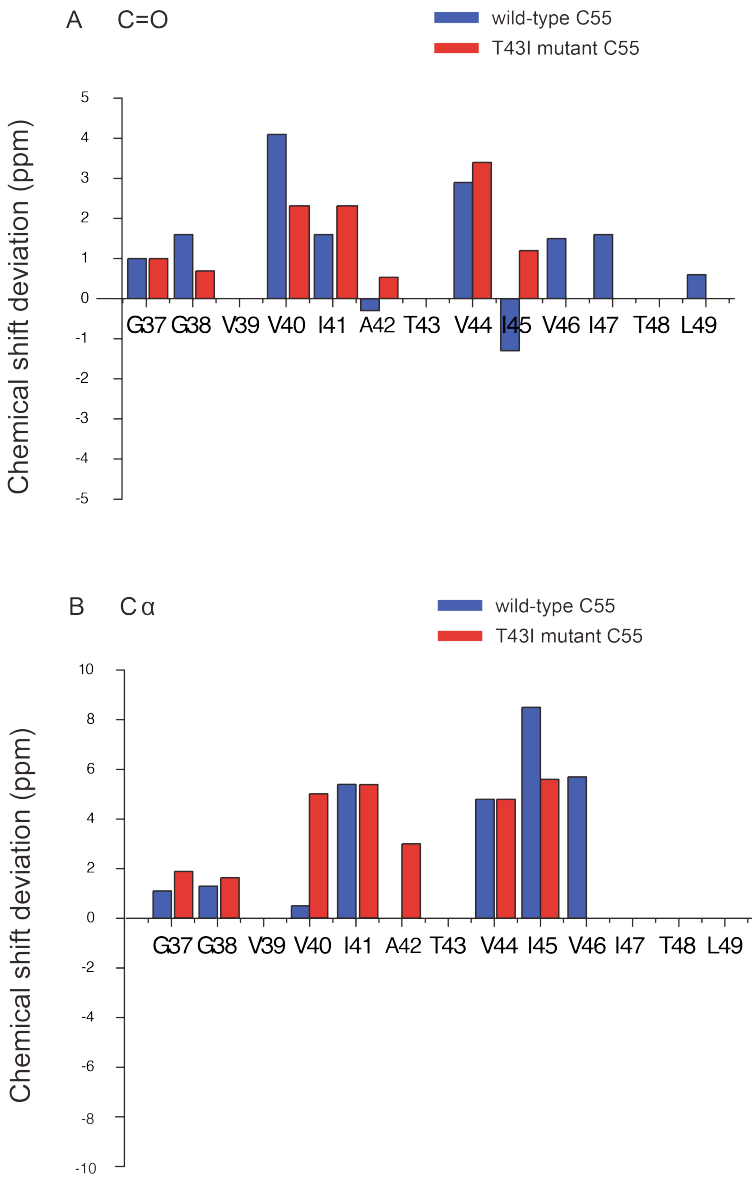

Figure 7-6. Chemical shift deviation of wild-type APP TM and T43I mutant peptide from average values. The secondary structure propensity predicted from deviation of chemical shifts is focus on upstream and downstream the site of T43I mutation. (A) Carbonyl chemical shift deviation from average values. (B) Cα carbon chemical shifts deviation from average values. The average chemical shift values are taken from the BMRB database (http://www.bmrb.wisc.edu/ref_info/ statful.htm). The deviations to higher chemical shift values (i.e. positive bars) correspond to α-helical secondary structure. The ratio of peptide to total lipid is 1: 50.

7.3 Discussion

Familial mutations in the APP gene fall into several clusters. One cluster corresponds to amino acid positions within the TM domain of the protein between Ala42, the γ-cleavage site that generates the toxic Aβ42 peptide and Leu49, the ε-cleavage site that initiates progressive cleavage of the β-CTF substrate by γ-secretase. This cluster involves amino acids Ala42, Thr43, Val44, Ile45, and Val46. We have targeted the T43I mutation and show that it induces global structural changes in the extracellular region of the protein, as well as local changes in the TM region at Ile45. These changes appear to shift the monomer – dimer equilibrium toward more monomer. *In vivo* processing analysis shows that the T43I mutation reduces the total amount of secreted Aβ peptides and increases the Aβ42/ Aβ40 ratio by decreased Aβ40 secretion. Here, both solution and solid state NMR are used to study the structures of wild-type and mutants in detergent and bilayer systems for comparison. The extracellular structure of β–CTF in detergent micelles , e.g. K17-L18-V18-F19-F20-A21, is different from that in bilayers [(45)].

7.3.1 The T43I mutation causes structural changes upstream of Thr43

The major γ-secretase cleavage sites within the β-CTF are at residues 38, 40 and 42. The TM cluster of FAD mutants occurs in the helical turn of amino acids that are just downstream of Ala42. De Jonghe *et al.* [(32)] found that T43I, V44M, V44A, I45V, V46I and V46L all increase the Aβ42/ Aβ40 ratio. All mutations except I45V decreased Aβ40 secretion, and all mutations except V44M increased the amount of secreted Aβ42. These results suggest there are local changes within the β-CTF substrate in the vicinity of the Val40 and Ala42 cleavage sites. However, there are several observations that imply that the FAD mutations within the TM domain can influence the structure of the γ-secretase substrate upstream of Thr43. For example, De Jonghe *et al.* [(32)] and Ancolio *et al.* (1999) found that mutations within the TM cluster of FAD mutants increased x-Aβ42. x-Aβ42

are peptide isoforms that start with cleavage at amino acid 11 (alternative β-sectretase cleavage) [6] or 17 (α-secretase cleavage) [84, 92].

The FTIR data presented in Figure 7-2 provide evidence for a change in the structure of the extracellular sequence of C55 upon mutation of Thr43. We observe reproducible changes in the intensities of the 1626 cm^{-1} and 1657 cm^{-1} bands. We have recently suggested that β-sheet/strand structure in the extracellular sequence influences the level of Aβ40 secretion by influencing γ-secretase cleavage (in Chapter 4 and 5). For example, mutations of the LVFF sequence disrupt the β-sheet structure in the extracellular domain and result in increase in the secretion of Aβ peptides.

Solution NMR studies suggest that the series of mutations at Thr43 all influence the structure of the β-CTF in the region of Gly37 and Gly38. These glycines have both been implicated in dimerization of the TM domain and destabilize the secondary structure. There are several lines of evidence indicate that dimerization may influence processing by the γ-secretase complex. In chapter 3, I have showed that TM peptides alone formed dimers mediated by their GxxxG motifs [20]. Mutation of GxxxG motifs in neuronal cell lines [23] or in CHO cells [21] gave different results. Munter *et al.* [23] found that mutations of Gly29 and Gly33 of the GxxxG motif gradually attenuate the strength of TM dimerization strength, reduce the formation of Aβ42 and increase Aβ38 and shorter Aβ species, while leaving the level of Aβ40 unaffected. Gorman et al. [25] using model peptides found that the mutations in the TM cluster of FAD mutations exhibited weaker dimerization than the wild-type sequence. Our results agree with Gorman et al. [25] in context of dimerization of APP TM T43I mutant. The mutations appear to influence both the G37-G38 and the extracellular regions.

7.3.2 Structural changes between Thr43 and ε-cleavage site induced by Thr43

One of the puzzling aspects of the TM cluster of FAD mutations involves how mutations in four consecutive amino acids (T43, V44, I45, V46) within one helical turn can lead to an increase in Aβ42 relative to Aβ40. The emerging consensus for the processing of APP to different length Aβ peptides is that proteolysis occurs by progressive cleavage of the TM domain of the β-CTF from the ε- to the γ-cut site [13]. The ε-cut site lies at the boundary between the hydrophobic core and the polar headgroup region of the bilayer. One of the first indications that the γ-secretase complex was able to cleave the β-CTF between the γ- and ε-cut sites was the isolation of Aβ46 peptides [14]. More recently, the Aβ43 and Aβ49 peptides have been detected [15-17]. Using the DAPT inhibitor that suppresses Aβ40, Qi-Takahara *et al.* [15] observed an intracellular buildup of Aβ43 and Aβ46. They proposed an α-helical model in which the β-CTF is cleaved at every three residues. Along with the detection of other longer intracellular Aβ peptides, including Aβ45 and Aβ48 and AICD 49 (49 residues), another product line starting from Aβ48 is sequentially to generate generate Aβ42 where is cleaved every three residues. The model suggests that the FAD mutations are responsible for increasing the number of peptides undergoing a shift from one product line to another. Our results show that there are irregular C=O chemical shifts of Ile45 and Ala42 of the wild-type within TM helix and the T43I mutation can positively shift this uncommon C=O frequencies of Ile45 and Ala42 along with a positive shifting of Gly38 and Val40 C=O. These observations are consistent with two distinct cleavage pathways.

7.4 Conclusions

The familial T43I mutation within the TM domain of the β-CTF leads to an increase in the ratio of the Aβ42 peptide relative to Aβ40 by decreasing the Aβ40

secretion. Aβ42, the most toxic spices to neuronal cells is the principal component of amyloid deposits within the brain parenchyma, and the Aβ42/ Aβ40 ratio is correlated with the onset age of Alzheimer's disease. FTIR measurements on C55, a 55-residue peptide corresponding to the extracellular and TM regions of the β-CTF, reveal an increase in β-sheet structure within the extracellular sequence. Solution and solid-state NMR measurements reveal structural changes both upstream and downstream of Thr43. Solution NMR measurements show the mutations at Thr43 lead to changes in the chemical shifts of Gly37 and Gly38 within the transmembrane domain. The T43I mutation leads to a local change at Ile45, located two residues toward the C terminus of the TM domain. Difference in the carbonyl and Cα carbon resonances of Ile45 (positive shift), Ala42 (positive shift), Val40 (negative shift) and G38 (negative shift) are consistent with an increased trend in local helical structure upon mutation that leads to the preference on the production of Aβ42 or Aβ40.

Chapter 8. General discussion and future plans

8.1 General discussion

The dissertation is mainly on the structural studies of C55 corresponding to extracellular and transmembrane domains of β–CTF in membrane bilayers. The *in vivo* Aβ secretion experiments by our collaborators set up a platform to monitor the correlation between structure and processing by the secretases, where we propose that structural variation of substrates can alter the substrate-enzyme interaction and leads to change in enzymatic cleavage.

8.2 Summary of results

8.2.1 The helix-to-coil transition at the TM-JM boundary is required for the

intramembranous cleavage

Processing of APP by the γ-secretase complex is the last step in the formation of the Aβ peptides associated Alzheimer's disease. In our structural studies of APP TM peptides in bilayers, we show that the TM domain forms an α-helical homodimer mediated by consecutive GxxxG motifs, but not GxxxA. We find that the APP TM helix is unraveled at the intracellular membrane boundary near the ε-cleavage site. Also, this helix-to-coil transition is required for γ-secretase processing; mutations that extend the TM α-helix inhibit ε-cleavage, leading to a low production of Aβ peptides and an accumulation of the α- and β-CTF. Our data are consistent with a progressive cleavage model where β-CTF proteolysis depends on the helix-to-coil transition at the TM-JM boundary and unraveling of the α-helix of TM substrate.

8.2.2 The Thr43 mutations decrease homodimerization with the secondary structure change between the γ-cut and ε-cut site

The familial T43I mutation within the TM domain of the β-CTF leads to an increase in the ratio of the Aβ42 peptide relative to Aβ40. Aβ42 is the principal component of amyloid deposits within the brain parenchyma, and the Aβ42/Aβ40 ratio is correlated with the onset age of Alzheimer's disease. FTIR measurements on C55, a 55-residue peptide corresponding to the extracellular and TM regions of the β-CTF, reveal an increase in β-sheet structure within the extracellular sequence. Solution and solid-state NMR measurements reveal structural changes both upstream and downstream of Thr43. Solution NMR measurements show that mutations at Thr43 lead to changes in the chemical shifts of Gly37 and Gly38 within the TM domain in micellar environments but

not bilayers. The T43I mutation leads to a local change at Ile45, located two residues toward the C- terminus of the TM domain in bilayers. Large shifts in the carbonyl and Cα carbon resonances of Ile45 are consistent with an increase in local helical structure upon mutation. These results argue that the mutations at Thr43 can influence both the extracellular and TM structure of β-CTF in micelles and bilayers.

8.2.3 Conformational change induced by the A21G mutation leads to increased Aβ secretion in Alzheimer's Disease

Solid-state NMR and Fourier transform infrared spectroscopy show that in membrane bilayers the extracellular sequence from Leu17 to Ala21 has β-secondary structure and that the transmembrane region is helical starting at Gly29. The familial A21G mutation reduces the β-structure near the site of the mutation and increases α-helical structure in the region from Gly25 to Gly29 at the junction between the extracellular and transmembrane domains. To further verify the role of extracellular β–structure, several mutations at A21 are made. The mutation of Ala21 to Leu or Phe reduces Aβ40 and Aβ42 production consistent with the hydrophobic character of these residues inhibiting the γ-secretase complex activity. In contrast, substitution of Ala21 with Glu similar to the downstream ED sequence, largely does not affect Aβ40 secretion, although it increases Aβ42 and decreases Aβ38 secretion.

8.2.4 Cholesterol and A21G mutation have the similar influence on the structure of β-CTF

Analogous to the familial A21G mutation which reduces the β-structure near the site of the mutation and increases α-helical structure in the transition region from Gly25 to

Gly29 at the junction between the extracellular and transmembrane domains, the changes in the structure of C55 upon incorporation of cholesterol into model lipids can also extend the TM helix and promote the formation of stronger C55 homodimer. The influence of the A21G mutation on structure and processing is similar to that caused by the membrane incorporation of cholesterol providing a common link between familial mutations and the cellular environment.

8.3 Future plans and current working model

8.3.1 The anti-parallel β-sheet structure on the extracellular sequence of β-CTF and its potential roles on the processing

FTIR spectra show that the β-CTF globally adopts TM α-helix and extracellular β–sheet structures. The ratio of integration on α-helix peak (at 1657 cm^{-1}) and extracellular β–sheet band (at 1626 cm^{-1}) is ~ 2.4: 1 corresponding to the numbers of 24 residues versus 10 residues (TM residues of G29 to L52). One explanation is the LVFFA sequence is part of the β–structure. Observation of 1695 cm^{-1} and Tri-Alanine scanning in the extracellular sequence is consistent with an intramolecular anti-parallel β–sheet conformation. Our latest Aβ secretion data on the FRH to AAA (i.e. leading to an increased Aβ secretion), HHQ to AAA (i.e. no effect Aβ-structure) and LVFF to AAAA (i.e. leading to an increased Aβ secretion and reducing the β-structure) β–CTF mutants support a registry of the region of RHDSGY --- LVFFAE in anti-parallel β–sheet formation with a complimentary interaction of positive charge of R5 and negative charge of E22 on both β–sheet ends. Those preliminary results raise the possibility of whether this intramolecular anti-parallel β–sheet structure can lead to the extended β-helix supramolecular structure [(93)] that has been observed in Aβ fibril formation. To further identify the potential roles on

influencing the processing, e.g. oligomerization, dimer-to-monomer equilibrium, higher resolution structures within this region can be established with more distance constraints.

8.3.2 The influence of liquid ordered domain (raft) on the structure of β-CTF

In my thesis studies, I found that the high concentration of cholesterol added in POPC: POPS model bilayers (unsaturated side chain) can influence the structure of β-CTF in two aspects, i) the extended TM helix ii) stronger TM dimerization on both wild-type and A21G C55. We infer that adding cholesterol increases the thickness of the bilayer [(78)] by 10 % (i.e. ~ 3 Å) and that this induces an increase in the helical structure between Gly25 and Gly29, in a fashion similar to that of A21G mutation. However, much less influence has been found on the extracellular β-sheet structure, e.g. the chemical shifts of Phe19 and Phe20 only show slightly shifting where the A21G mutation is just next to. To further verify whether the thickness induced by the rich cholesterol in bilayers influence the TM structure of β-CTF, incorporation of peptides into thicker bilayer (e.g. with longer acyl chains of C18, C20 or C22) or saturate acyl chains (e.g. DPPC) should also lead to TM structural variation and dimerization. FTIR (i.e. serve to monitor the sample homogeneity) and solid-state NMR (i.e. serve to monitor the TM structure) are used to investigate the structure change. In physiological aspect, the accumulation of cholesterol in Neiman Pick type C (NPC) cells promotes the aggregation of APP or β-CTF in lipid order domains (raft) where the secreted Aβ peptides generated [(77)].

8.3.3 The Thr43 mutations can influence the structure of β-CTF between γ–and ε–cut site

In Chapter 7, I found that the Thr43 mutation can influence the secondary structure at Gly37-Gly38 upstream γ–cleavage site and Ile45 between γ– and ε-cleavage site either

in micelles or bilayers. The DARR constraints show that the mutation influences the dimer-to-monomer equilibrium of T43I mutant TM peptides toward monomer. To establish the structure variation at the TM-JM boundary caused by the T43I mutation, we need full chemical shift information of T43I mutant β-CTF in this region. Previously, we have successfully assigned 78 % of wild-type C55 proteins with a few residues missing backbone nucleus frequencies. The 3D data for assignment are collected at ^{1}H frequency of 600 MHz. To optimize the resolution and sensitivity of spectrum, the spectrum can be taken in higher field of 850 MHz (at ^{1}H frequency) with cryoprobe (~ 2-3 fold). The successful assignment on the wild-type C55 can extend the structure studies between γ– and ε–cut site upon the Thr43 mutations.

8.3.4 Current working model

In this thesis, several structure elements have been characterized to influence the processing of β–CTF. The Thr43 mutation can influence the secondary structure at Gly37-Gly38 upstream γ–cleavage site and residues, e.g. Ile45 between γ– and ε-cleavage site either in micelles or bilayers that have been attributed to the different monomer-to-dimer equilibrium. Those structure variations within transmembrane domains also affect the extracellular structure that has been identified as β–structure in bilayers and proposed as an intramolecular anti-parallel β–sheet in the region of HDSGY - - - LVFFA with the complementary ionic interactions between Arg5 to Glu22 and Glu11 to Lys16. Our FTIR results support an increasing β–structure propensity upon Thr43 mutations. The Aβ secretion in double mutations at A21G and T43I shows higher Aβ42/ Aβ40 ratio without increasing the total Aβ generation is similar to the phenotype of single T43I mutation and

further implicates the T43 mutations show the inhibitory effect of extracellular sequence with an induced stronger β–structure. Furthermore, the well-defined anti-parallel β–sheet in the region of RHDSGYE - - - KLVFFAKE within single C55 peptide is of interesting since the anti-parallel β–sheets of Aβ peptide constitute to the β-helix formation of fibrils. In surface of bilayers, the formation of this supramolecular structure can have influence on the oligomerization state, TM dimer-to-monomer equilibrium, secondary structure variation of β-CTF and interaction with membranes those can attribute to the regulation of Aβ secretion. The future plans can be focused on i) establishment of intramolecular anti-parallel β–sheet with more distance constraints. ii) supramolecular structure of extracellular anti-parallel β–sheet. iii) interaction of extracellular domains with lipid bilayers iv) structure comparison of β–CTF in different lipid compositions between cholesterol-rich lipids and lipid raft microdomain.

Bibliography

1. Nikolaev, A., McLaughlin, T., O'Leary, D. D. M., and Tessier-Lavigne, M. (2009) APP binds DR6 to trigger axon pruning and neuron death via distinct caspases, *Nature 457*, 981-U981.
2. Cao, X. W., and Südhof, T. C. (2001) A transcriptively active complex of APP with Fe65 and histone acetyltransferase Tip60, *Science 293*, 115-120.
3. Thinakaran, G., and Koo, E. H. (2008) Amyloid precursor protein trafficking, processing, and function, *J. Biol. Chem. 283*, 29615-29619.
4. Watanabe, T., Hikichi, Y., Willuweit, A., Shintani, Y., and Horiguchi, T. (2012) FBL2 Regulates Amyloid Precursor Protein (APP) Metabolism by Promoting Ubiquitination-Dependent APP Degradation and Inhibition of APP Endocytosis, *Journal of Neuroscience 32*, 3352-3365.
5. Tian, Y., Crump, C. J., and Li, Y.-M. (2010) Dual role of α-secretase cleavage in the regulation of γ-secretase activity for amyloid production, *J. Biol. Chem. 285*, 32549-32556.
6. Vassar, R., Bennett, B. D., Babu-Khan, S., Kahn, S., Mendiaz, E. A., Denis, P., Teplow, D. B., Ross, S., Amarante, P., Loeloff, R., Luo, Y., Fisher, S., Fuller, J., Edenson, S., Lile, J., Jarosinski, M. A., Biere, A. L., Curran, E., Burgess, T., Louis, J. C., Collins, F., Treanor, J., Rogers, G., and Citron, M. (1999) β-secretase cleavage of Alzheimer's amyloid precursor protein by the transmembrane aspartic protease BACE, *Science 286*, 735-741.
7. Wolfe, M. S., Xia, W. M., Ostaszewski, B. L., Diehl, T. S., Kimberly, W. T., and Selkoe, D. J. (1999) Two transmembrane aspartates in presenilin-1 required for presenilin endoproteolysis and γ-secretase activity, *Nature 398*, 513-517.
8. Burdick, D., Soreghan, B., Kwon, M., Kosmoski, J., Knauer, M., Henschen, A., Yates, J., Cotman, C., and Glabe, C. (1992) Assembly and aggregation properties of synthetic Alzheimer's A4/β amyloid peptide analogs, *J. Biol. Chem. 267*, 546-554.
9. Wiley, J. C., Hudson, M., Kanning, K. C., Schecterson, L. C., and Bothwell, M. (2005) Familial Alzheimer's disease mutations inhibit γ-secretase-mediated liberation of β-amyloid precursor protein carboxy-terminal fragment, *J. Neurochem. 94*, 1189-1201.
10. Hecimovic, S., Wang, J., Dolios, G., Martinez, M., Wang, R., and Goate, A. M. (2004) Mutations in APP have independent effects on Aβ and CTFγ generation, *Neurobiology of Disease 17*, 205-218.
11. Chandu, D., Huppert, S. S., and Kopan, R. (2006) Analysis of transmembrane domain mutants is consistent with sequential cleavage of Notch by γ-secretase, *J. Neurochem. 96*, 228-235.
12. Kakuda, N., Funamoto, S., Yagishita, S., Takami, M., Osawa, S., Dohmae, N., and Ihara, Y. (2006) Equimolar production of amyloid β-protein and amyloid precursor protein intracellular domain from β-carboxyl-terminal fragment by γ-secretase, *J. Biol. Chem. 281*, 14776-14786.

13. De Strooper, B. (2007) Loss-of-function presenilin mutations in Alzheimer disease - Talking Point on the role of presenilin mutations in Alzheimer disease, *EMBO Rep. 8*, 141-146.
14. Yu, C. J., Kim, S. H., Ikeuchi, T., Xu, H. X., Gasparini, L., Wang, R., and Sisodia, S. S. (2001) Characterization of a presenilin-mediated amyloid precursor protein carboxyl-terminal fragment γ - Evidence for distinct mechanisms involved in γ-secretase processing or the APP and Notch1 transmembrane domains, *J. Biol. Chem. 276*, 43756-43760.
15. Qi-Takahara, Y., Morishima-Kawashima, M., Tanimura, Y., Dolios, G., Hirotani, N., Horikoshi, Y., Kametani, F., Maeda, M., Saido, T. C., Wang, R., and Ihara, Y. (2005) Longer forms of amyloid β protein: implications for the mechanism of intramembrane cleavage by γ-secretase, *J. Neurosci. 25*, 436-445.
16. Yagishita, S., Morishima-Kawashima, M., Tanimura, Y., Ishiura, S., and Ihara, Y. (2006) DAPT-induced intracellular accumulations of longer amyloid β-proteins: Further implications for the mechanism of intramembrane cleavage by γ-secretase, *Biochemistry 45*, 3952-3960.
17. Zhao, G. J., Cui, M. Z., Mao, G. Z., Dong, Y. Z., Tan, J. X., Sun, L. S., and Xu, X. M. (2005) γ-cleavage is dependent on ζ-cleavage during the proteolytic processing of amyloid precursor protein within its transmembrane domain, *J. Biol. Chem. 280*, 37689-37697.
18. Mowrer, K. R., and Wolfe, M. S. (2008) Promotion of BACE1 mRNA alternative splicing reduces amyloid β-peptide production, *J. Biol. Chem. 283*, 18694-18701.
19. Munter, L.-M., Botev, A., Richter, L., Hildebrand, P. W., Althoff, V., Weise, C., Kaden, D., and Multhaup, G. (2010) Aberrant amyloid precursor protein (APP) processing in hereditary forms of Alzheimer disease caused by APP familial Alzheimer disease mutations can be rescued by mutations in the APP GxxxG motif, *J. Biol. Chem. 285*, 21636-21643.
20. Sato, T., Tang, T. C., Reubins, G., Fei, J. Z., Fujimoto, T., Kienlen-Campard, P., Constantinescu, S. N., Octave, J. N., Aimoto, S., and Smith, S. O. (2009) A helix-to-coil transition at the ε-cut site in the transmembrane dimer of the amyloid precursor protein is required for proteolysis, *Proc. Natl. Acad. Sci. U. S. A. 106*, 1421-1426.
21. Kienlen-Campard, P., Tasiaux, B., Van Hees, J., Li, M., Huysseune, S., Sato, T., Fei, J. Z., Aimoto, S., Courtoy, P. J., Smith, S. O., Constantinescu, S. N., and Octave, J. N. (2008) Amyloidogenic processing but not amyloid precursor protein (APP) intracellular C-terminal domain production requires a precisely oriented APP dimer assembled by transmembrane GXXXG motifs, *J. Biol. Chem. 283*, 7733-7744.
22. Eggert, S., Midthune, B., Cottrell, B., and Koo, E. H. (2009) Induced dimerization of the amyloid precursor protein leads to decreased amyloid-β protein production, *J. Biol. Chem. 284*, 28943-28952.
23. Munter, L. M., Voigt, P., Harmeier, A., Kaden, D., Gottschalk, K. E., Weise, C., Pipkorn, R., Schaefer, M., Langosch, D., and Multhaup, G. (2007) GxxxG motifs within the amyloid precursor protein transmembrane sequence are critical for the etiology of Aβ42, *EMBO J. 26*, 1702-1712.

24. Richter, L., Munter, L.-M., Ness, J., Hildebrand, P. W., Dasari, M., Unterreitmeier, S., Bulic, B., Beyermann, M., Gust, R., Reif, B., Weggen, S., Langosch, D., and Multhaup, G. (2010) Amyloid beta 42 peptide (Aβ42)-lowering compounds directly bind to Aβ and interfere with amyloid precursor protein (APP) transmembrane dimerization, *Proc. Natl. Acad. Sci. U. S. A. 107*, 14597-14602.
25. Gorman, P. M., Kim, S., Guo, M., Melnyk, R. A., McLaurin, J., Fraser, P. E., Bowie, J. U., and Chakrabartty, A. (2008) Dimerization of the transmembrane domain of amyloid precursor proteins and familial Alzheimer's disease mutants., *BMC Neurosci. 9*, 17, 1-11.
26. Tian, Y., Bassit, B., Chau, D. M., and Li, Y. M. (2010) An APP inhibitory domain containing the Flemish mutation residue modulates γ-secretase activity for Aβ production, *Nat. Struct. Mol. Biol. 17*, 151-158.
27. Portelius, E., Bogdanovic, N., Gustavsson, M., Volkmann, I., Brinkmalm, G., Zetterberg, H., Winblad, B., and Blennow, K. (2010) Mass spectrometric characterization of brain amyloid beta isoform signatures in familial and sporadic Alzheimer's disease, *Acta Neuropathologica 120*, 185-193.
28. Citron, M., Oltersdorf, T., Haass, C., McConlogue, L., Hung, A. Y., Seubert, P., Vigopelfrey, C., Lieberburg, I., and Selkoe, D. J. (1992) Mutation of the beta-amyloid precursor protein in familial Alzheimer's disease increases beta-protein production., *Nature 360*, 672-674.
29. Di Fede, G., Catania, M., Morbin, M., Rossi, G., Suardi, S., Mazzoleni, G., Merlin, M., Giovagnoli, A. R., Prioni, S., Erbetta, A., Falcone, C., Gobbi, M., Colombo, L., Bastone, A., Beeg, M., Manzoni, C., Francescucci, B., Spagnoli, A., Cantù, L., Del Favero, E., Levy, E., Salmona, M., and Tagliavini, F. (2009) A recessive mutation in the APP gene with dominant-negative effect on amyloidogenesis, *Science 323*, 1473-1477.
30. Johnston, J. A., Cowburn, R. F., Norgren, S., Wiehager, B., Venizelos, N., Winblad, B., Vigopelfrey, C., Schenk, D., Lannfelt, L., and Oneill, C. (1994) Increased β-amyloid release and levels of amyloid precursor protein (APP) in fibroblast cell lines from family members with the Swedish Alzheimer's disease APP670/671 mutation, *FEBS Lett. 354*, 274-278.
31. Wolfe, M. S. (2007) When loss is gain: Reduced presenilin proteolytic function leads to increased Aβ42/Aβ40 - Talking Point on the role of presenilin mutations in Alzheimer disease, *EMBO Rep. 8*, 136-140.
32. De Jonghe, C., Esselens, C., Kumar-Singh, S., Craessaerts, K., Serneels, S., Checler, F., Annaert, W., Van Broeckhoven, C., and De Strooper, B. (2001) Pathogenic APP mutations near the γ-secretase cleavage site differentially affect Aβ secretion and APP C-terminal fragment stability, *Hum. Mol. Genet. 10*, 1665-1671.
33. De Jonghe, C., Zehr, C., Yager, D., Prada, C. M., Younkin, S., Hendriks, L., Van Broeckhoven, C., and Eckman, C. B. (1998) Flemish and Dutch mutations in amyloid β precursor protein have different effects on amyloid β secretion, *Neurobiology of Disease 5*, 281-286.
34. Hendriks, L., van Duijn, C. M., Cras, P., Cruts, M., Van Hul, W., van Harskamp, F., Warren, A., McInnis, M. G., Antonarakis, S. E., Martin, J. J., Hofman, A., and Van Broeckhoven, C. (1992) Presenile dementia and cerebral haemorrhage linked

to a mutation at codon 692 of the β-amyloid precursor protein gene, *Nat. Genet. 1*, 218-221.
35. Levy, E., Carman, M. D., Fernandez-Madrid, I. J., Power, M. D., Lieberburg, I., van Duinen, S. G., Bots, G. T., Luyendijk, W., and Frangione, B. (1990) Mutation of the Alzheimer's disease amyloid gene in hereditary cerebral hemorrhage, Dutch type, *Science 248*, 1124-1126.
36. Kamino, K., Orr, H. T., Payami, H., Wijsman, E. M., Alonso, M. E., Pulst, S. M., Anderson, L., O'Dahl, S., Nemens, E., White, J. A., Sadovnick, A. D., Ball, M. J., Kaye, J., Warren, A., McInnis, M. G., Antonarakis, S. E., Korenberg, J. R., Sharma, V., Kukull, W., Larson, E., Heston, L. L., Martin, G. M., Bird, T. D., and Schellenberg, G. D. (1992) Linkage and mutational analysis of familial Alzheimer disease kindreds for the APP gene region, *Am. J. Hum. Genet. 51*, 998-1014.
37. Grabowski, T. J., Cho, H. S., Vonsattel, J. P., Rebeck, G. W., and Greenberg, S. M. (2001) Novel amyloid precursor protein mutation in an Iowa family with dementia and severe cerebral amyloid angiopathy, *Ann. Neurol. 49*, 697-705.
38. Nilsberth, C., Westlind-Danielsson, A., Eckman, C. B., Condron, M. M., Axelman, K., Forsell, C., Stenh, C., Luthman, J., Teplow, D. B., Younkin, S. G., Naslund, J., and Lannfelt, L. (2001) The 'Arctic' APP mutation (E693G) causes Alzheimer's disease by enhanced Aβ protofibril formation, *Nat. Neurosci. 4*, 887-893.
39. Van Broeckhoven, C., Haan, J., Bakker, E., Hardy, J. A., Van Hul, W., Wehnert, A., Vegter-Van der Vlis, M., and Roos, R. A. (1990) Amyloid β protein precursor gene and hereditary cerebral hemorrhage with amyloidosis (Dutch), *Science 248*, 1120-1122.
40. Van Nostrand, W. E., Melchor, J. P., Cho, H. S., Greenberg, S. M., and Rebeck, G. W. (2001) Pathogenic effects of D23N Iowa mutant amyloid β-protein, *J. Biol. Chem. 276*, 32860-32866.
41. Ren, Z., Schenk, D., Basi, G. S., and Shapiro, I. P. (2007) Amyloid β-protein precursor juxtamembrane domain regulates specificity of γ-secretase-dependent cleavages, *J. Biol. Chem. 282*, 35350-35360.
42. Kivipelto, M., Helkala, E. L., Laakso, M. P., Hanninen, T., Hallikainen, M., Alhainen, K., Soininen, H., Tuomilehto, J., and Nissien, A. (2001) Midlife vascular risk factors and Alzheimer's disease in later life: longitudinal, population based study, *Br. Med. J. 322*, 1447-1451.
43. Refolo, L. M., Pappolla, M. A., Malester, B., LaFrancois, J., Bryant-Thomas, T., Wang, R., Tint, G. S., Sambamurti, K., and Duff, K. (2000) Hypercholesterolemia accelerates the Alzheimer's amyloid pathology in a transgenic mouse model, *Neurobiology of Disease 7*, 690-691.
44. Umeda, T., Tomiyama, T., Kitajima, E., Idomoto, T., Nomura, S., Lambert, M. P., Klein, W. L., and Mori, H. (2012) Hypercholesterolemia accelerates intraneuronal accumulation of A beta oligomers resulting in memory impairment in Alzheimer's disease model mice, *Life Sci. 91*, 1169-1176.
45. Beel, A. J., Mobley, C. K., Kim, H. J., Tian, F., Hadziselimovic, A., Jap, B., Prestegard, J. H., and Sanders, C. R. (2008) Structural studies of the transmembrane C-terminal domain of the amyloid precursor protein (APP): Does APP function as a cholesterol sensor?, *Biochemistry 47*, 9428-9446.

46. Wahrle, S., Das, P., Nyborg, A. C., McLendon, C., Shoji, M., Kawarabayashi, T., Younkin, L. H., Younkin, S. G., and Golde, T. E. (2002) Cholesterol-dependent γ-secretase activity in buoyant cholesterol-rich membrane microdomains, *Neurobiology of Disease 9*, 11-23.
47. Simons, M., Keller, P., De Strooper, B., Beyreuther, K., Dotti, C. G., and Simons, K. (1998) Cholesterol depletion inhibits the generation of β-amyloid in hippocampal neurons, *Proc. Natl. Acad. Sci. U. S. A. 95*, 6460-6464.
48. Osenkowski, P., Ye, W., Wang, R., Wolfe, M. S., and Selkoe, D. J. (2008) Direct and potent regulation of γ-secretase by its lipid microenvironment, *J. Biol. Chem. 283*, 22529-22540.
49. London, E. (2005) How principles of domain formation in model membranes may explain ambiguities concerning lipid raft formation in cells, *Biochim. Biophys. Acta-Mol. Cell Res. 1746*, 203-220.
50. Smith, S. O., Eilers, M., Song, D., Crocker, E., Ying, W. W., Groesbeek, M., Metz, G., Ziliox, M., and Aimoto, S. (2002) Implications of threonine hydrogen bonding in the glycophorin A transmembrane helix dimer, *Biophys. J. 82*, 2476-2486.
51. Lu, Z., Van Horn, W. D., Chen, J., Mathew, S., Zent, R., and Sanders, C. R. (2012) Bicelles at low concentrations, *Mol. Pharm. 9*, 752-761.
52. Takegoshi, K., Nakamura, S., and Terao, T. (2001) ^{13}C-^{1}H dipolar-assisted rotational resonance in magic-angle spinning NMR, *Chemical Physics Letters 344*, 631-637.
53. Adams, P. D., Engelman, D. M., and Brünger, A. T. (1996) Improved prediction for the structure of the dimeric transmembrane domain of glycophorin A obtained through global searching, *Proteins: Structure, Function, and Genetics 26*, 257-261.
54. Feng, L., Yan, H. C., Wu, Z. R., Yan, N., Wang, Z., Jeffrey, P. D., and Shi, Y. G. (2007) Structure of a site-2 protease family intramembrane metalloprotease, *Science 318*, 1608-1612.
55. Li, S. C., and Deber, C. M. (1992) Glycine and β-branched residues support and modulate peptide helicity in membrane environments, *FEBS Lett. 311*, 217-220.
56. Li, S. C., and Deber, C. M. (1992) Influence of glycine residues on peptide conformation in membrane environments, *International Journal of Peptide and Protein Research 40*, 243-248.
57. Wang, H., Barreyro, L., Provasi, D., Djemil, I., Torres-Arancivia, C., Filizola, M., and Ubarretxena-Belandia, I. (2011) Molecular determinants and thermodynamics of the amyloid precursor protein transmembrane domain implicated in Alzheimer's disease, *J. Mol. Biol. 408*, 879-895.
58. Ramelota, T. A., and Nicholson, L. K. (2001) Phosphorylation-induced structural changes in the amyloid precursor protein cytoplasmic tail detected by NMR, *J. Mol. Biol. 307*, 871-884.
59. Funamoto, S., Morshima-Kawashima, M., Tanimura, Y., Hirotani, N., Saido, T. C., and Ihara, Y. (2004) Truncated carboxyl-terminal fragments of β-amyloid precursor protein are processed to amyloid β-proteins 40 and 42, *Biochemistry 43*, 13532-13540.
60. Kühne, W. (1878) On the stable colours of the retina, *Journal of Physiology 1*, 109-212.

61. Kukar, T. L., Ladd, T. B., Robertson, P., Pintchovski, S. A., Moore, B., Bann, M. A., Ren, Z., Jansen-West, K., Malphrus, K., Eggert, S., Maruyama, H., Cottrell, B. A., Das, P., Basi, G. S., Koo, E. H., and Golde, T. E. (2011) Lysine 624 of the amyloid precursor protein (APP) is a critical determinant of amyloid β peptide length: Support for a sequential model of γ-secretase intramembrane proteolysis and regulation by the amyloid β precursor protein (APP) juxtamembrane region, *J. Biol. Chem. 286*, 39804-39812.
62. Paravastua, A. K., Leapman, R. D., Yau, W. M., and Tycko, R. (2008) Molecular structural basis for polymorphism in Alzheimer's β-amyloid fibrils, *Proc. Natl. Acad. Sci. U. S. A. 105*, 18349-18354.
63. Barrett, P. J., Song, Y., Van Horn, W. D., Hustedt, E. J., Schafer, J. M., Hadziselimovic, A., Beel, A. J., and Sanders, C. R. (2012) The amyloid precursor protein has a flexible transmembrane domain and binds cholesterol, *Science 336*, 1168-1171.
64. Beel, A. J., Sakakura, M., Barrett, P. J., and Sanders, C. R. (2010) Direct binding of cholesterol to the amyloid precursor protein: An important interaction in lipid-Alzheimer's disease relationships?, *Biochim. Biophys. Acta Mol. Cell Biol. Lipids 1801*, 975-982.
65. Tycko, R. (2011) Solid-State NMR sudies of amyloid fibril structure, *Annu. Rev. Phys. Chem. 62*, 279-299.
66. Saito, H. (1986) Conformation-dependent C-13 chemical-shifts - a new means of conformational characterization as obtained by high-resolution solid-state C-13 NMR, *Magn. Reson. Chem. 24*, 835-852.
67. Wishart, D. S., and Sykes, B. D. (1994) The ^{13}C Chemical-Shift Index: A Simple Method for the Identification of Protein Secondary Structure Using ^{13}C Chemical-Shift Data, *J. Biomol. NMR 4*, 171-180.
68. Nadezhdin, K. D., Bocharova, O. V., Bocharov, E. V., and Arseniev, A. S. (2012) Dimeric structure of transmembrane domain of amyloid precursor protein in micellar environment, *FEBS Lett. 586*, 1687-1692.
69. Kaden, D., Harmeier, A., Weise, C., Munter, L. M., Althoff, V., Rost, B. R., Hildebrand, P. W., Schmitz, D., Schaefer, M., Lurz, R., Skodda, S., Yamamoto, R., Arlt, S., Finckh, U., and Multhaup, G. (2012) Novel APP/Aβ mutation K16N produces highly toxic heteromeric Aβ oligomers, *EMBO Mol. Med. 4*, 647-659.
70. Betts, V., Leissring, M. A., Dolios, G., Wang, R., Selkoe, D. J., and Walsh, D. M. (2008) Aggregation and catabolism of disease-associated intra-Aβ mutations: reduced proteolysis of AβA21G by neprilysin, *Neurobiology of Disease 31*, 442-450.
71. Paul, C., Wang, J. P., Wimley, W. C., Hochstrasser, R. M., and Axelsen, P. H. (2004) Vibrational coupling, isotopic editing, and β-sheet structure in a membrane-bound polypeptide, *J. Am. Chem. Soc. 126*, 5843-5850.
72. Russ, W. P., and Engelman, D. M. (2000) The GxxxG motif: A framework for transmembrane helix-helix association, *J. Mol. Biol. 296*, 911-919.
73. Minor, D. L., and Kim, P. S. (1994) Measurement of the β-sheet-forming propensities of amino acids, *Nature 367*, 660-663.
74. Ben Khalifa, N., Tyteca, D., Marinangeli, C., Depuydt, M., Collet, J.-F., Courtoy, P. J., Renauld, J.-C., Constantinescu, S., Octave, J.-N., and Kienlen-Campard, P.

(2012) Structural features of the KPI domain control APP dimerization, trafficking, and processing, *FASEB J. 26*, 855-867.
75. Calderon, R. O., Attema, B., and Devries, G. H. (1995) LIPID-COMPOSITION OF NEURONAL CELL-BODIES AND NEURITES FROM CULTURED DORSAL-ROOT GANGLIA, *Journal of Neurochemistry 64*, 424-429.
76. Brown, D. A., and London, E. (1998) Functions of lipid rafts in biological membranes, *Annu. Rev. Cell. Dev. Biol. 14*, 111-136.
77. Kosicek, M., Malnar, M., Goate, A., and Hecimovic, S. (2010) Cholesterol accumulation in Niemann Pick type C (NPC) model cells causes a shift in APP localization to lipid rafts, *Biochem. Biophys. Res. Commun. 393*, 404-409.
78. Kučerka, N., Nieh, M.-P., Pencer, J., Sachs, J. N., and Katsaras, J. (2009) What determines the thickness of a biological membrane, *Gen. Physiol. Biophys. 28*, 117-125.
79. Janssen, J. C., Beck, J. A., Campbell, T. A., Dickinson, A., Fox, N. C., Harvey, R. J., Houlden, H., Rossor, M. N., and Collinge, J. (2003) Early onset familial Alzheimer's disease - Mutation frequency in 31 families, *Neurology 60*, 235-239.
80. Wakutani, Y., Watanabe, K., Adachi, Y., Wada-Isoe, K., Urakami, K., Ninomiya, H., Saido, T. C., Hashimoto, T., Iwatsubo, T., and Nakashima, K. (2004) Novel amyloid precursor protein gene missense mutation (D678N) in probable familial Alzheimer's disease, *J. Neurol. Neurosurg. Psychiatry 75*, 1039-1042.
81. Hori, Y., Hashimoto, T., Wakutani, Y., Urakami, K., Nakashima, K., Condron, M. M., Tsubuki, S., Saido, T. C., Teplow, D. B., and Iwatsubo, T. (2007) The Tottori (D7N) and English (H6R) familial Alzheimer disease mutations accelerate A beta fibril formation without increasing protofibril formation, *J. Biol. Chem. 282*, 4916-4923.
82. Pasalar, P., Najmabadi, H., Noorian, A. R., Moghimi, B., Jannati, A., Soltanzadeh, A., Krefft, T., Crook, R., and Hardy, J. (2002) An Iranian family with Alzheimer's disease caused by a novel APP mutation (Thr714Ala), *Neurology 58*, 1574-1575.
83. Kumar-Singh, S., De Jonghe, C., Cruts, M., Kleinert, R., Wang, R., Mercken, M., De Strooper, B., Vanderstichele, H., Lofgren, A., Vanderhoeven, I., Backhovens, H., Vanmechelen, E., Kroisel, P. M., and Van Broeckhoven, C. (2000) Nonfibrillar diffuse amyloid deposition due to a γ_{42}-secretase site mutation points to an essential role for N-truncated $A\beta_{42}$ in Alzheimer's disease, *Hum. Mol. Genet. 9*, 2589-2598.
84. Ancolio, K., Dumanchin, C., Barelli, H., Warter, J. M., Brice, A., Campion, D., Frébourg, T., and Checler, F. (1999) Unusual phenotypic alteration of β amyloid precursor protein (β APP) maturation by a new Val-715 -> Met βAPP-770 mutation responsible for probable early-onset Alzheimer's disease, *Proc. Natl. Acad. Sci. U. S. A. 96*, 4119-4124.
85. Cruts, M., Dermaut, B., Rademakers, R., Van den Broeck, M., Stögbauer, F., and Van Broeckhoven, C. (2003) Journal of Neurology, *J. Neurol. 250*, 1374-1375.
86. Eckman, C. B., Mehta, N. D., Crook, R., Pereztur, J., Prihar, G., Pfeiffer, E., GraffRadford, N., Hinder, P., Yager, D., Zenk, B., Refolo, L. M., Prada, C. M., Younkin, S. G., Hutton, M., and Hardy, J. (1997) A new pathogenic mutation in the APP gene (1716V) increases the relative proportion of Aβ42(43), *Hum. Mol. Genet. 6*, 2087-2089.

87. Goate, A., Chartier-Harlin, M. C., Mullan, M., Brown, J., Crawford, F., Fidani, L., Giuffra, L., Haynes, A., Irving, N., James, L., Mant, R., Newton, P., Rooke, K., Roques, P., Talbot, C., Pericak-Vance, M., Roses, A., Williamson, R., Rossor, M., Owen, M., and Hardy, J. (1991) Segregation of a missense mutation in the amyloid precursor protein gene with familial Alzheimer's disease, *Nature 349*, 704-706.
88. Murrell, J. R., Hake, A. M., Quaid, K. A., Farlow, M. R., and Ghetti, B. (2000) Early-onset Alzheimer disease caused by a new mutation (V717L) in the amyloid precursor protein gene, *Arch. Neurol. 57*, 885-887.
89. Chartierharlin, M. C., Crawford, F., Houlden, H., Warren, A., Hughes, D., Fidani, L., Goate, A., Rossor, M., Roques, P., Hardy, J., and Mullan, M. (1991) Early-onset Alzheimer's disease caused by mutations at codon 717 of the β-amyloid precursor protein gene, *Nature 353*, 844-846.
90. Kwok, J. B. J., Li, Q. X., Hallupp, M., Whyte, S., Ames, D., Beyreuther, K., Masters, C. L., and Schofield, P. R. (2000) Novel Leu723Pro amyloid precursor protein mutation increases amyloid β42(43) peptide levels and induces apoptosis, *Ann. Neurol. 47*, 249-253.
91. Edwards-Lee, T., Ringman, J. M., Chung, J., Werner, J., Morgan, A., Hyslop, P. S., Thompson, P., Dutton, R., Mlikotic, A., Rogaeva, E., and Hardy, J. (2005) An African American family with earlyonset Alzheimer disease and an APP (T714I) mutation, *Neurology 64*, 377-379.
92. Wang, R., Meschia, J. F., Cotter, R. J., and Sisodia, S. S. (1991) Secretion of the beta-A4 amylid precursor protein identification of a cleavage site in cultured-mammalian-cells *J. Biol. Chem. 266*, 16960-16964.
93. Antzutkin, O. N., Leapman, R. D., Balbach, J. J., and Tycko, R. (2002) Supramolecular structural constraints on Alzheimer's β-amyloid fibrils from electron microscopy and solid-state nuclear magnetic resonance, *Biochemistry 41*, 15436-15450.

Appendix

A.1 Averaged ^{13}C Chemical shift values

(updated on 23/05/2013 from BMRB database)

Amino acid type	Atom	Number	Averaged chemical shift (ppm)	Deviation (ppm)
ALA	C	32958	177.72	3.3
ALA	CA	45121	53.17	2.1
ALA	CB	42930	19.07	2.47
ARG	C	21348	176.38	3.27
ARG	CA	29802	56.77	2.42
ARG	CB	27819	30.73	2.19
ARG	CG	18515	27.23	1.73
ARG	CD	18753	43.16	1.47
ARG	CZ	467	160.46	4.28
ASP	C	26455	176.39	2.69
ASP	CA	36270	54.69	2.13
ASP	CB	34461	40.9	2.08
ASP	CG	704	178.42	11.8
ASN	C	17903	175.21	3.51
ASN	CA	24979	53.54	2.01
ASN	CB	23770	38.71	2.05
ASN	CG	1883	176.44	6.76
CYS	C	7157	174.84	3.69
CYS	CA	10230	58.2	3.37
CYS	CB	9657	32.85	6.22
GLU	C	34861	176.81	3.74
GLU	CA	47369	57.33	2.18
GLU	CB	44617	30.04	2.19
GLU	CG	31217	36.12	1.65
GLU	CD	717	181.8	7.8
GLN	C	18333	176.3	3.23
GLN	CA	25426	56.59	2.2
GLN	CB	23993	29.22	2.1
GLN	CG	16885	33.78	1.88
GLN	CD	1778	179.39	6.74
GLY	C	32448	173.84	3.21
GLY	CA	44985	45.38	1.66

Amino acid type	Atom	Number	Averaged chemical shift (ppm)	Deviation (ppm)
HIS	C	9494	175.15	4.3
HIS	CA	13518	56.56	2.84
HIS	CB	12762	30.29	2.42
HIS	CG	141	131.32	6.24
HIS	CD2	5218	119.9	5.8
HIS	CE1	4109	137.28	5.39
ILE	C	23590	175.81	3.62
ILE	CA	32127	61.62	2.75
ILE	CB	30185	38.61	2.23
ILE	CG1	20799	27.71	2.07
ILE	CG2	22166	17.56	2.02
ILE	CD1	22286	13.49	2.48
LEU	C	38604	176.97	3.34
LEU	CA	52871	55.65	2.2
LEU	CB	49837	42.3	2.06
LEU	CG	32621	26.81	1.57
LEU	CD1	35667	24.72	2.04
LEU	CD2	34018	24.1	2.12
LYS	C	31384	176.59	6.35
LYS	CA	43294	56.94	2.26
LYS	CB	40799	32.81	2.06
LYS	CG	27502	24.92	1.61
LYS	CD	26052	28.97	1.55
LYS	CE	25242	41.88	1.37
MET	C	9378	176.18	2.8
MET	CA	13202	56.15	2.31
MET	CB	12254	33	2.49
MET	CG	8073	32.04	1.73
MET	CE	6114	17.19	2.51
PHE	C	16573	175.42	3.46
PHE	CA	22574	58.12	2.65
PHE	CB	21355	40	2.38
PHE	CG	248	136.93	13.06
PHE	CD1	9369	131.34	4.1
PHE	CD2	6648	131.38	3.93
PHE	CE1	8246	130.48	3.83
PHE	CE2	5844	130.57	3.36
PHE	CZ	6315	129.02	3.93

Amino acid type	Atom	Number	Averaged chemical shift (ppm)	Deviation (ppm)
PRO	C	17323	176.61	4.62
PRO	CA	25033	63.32	2.27
PRO	CB	23639	31.88	1.79
PRO	CG	16967	27.24	1.81
PRO	CD	17101	50.3	1.95
SER	C	28442	174.61	2.6
SER	CA	39364	58.72	2.22
SER	CB	36773	63.72	5.68
THR	C	24312	174.52	2.34
THR	CA	33749	62.25	2.66
THR	CB	31584	69.61	6.99
THR	CG2	22730	21.59	2.03
TRP	C	5320	176.14	2.6
TRP	CA	7263	57.68	2.66
TRP	CB	6860	30.12	2.82
TRP	CG	191	110.28	6.92
TRP	CD1	3615	126.3	4.02
TRP	CD2	129	128.17	1.93
TRP	CE2	164	138.38	7.07
TRP	CE3	3083	120.22	3.76
TRP	CZ2	3476	114.04	4.04
TRP	CZ3	3110	121.2	3.36
TRP	CH2	3260	123.62	3.71
TYR	C	13494	175.36	3.38
TYR	CA	18839	58.13	2.63
TYR	CB	17669	39.33	2.71
TYR	CG	237	128.12	12.18
TYR	CD1	8528	132.42	4.85
TYR	CD2	5735	132.42	4.78
TYR	CE1	8460	117.71	3.92
TYR	CE2	5671	117.78	3.02
TYR	CZ	184	154.65	17.33
VAL	C	30803	175.63	2.41
VAL	CA	42092	62.53	2.92
VAL	CB	39626	32.75	2
VAL	CG1	29219	21.53	1.93
VAL	CG2	28192	21.33	2.07

A.2 Chemical shift table of the extracellular region of β-CTF

Table 1

wild type C55
A21G mutant

	Carbonyl	Carbonyl	Carbonyl	Cα	Cα	Cα
Residue	DMPC/PG	POPC/PS	POPC/PS/Chol	DMPC/PG	POPC/PS	POPC/PS/Chol
Leu 17	174.3	174.5	174.6	53.5	53.8	53.7
	173.9		174.6	53.3		53.6
Val 18	173.9			61.0		
	173.6			60.5		
Phe 19	172.6	172.6	173.2	56.1	56.5	57.6
	174.5			57.1		
Phe 20	171.1	171.3	171.4	55.2	54.6	54.6
	174.4			56.0		
Ala 21	174.5			49.6		
Gly 21	172.5			45.1		
Val 24	175.3	173.1		61.5	61.0	60.8
	175.7			63.2		
Gly 25	172.3	172.5		44.4	44.1	44.0
	175.7		176.2	45.6		47.6
Gly 29	175.4	174.7	174.7	47.0	46.6	46.7
	175.2			47.3		
Ala 30	178.6	179.0	178.6	54.8	55.0	
	178.8		178.9	54.9		54.8
Ile 31	177.8	178.5	178.3			
	177.9					

* The chemical shift values are referenced to Glycine

CO, and adjusted to DSS by adding 2.01 ppm.

A.3 Chemical shift table of the transmembrane domain of β-CTF

wild type APP TM peptide
T43I mutant APP TM peptide

Residue	Carbonyl	Ca	Cb
Gly 33	175.2	47.6	N.D.
Gly 37	174.9 174.9	46.6 47.7	N.D.
Gly 38	175.5 174.4	46.8 47.3	N.D.
Val 40	179.8 177.5	62.6 67.5	34.7 31.1
Ile 41	177.2 176.8	66.4 66.4	38.1 37.8
Ala 42	177.4 178.7	N.D. 55.8	N.D. 18.2
Val 44	178.6 179.1	66.9 66.9	31.2 31.0
Ile 45	174.3 176.8	69.5 66.6	36.2 37.4
Val 46	177.2	67.8	31.5
Ile 47	177.2	N.D.	N.D.
Leu 49	177.5	N.D.	N.D.

* The chemical shift values are referenced to Glycine CO, and adjusted to DSS by adding 2.01 ppm.

A.4 1H, 15N – TROSY HSQC spectrum of the wild-type C55 in LMPG micelles